The role of the receptor tyrosine kinase TrkA in checkpoint activation, DSB repair, and survival of neuroblastoma cell lines

Inaugural-Dissertation
zur
Erlangung des Doktorgrades

Dr. rer. nat.

der Fakultät für Biologie

an der Universität Duisburg-Essen

vorgelegt von

Ines Rudolf

aus Essen

Essen, Juni 2015

Die der vorliegenden Arbeit zugrunde liegenden Experimente wurden im hämatologisch-onkologischen Labor der Kinderklinik III des Universitätsklinikum Essen im Rahmen des DFG-Graduiertenkollegs 1739 durchgeführt.

1. **Gutachter:** PD Dr. rer. nat. Alexander Schramm

2. Gutachter: Prof. Dr. phil. nat. Shirley Knauer

Vorsitzender des Prüfungsausschusses: Prof. Dr. phil. nat. George Iliakis

Tag der mündlichen Prüfung: 08.09.2015

Table of Contents

Introduction

1 Neuroblastoma: Etiology, genetics and clinical subtypes

1.1 Epidemiology and genetic predisposition

Neuroblastoma comprises 8-10% of all childhood cancers, accounts for 15% of pediatric cancer deaths, and is the most common solid tumor in childhood [1, 2]. The tumor derives from primitive sympathetic neural precursors and arises most often in the adrenal medulla [3]. Neuroblastoma is characterized by a broad heterogeneity regarding the outcome of the disease. Clinical courses range from spontaneous regression to development of metastasis or relapse accompanied by therapy resistance and infaust outcome [4]. In Germany, approx. 150 new cases of neuroblastoma are diagnosed each year (Cancer Registry, Mainz).

The likelihood of spontaneous regression in infants below 18 months of age is very high, even without chemotherapy [5-8]. On the other hand, the survival rate for children 18 months or older is only 40-50%, as neuroblastomas are often unresectable, metastatic and require intensive multi-modal therapy [1, 9]. The incidence of neuroblastoma is 1 in 7000 live births, 40% of patients are diagnosed in the first year of life with the incidence rate of neuroblastoma being twice that of leukemia in this age group, and 96% tumors are diagnosed before the age of 10 [10]. Patients are divided into very low (5-year event-free survival (EFS) >85%), low- (5-year EFS >75% to ≤85%), intermediate- (5-year EFS ≥50% to ≤75% and high-risk patients (5-year EFS <50%), where neuroblastomas of high-risk patients are frequently resistant to therapies and 60-70% patients succumb to the disease [11]. Only about 1-2% of children with neuroblastoma have a family history of the tumor [12-14]. Hereditary neuroblastomas are caused by germline mutations in ALK (anaplastic lymphoma kinase, 75%) [12, 15, 16] and PHOX2B (paired-like homeobox 2B gene; 5%) [10, 17]. Whole genome analyses of neuroblastomas have identified activating mutations or rearrangements of *ALK* (8-10% of sporadic tumors) [18] and mutations in *ATRX*, *ARID1A*, *ARID1B*, *MYCN*, *PTPN11* and *NRAS* (1-3% of tumors) [4, 18-21]. Genome-wide association studies have identified neuroblastoma-associated polymorphisms in *BARD1*, *LMO1* and *LIN28B* [22-26].

Nevertheless, most neuroblastomas occur spontaneously with the underlying factors remaining largely unknown [4, 17, 27]. Further research is necessary to better characterize different types of neuroblastoma and develop effective therapies according to prognosis of each patient.

1.2 Pathogenesis

Neuroblastoma arises within the neuronal ganglia of the peripheral sympathetic nervous system, which derive from ventrolateral neural crest cells. During early embryogenesis, the neural crest cells undergo epithelial-to-mesenchymal transition at the edge of the neural tube to form the enteric nervous system, melanocytes, dorsal root and sympathetic ganglia, and the chromaffin cells of the adrenal medulla [28]. The differentiation of pluripotent neural crest cells and neural crest formation depends on the interplay of multiple transcription factors, signaling pathways and epigenetic regulatory mechanisms [28, 29]. As a developmental malignancy, the pathologic heterogeneity of neuroblastoma may be explained by the unique developmental biology of the neural crest [30, 31]. Expression profiling of fetal adrenal neuroblasts, normal fetal adrenal cortical cells, and neuroblastoma cells found differential expression of genes involved in earlier (*ASCL1*) and later (*DLK1*) developmental stages of neural crest development in favorable and unfavorable tumors [32]. Moreover, zebrafish studies have shown varying effects of *PHOX2B* aberrations on differentiation and confirmed its requirement for the development of neural crest-derived cells that comprise the sympathetic ganglia [33].

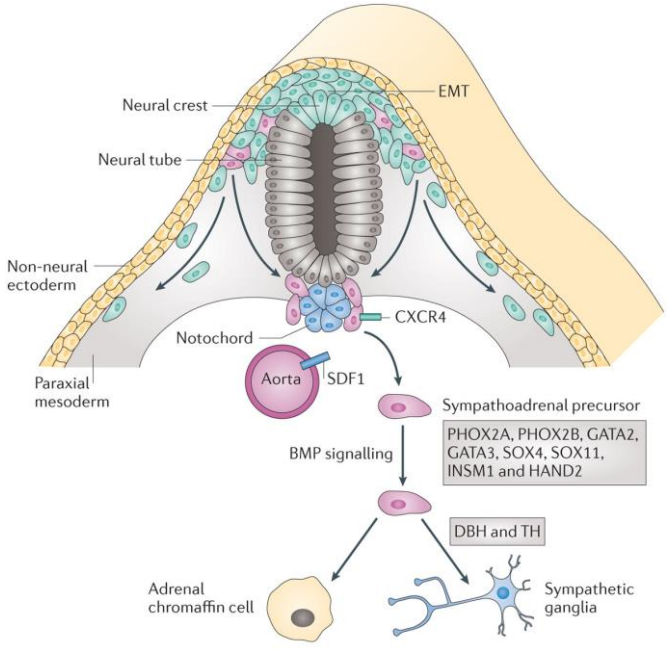

Figure 1: Differentiation of neural crest cells [34].

Migrating neural crest cells undergo epithelial-mesenchymal transition (EMT) as they migrate. Migration towards the dorsal aorta is in part directed by the chemoattractant CXR4 (CXC chemokine receptor 4), expressed on neural crest progenitor cells, and SDF1 (stromal cell derived factor 1), expressed on the dorsal aorta, and commits cells to the sympathoadrenal lineage. Bone morphogenetic protein (BMP) signaling induces the differentiation programme of migrating neural crest progenitor cells.

About 60% of tumors arise from abdominal paraspinal ganglia, 30% within the adrenal medulla and 10% are found from sympathetic ganglia in the chest, head/ neck and pelvis [35]. The degree of differentiation of neural crest cells has been shown to be an indicator for long-term survival [36]. Patients with tumors displaying high differentiation have a more favorable outcome than patients with tumors characterized by more primitive crest-like cells.

During neural tube formation in the embryogenesis of vertebrates, the early neural crest precursors acquire multi-potent differentiation potential through an elaborate mechanism involving transcription factors and epigenetic regulation [37, 38]. Different transformation steps during these early stages of neural crest maturation and the developmental stage of neural crest precursors might reflect the various neuroblastoma phenotypes and cause the observed clinical and pathological heterogeneity [39, 40].

The term '*in situ* neuroblastoma' refers to microscopic foci of neuroblastic cells that were found in adrenal glands of infants (<3 months of age) who had died for various reasons [41]. It was proposed that these neuroblastic nodules might eventually become clinically detectable neuroblastoma. However, further studies of adrenal glands of spontaneously aborted fetuses showed that neuroblastic nodules were present in all fetuses. It has been proposed that the neuroblastic nodules were not malignant neuroblastomas *in situ*, but elements of normal sympathoadrenal development, which contain the cells that can eventually give rise to adrenal neuroblastomas. This led to the hypothesis that genes like *PHOX2B*, which are involved in neural crest development, might also play a role in spontaneous regression of neuroblastoma [42].

1.3 Neuroblastoma staging

The International Neuroblastoma Staging System (INSS) has been established in 1988 to facilitate the comparison of clinical and laboratory studies and ranged from Stage I (localized tumors, complete resection), Stage II (small tumors, incomplete resection, possible lymph node involvement), Stage III (large tumors crossing anatomical midline of patient, incomplete resection) to Stage IV (metastatic tumors) and Stage IVS (< 1 year of age, liver/ skin/ bone marrow metastases) [43].

A newer staging system designated 'International Neuroblastoma Risk Group (INRG) staging system' involves radiographic image-defined risk factors (IDRFs) and stages tumors based on involvement of vital structures (stage L1 vs. L2), presence of metastases (stage M) and age of 18 months or older (stage MS, Table1) [44].

Neuroblastoma is the tumor with the highest rate of spontaneous regression [45, 46]. The 'S' in Stage IVS or MS refers to 'special' and describes the phenomenon of spontaneous regression seen in neuroblastoma. A clinical phenotype with a specific metastatic spread to the liver, skin and bone marrow was observed to be associated with a very good prognosis and an age of less than 12 months at the time of diagnosis [47, 48].

Table 1: International Neuroblastoma Risk Group (INRG) staging system from Monclair et al. JCO 2009

Stage	**Definition**
L1	Localized tumor not involving vital structures as defined by the list of image-defined risk factors and confined to one body compartment.
L2	Locoregional tumor with presence of one or more image-defined risk factors.
M	Distant metastatic disease (except stage MS).
MS	Metastatic disease in children younger than 18 months with metastases confined to skin, liver, and/or bone marrow.

The INRG pre-treatment classification schema involves INRG staging, chromosomal aberrations, prognosis-associated clinical and biological factors, age, histology, differentiation, MYCN status and ploidy and is used to evaluate the patient and determine their risk group. Treatment recommendations are then made based on this classification and the resulting risk group of the patient [11].

1.4 Treatment

Based on the clinical heterogeneity of neuroblastoma and the event-free and overall survival of patients in cooperative group clinical trials treatment recommendations range from observation to multi-modal therapies. For non-high risk groups showing an EFS greater than 90%, therapy should be reduced as much as possible to avoid long-term complications from cancer treatment. Efforts addressing the treatment options for children with localized disease, young age (<18 months) and favorable genetics show excellent outcome with observation, resection alone and restricted use of chemotherapy [49-51]. Children with other lower-risk lesions are treated based on the presence of image-defined risk factors (IDRFs), where complete resection is pursued for INRG L1 tumors and INRG L2 tumors with incomplete resection are treated according to their biological features [52, 53]. Tumors associated with a

high risk are characterized by MYCN amplification, INRG Stage M and an age of >18 months. Therapies are multi-modal and involve surgery, chemotherapy, irradiation, biologics like cis-retinoic acid, and immunotherapy. Collective efforts are focused on the identification of biomarkers to identify treatment responders and non-responders. The measurement of minimal residual disease markers in the bloodstream and bone marrow, and a radiographic, semi-quantitative metaiodobenzylguanidine (MIBG) scoring system are currently the most studied indicators [31, 54, 55].

1.5 Molecular characteristics of neuroblastoma

The clinical heterogeneity of neuroblastoma is reflected by its variety of biological and genetic features. The most important molecular features correlating with the differences in clinical outcome are the status of the *MYCN* oncogene, which is amplified in about 20% of all NB [56], loss of heterozygosity at chromosomes 1p [57] or 11q [58], trisomy of 17q [59], and high expression of the neurotrophin receptor TrkB/NTRK2 [60], all of which are linked to unfavorable outcome [61]. Near-triploidy [62] and a high expression of TrkA/NTRK1 [63], on the other hand, are associated with far less aggressive tumors that often regress spontaneously [64].

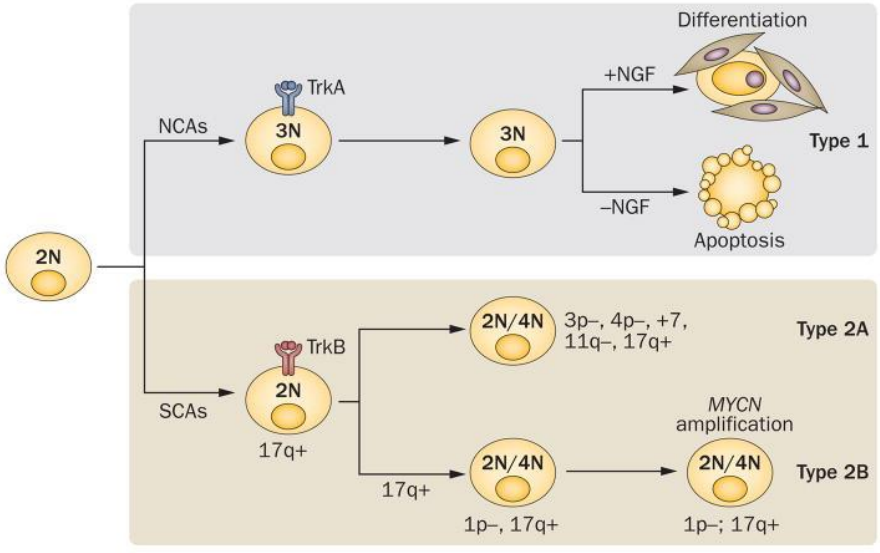

Figure 2: Genomic model of neuroblastoma development [42].

Based on their molecular features, neuroblastomas can be subdivided into three different types, Type 1, Type 2 and Type 2A. Type 1 neuroblastomas are characterized by numerical chromosomal aberrations (NCAs), near-triploidy and expression of the receptor-tyrosine kinase TrkA/NTRK1. Tumors of this type differentiate in the presence of NGF, undergo apoptosis in its absence and have a favorable outcome. Type 2 tumors show

TrkB/NTRK2 expression and segmental chromosomal aberrations (SCAs), which further subdivide this type into 2A and 2B. Type 2A tumors show loss of 3p, 4p and/or 11q and gain of 17q or chromosome 7. Tumors of the type 2B show 1p depletion and gain of 17q as well as *MYCN* amplification, which makes it the most aggressive and quickly progressing subtype.

Based on these characteristics, neuroblastoma is divided into different subtypes. According to a widely accepted model these different genetic subtypes can arise from a common precursor cell type of the sympatho-adrenal lineage [4]. We have demonstrated in mice that overexpression of *MYCN* or mutated *ALK* is sufficient to induce tumorigenic properties in pluripotent neural crest precursor cells [65]. In human neuroblastoma, it is hypothesized that mitotic dysfunctions give rise to two different subtypes; one presenting with a hyper-diploid or near-triploid karyotype and the other defined by chromosomal aberrations such as loss of 1p or trisomy of chromosome 17q. The first subtype is characterized by numerical chromosomal aberrations (NCAs) and high TrkA/NTRK1 expression. Tumors of this subtype respond well to low-dose chemotherapy or even differentiate and regress without cytotoxic treatment. This can be mimicked *in vitro*, as induction of differentiation in TrkA/NTRK1-expressing neuroblastoma cells could be achieved by ligand-mediated activation of TrkA/NTRK1 [66].

The second subtype is associated with a diploid or tetraploid karyotype involving high genomic instability comprising different distinct segmental chromosomal aberrations (SCAs). This subtype is further divided into two subsets, one of which displays 17q gain and deletion of 11q and 14q (Type 2A), and the other displaying 17q gain coupled with allelic loss of 1p often involving *MYCN* amplification and TrkB/NTRK2 + BDNF expression (Type 2B). Co-expression of TrkB/NTRK2 and its ligand BDNF (brain derived growth factor) is believed to act as an autocrine survival pathway.

2 Trk receptors: physiological role and signaling pathways

2.1 Trk receptors in neuronal development

Trk (tropomyosin receptor kinases) receptors are transmembrane proteins that are critically involved in cell survival and differentiation during neuronal development [67]. They consist of three family members, TrkA/NTRK1, TrkB/NTRK2 and TrkC/NTRK3, which bind to distinct neurotrophin ligands - nerve growth factor (NGF), brain-derived neurotrophic factor (BDNF), and neurotrophin-3 (NT3), respectively - and are characterized by differential structures and functions. Neurotrophins exert distinct functions ranging from differentiation

and neuronal survival to synaptogenesis and activity-dependent forms of synaptic plasticity [68, 69]. While mature neurotrophins preferentially bind to Trk receptors, pro-neurotrophins bind to the p75 neurotrophin receptor ($p75^{NTR}$), which is non-selective and has similar albeit low affinity for all neurotrophins [70, 71]. Unprocessed pro-neurotrophins and neurotrophins exert different functions when binding to different receptors. Binding of mature neurotrophins to Trk receptors activates survival pathways, whereas binding of pro-neurotrophins to $p75^{NTR}$ induces apoptosis [72]. However, TrkA/NTRK1 and TrkC/NTRK3 have also been classified as dependence receptors, since apoptotic signals are induced in the absence of ligand activation [73, 74]. The ability of neurotrophins to induce opposing effects on cell survival have led to the proposal of a 'yin and yang' model [75]. According to this model, binary neurotrophin actions are dependent on proteolytic cleavage of neurotrophins (pro- vs. mature neurotrophins) and the class of receptors (Figure 3).

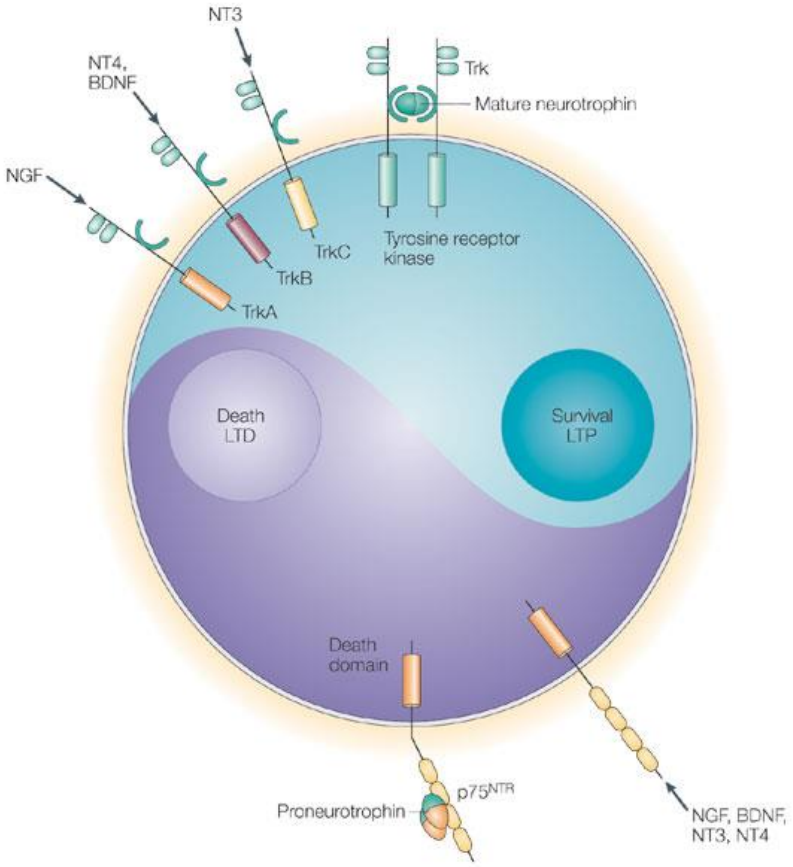

Figure 3: The "yin and yang" model of neurotrophin receptors and neurotrophin function [75].
Neurotrophin-mediated signaling can lead to opposing cellular effects – survival or apoptosis. Binding of immature pro-neurotrophins to $p75^{NTR}$ induces apoptosis (LTD: long-term depression), while activation of a mature neurotrophin to its specific Trk receptor activates survival pathways (LTP: long-term potentiation).

The receptor tyrosine kinase TrkA/NTRK1 is the high-affinity receptor for NGF. Activation of TrkA/NTRK1 by NGF induces recruitment of different proteins to the intracellular domain of TrkA/NTRK1 and leads to the activation of signaling pathways associated with activation of gene expression, proliferation and neuronal growth. Brain-derived growth factor, BDNF, and NT-4 are high and low affinity ligands for TrkB/NTRK2, respectively. TrkB/NTRK2 transduces signaling via PI3K, Ras and PLCγ. Activation of TrkC leads to neurogenesis via binding of NT-3. TrkA/NTRK1 (and TrkC/NTRK3) is implicated in the development of sensory and sympathetic neurons, while TrkB/NTRK2 is important for motor neuron development [67, 76].

The receptors form homodimers upon binding of their respective ligand to the extracellular immunoglobulin G (IgG) domain. This is followed by receptor auto-phosphorylation and subsequent activation of various signaling cascades. As a first step, binding of the adaptor protein Shc (Src homology 2-containing protein) and the effector protein PLCγ1 to the major docking sites (Tyr^{496} in the juxtamembrane region and Tyr^{791} in the tail of the intracellular domain) initiate activation of the PI3K/Akt and Ras/MAPK (mitogen-activated protein kinase) pathways [77]. These pathways can ultimately induce cell survival (PI3K/Akt), or cell survival and differentiation (Ras/MAPK). Conversely, depending on the level of differentiation, inhibition of TrkA/NTRK1 activation or withdrawal of NGF has been shown to induce apoptosis [78].

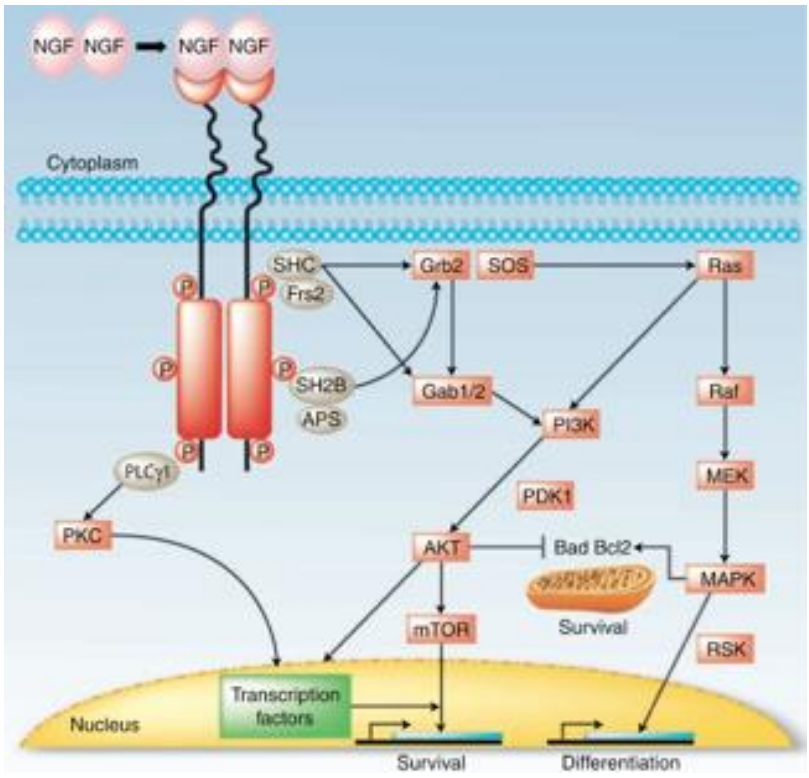

Figure 4: Signal transduction pathway of the TrkA/NTRK1 tyrosine kinase receptor [79].
Binding of the ligand NGF causes receptor homodimerization activating the tyrosine kinase and leading to trans-phosphorylation of at least five tyrosine residues. Auto-phosphorylation serves as docking sites for downstream effectors SHC, SH2B, PLCγ1 on Y490, Y674, and Y785, respectively.

Physiologically, retrograde signaling through internalization of activated TrkA/NTRK1 and axonal transport to nerves has been described to promote neuronal survival *in vitro* and *in vivo* [80-82]. NGF-mediated activation of TrkA/NTRK1 can induce uptake of the ligand-receptor complex via endosomes facilitating the co-transportation of TrkA/NTRK1 and NGF to cell bodies [83-85].

2.2 Trk receptors in cancer biology

NTRK genes are involved in a variety of cancer entities through abnormal gene expression or gene rearrangement. Unfavorable Wilms tumors show *TrkB/NTRK2* over-expression [86], while *TrkC/NTRK3* over-expression is associated with a favorable outcome in medulloblastomas [87]. Abnormal expression of *NTRK* genes is also found in medullary thyroid carcinomas [88], prostate cancers [89, 90], and breast cancers [91, 92]. Papillary thyroid carcinomas frequently show activated TrkA/NTRK1 expression through the formation of chimeric receptor genes with different partner genes. Intra- or inter-chromosomal

rearrangements juxtapose the tyrosine kinase domain of *TrkA/NTRK1* to various genes including *TPM3*, *TPR*, *TFG* and *tropomyosin* [93, 94]. In mesoblastic nephroma and congenital fibrosarcoma a translocation t(12;15)(p13;q25) gives rise to a chimeric TrkC/NTRK3-ETV6 protein [95, 96].

2.3 Trk receptors in neuroblastoma

Trk neurotrophin receptors are major factors in the development as well as the maintenance of the peripheral and central nervous systems. High levels of TrkA/NTRK1 are correlated with a favorable outcome, low stage, young age at diagnosis, genomic integrity, and absence of *MYCN* amplification [63, 97, 98]. On the other hand, expression of TrkB/NTRK2 and its ligand BDNF is associated with an unfavorable prognosis, chromosomal aberrations, and *MYCN* amplification [60, 99].

High levels of TrkA/NTRK1 are also found in tumors of children with low-stage neuroblastoma staged as 4S [63, 97]. These tumors often undergo spontaneous differentiation or regression even without therapy. *In vitro,* neuroblastoma cells with ectopic TrkA/NTRK1 expression undergo neuronal differentiation or die by apoptosis within a week in the presence or absence of NGF, respectively [63, 100]. Spontaneous regression in patients with TrkA/NTRK1-expressing tumors might be caused by the same mechanism of dependence on the expression of NGF. It has been shown that a high amount of Schwann cells in the tumor microenvironment is correlated with enhanced tumor cell differentiation and a favorable outcome [11, 101]. A TrkA/NTRK1-dependent intercellular communication mechanism via NRG1-secretion has recently been shown to attract Schwann cells to the tumor cells, which then produce NGF and induce neuroblastic differentiation [102]. By contrast, invasive potential, metastasis, angiogenesis and drug resistance characterize neuroblastomas with high levels of TrkB/NTRK2 and its ligand BDNF [103]. This autocrine pathway is found in 50-60% of high-risk neuroblastomas [60, 99, 104, 105]. Inhibition of TrkB/NTRK2 induces apoptosis and sensitizes neuroblastoma cells to chemotherapy *in vitro* [106-109].

Taking advantage of the TrkA/NTRK1-mediated induction of apoptosis and tumor regression has become one of the most promising approaches in the induction of neuroblastoma regression. Inhibition of TrkA/NTRK1-signaling through the use of small molecule inhibitors like Lestaurtinib (CEP-107) has been shown to have anti-tumor efficacy on neuroblastoma xenografts [107, 108], but this molecule is not being used in clinical studies. However, new second generation Trk inhibitors are evaluated in phase I clinical trials and could induce

regression in TrkA/NTRK1-expressing tumors, while at the same time inhibiting TrkB/NTRK2-signaling in high-risk TrkB/NTRK2-expressing neuroblastomas [42].

2.4 TrkA and DNA double-strand break repair

A crucial determinant of genomic integrity is the capability of repairing DNA double-strand breaks (DSBs) [110]. Homologous recombination repair (HRR) requires the presence of a sister-chromatid; therefore, this pathway of DSB repair cannot be used during all phases of the cell cycle. Non-homologous end joining (NHEJ), however, ligates broken ends without the requirement for a homologous template, making this repair pathway independent of cell cycle phases. NHEJ is thus considered to be the major DSB repair pathway in mammalian cells [111] (Figure 5).

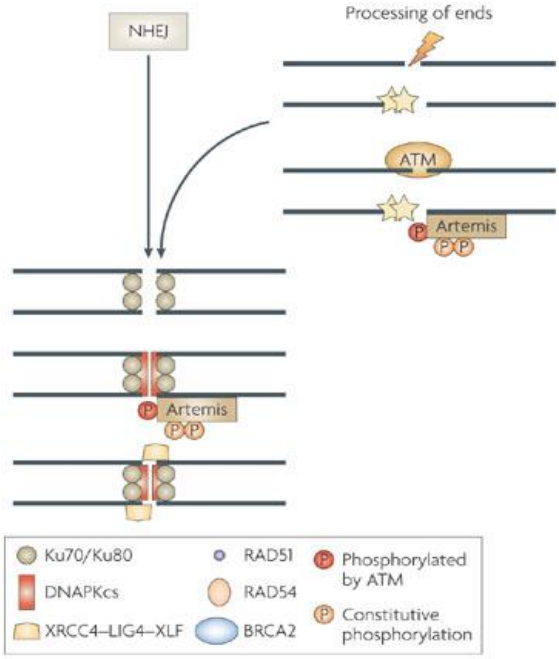

Figure 5: Non-homologous end-joining (NHEJ) (adapted from [112]).

Non-homologous end joining involves a repair machinery consisting of at least six core factors [113]. A Ku70/Ku80 heterodimer binding to double-strand endings recruits DNA-PK_{CS} (DNA-dependent protein kinase catalytic subunit). This induces the formation of the DNA-PK-Artemis-complex by binding of the Artemis endonuclease to DNA-PK_{CS}, activating its kinase activity in the process. Following the processing of the DSB ends, a second complex (XRCC4-LIG4-XLF-PAXX [114]), which executes final rejoining steps, is recruited by DNA-PK-Artemis [115].

Classical NHEJ (c-NHEJ) joins DNA ends without a mechanism ensuring the correct restoration of the damaged sequence, which makes this repair pathway error-prone and associated with nucleotide exchanges, sequence alterations and base pair addition or deletion [116]. Moreover, NHEJ might lead to the joining of ends of different origin, manifesting in the formation of chromosomal translocations. However, the classical NHEJ has been shown to have a crucial role in the suppression of translocation [117]. Recently, an alternative pathway to c-NHEJ and HRR has been proposed as a backup mechanism to the aforementioned mechanisms [118-120]. The alternative end joining pathway (A-EJ) functions throughout the cell cycle, like c-NHEJ, but is functionally enhanced in S- and G_2-phases [121-123]. A-EJ has a higher probability of chromosomal translocations and other sequence alterations [124].

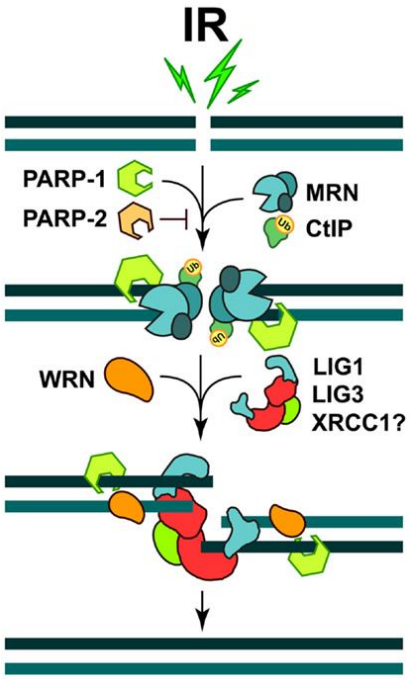

Figure 6: Repair of DSBs by alternative end joining (A-EJ), adapted from [125].
Factors involved in the A-EJ pathway are PARP-1, PARP-2, MRN and CtIP. Either Ligase 1 or 3 (LIG1, 3) mediates the ligation of ends after processing is complete. Since A-EJ is a backup-mechanism and is initiated only after failure of c-NHEJ or HRR, repair by A-EJ might start at any point during repair, depending on where the classical pathways failed.

High expression of the neurotrophin receptor TrkA/NTRK1 is a feature of favorable neuroblastomas and correlates with a lack of chromosomal changes [63]. Contrastingly, high expression of TrkB/NTRK2 is found in unfavorable, aggressive neuroblastomas and is associated with genomic instability [60]. Previous experiments in our research group have

shown that stably TrkA/NTRK1-expressing neuroblastoma cells (SY5Y-TrkA) show alterations in the expression pattern of factors associated with non-homologous end joining. Specifically, gene expression analyses (Affymetrix U95A microarray chips) of DNA repair-factors revealed an up-regulation of *XRCC4* in stably TrkA/NTRK1-expressing SY5Y cells [126] (Figure 7).

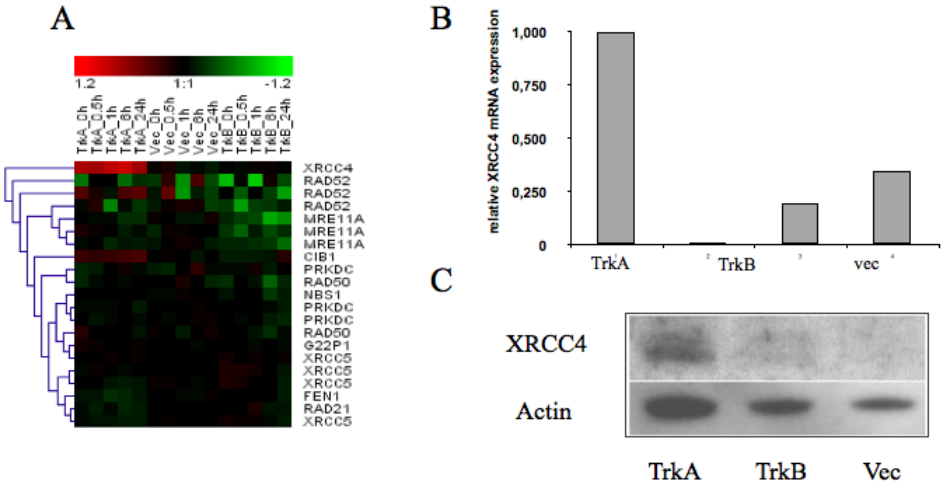

Figure 7: Up-regulation of the NHEJ-factor XRCC4 in stably TrkA/NTRK1-expressing SY5Y neuroblastoma cells (adapted from [126]).

Microarray analysis of expression levels of DNA-repair factors show up-regulation of *XRCC4* in TrkA/NTRK1-expressing SY5Y cells compared to TrkB/NTRK2-positive cells and the vector control SY5Y-Vec (A). Analyses of the relative *XRCC4* expression levels confirmed *XRCC4*-upregulation on the mRNA- (B) as well as on the protein level (C).

Analyses of primary neuroblastomas additionally showed enhanced XRCC4 expression in tumors with high TrkA/NTRK1 levels. A differential effect of TrkA/NTRK1 on NHEJ-mediated DNA repair capacity in comparison to TrkA/NTRK1-negative neuroblastoma cells could be reverted by knockdown of *XRCC4* suggesting an effect of TrkA/NTRK1-signaling on the DNA damage response [126].

2.5 Molecular determinants in the DDR following ionizing radiation

Induction of DNA double-strand breaks by ionizing irradiation (IR) triggers a DNA damage response (DDR) consisting of signal transduction pathways regulating DNA repair and cell cycle control. The first step in the DNA damage response is the activation of the Mre11-Rad50-NBS1 (MRN) complex [127, 128], which acts as an initial DNA damage sensor and activates ATM (Ataxia Telangiectasia Mutated) [129] (Figure 8).

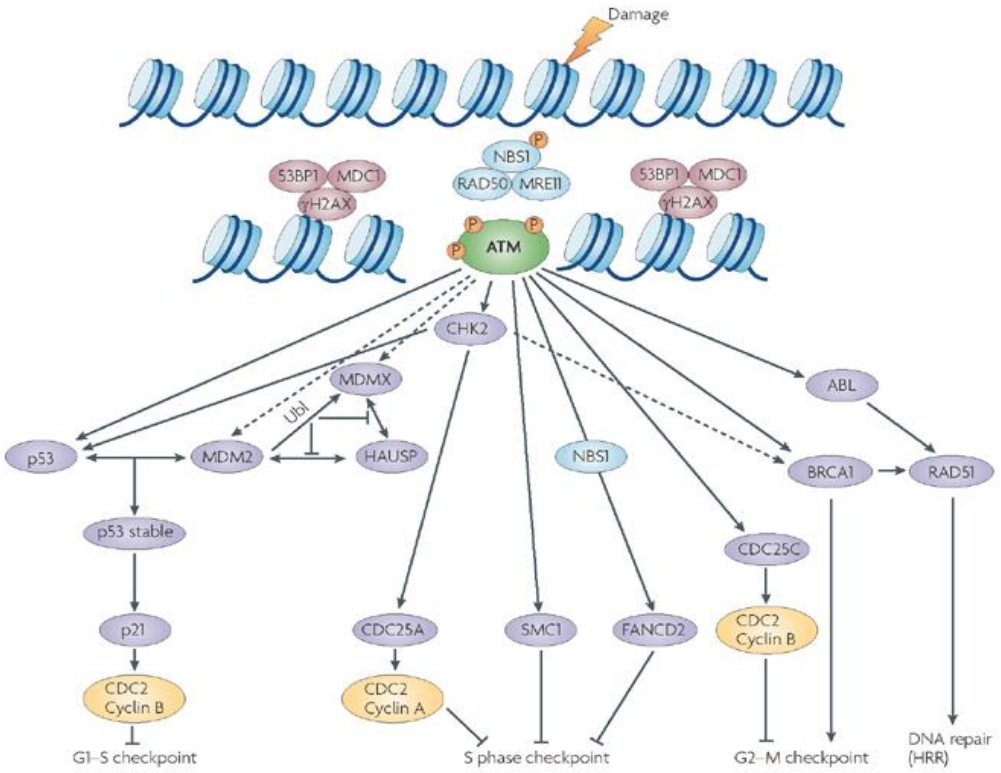

Figure 8: ATM activation and signalling to downstream substrates in response to DNA double-strand breaks [130].

Ataxia-telangiectasia mutated (ATM) is activated by DNA damaging agents such as ionizing radiation (IR) and results in the activation of the MRE11-RAD50-NBS1 (MRN) complex. Phosphorylation of a number of downstream substrates contributes to the control of checkpoints including the G_1-S checkpoint to ensure tight regulation. This is also true for both the intra-S phase and G_2-M phase checkpoint control. Many players in different pathways are involved to achieve efficient checkpoint control.

ATM subsequently phosphorylates S-139 at the C-terminus of H2AX, a modified form of histone 2A, producing γH2AX [131]. γH2AX recruits the mediator protein MDC1 (Mediator of DNA damage checkpoint 1) by binding to its BRCT domains [132]. The formation of a complex consisting of MDC1, H2AX and 53BP1 is thought to mainly function in the amplification of the ATM signal [133]. MDC1 binds to the FHA-domain of NBS1 recruiting the MRN complex to γH2AX-bound DSBs possibly resulting in the retention of ATM at the double strand-break [134].

Signaling to the checkpoint machinery is mainly achieved via the transducer kinases Chk1 and Chk2 [135, 136]. Chk1 and Chk2 interact with cyclin-dependent kinases (Cdks) controlling cell cycle progression in the case of DNA damage or a lack of chromosomal integrity. However, signaling pathways leading to checkpoint arrests strongly depend on the phase of the cell cycle in which DSBs occur. In cells that undergo irradiation while in G_1-

phase, the G_1/S-checkpoint arrest is achieved by ATM activation and subsequent Chk2/p53 activation [137, 138]. Due to the presence of a replication fork, ionizing radiation in S-phase can additionally lead to the activation of ATR [139]. ATR (Rad3 related) is then involved in the phosphorylation and activation of Chk1, while Chk2 activation is achieved via ATM [140]. In G_2 phase, cell cycle checkpoint arrest following IR is mainly ATM-dependent [141].

2.6 Cellular systems for ectopic expression of TrkA/NTRK1

The Trk-negative neuroblastoma cell line SY5Y was previously stably transfected with either human *TrkA/NTRK1* cDNA, human *TrkB/NTRK2* cDNA or the empty pLNCX vector to be used in the analyses of DSB repair factor expression [126].

The cellular SY5Y Trk-system generated in our lab displays the same characteristics associated with TrkA/NTRK1- or TrkB/NTRK2-expression upon ligand stimulation previously described in primary neuroblastomas [142] (Figure 9).

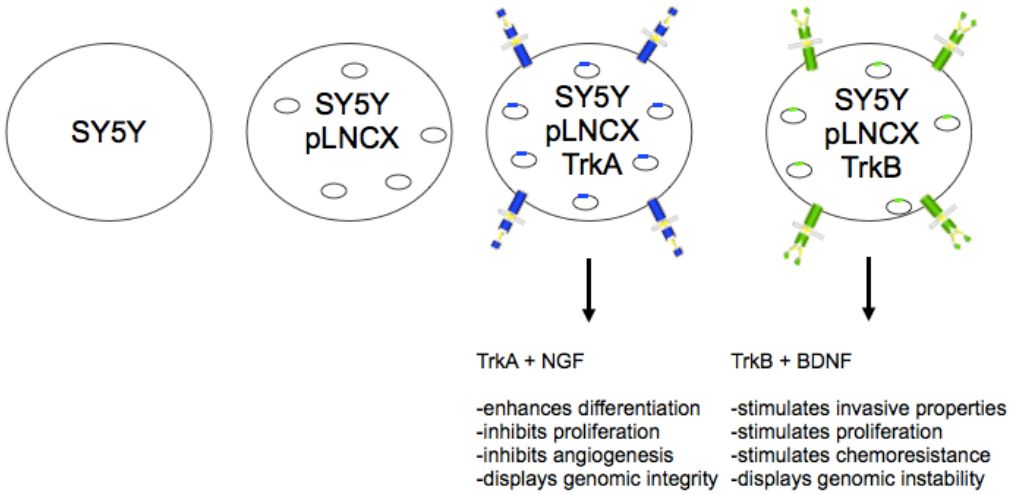

Figure 9: Stably Trk/NTRK-expressing SY5Y-transfectants mirror *in vivo* characteristics of the respective subgroup of primary neuroblastoma.

The neuroblastoma cell line SY5Y was stably transfected with human *TrkA/NTRK1*- or *TrkB/NTRK2*-cDNA in order to study the effects of Trk/NTRK receptor signaling. TrkA/NTRK1-expressing SY5Y cells displayed inhibition of proliferation and angiogenesis, enhanced differentiation and genomic integrity. Contrastingly, TrkB/NTRK2-expression was associated with stimulation of invasive properties, proliferation and chemoresistance and displayed genomic instability.

Trk/NTRK receptor activation by NGF in TrkA/NTRK1-expressing SY5Y cells resulted in cell differentiation. Consistent with this phenotype gene expression profiling of SY5Y-TrkA cells revealed up-regulation of differentiation related factors, pro-apoptotic proteins and angiogenesis inhibitors. By contrast, SY5Y-TrkB cells displayed up-regulation of genes associated with invasion- and therapy resistance upon stimulation with BDNF [142].

A limitation of this model is that high ectopic TrkA/NTRK1-expression in SY5Y-TrkA cells results in auto-phosphorylation and auto-activation of TrkA/NTRK1. Over time the induction of pro-differentiation programs by TrkA/NTRK1 expression culminates in counter-selection processes and presents as a severe limitation of cellular systems with stable TrkA/NTRK1-expression. A resistance mechanism evolved in bacteria is used to create a switch controlling the expression of a specific target gene [143]. The generation of a fusion protein of the Tet Repressor DNA binding protein (TetR) and the transactivating domain of VP16 from the Herpes simplex virus creates a reverse tetracycline-controlled transactivator (rtTA). Binding of the rtTA to the tet Operon (*tetO*) sequence is only possible through a conformational change induced by tetracycline, which activates transcription of the target gene [144]. Tetracycline-conditional expression of *TrkA/NTRK1* in neuroblastoma cells is thus possible in SY5Y-TR TrkA, IMR5-TR TrkA (generated by Dr. rer. nat. Sven Lindner, Group of Prof. Dr. J. H. Schulte), and NGP-TR TrkA (generated as part of this project).

3 The MYC protein family

3.1 The MYC oncogene

The MYC protein plays a role in cell growth, proliferation, stem cells, and in the tumorigenesis of different human cancers [10, 145-147]. The MYC family of transcription factors includes c-MYC (commonly referred to as MYC), MYCN and LMYC all of which are characterized by a basic helix-loop-helix (bHLH) domain. While expression of MYCN is restricted to the nervous system, MYCN was able to substitute for c-MYC in murine development [148]. LMYC function is not as well understood, but elevated levels and LMYC polymorphisms have been associated with lung cancers [149]. Aberrant MYC expression is sufficient to induce tumorigenesis in several different transgenic mouse tissues [150-152]. Regression of tumors in mouse models with inducible MYC-expression upon MYC-withdrawal suggests a role for MYC in tumor maintenance in addition to tumor initiation [153]. A role of MYC in the epithelial-mesenchymal-transition (EMT) and metastasis has

been observed through the regulation of miR-9, which exerts its function on the cell adhesion protein E-Cadherin, and through the transactivation of Bmi-1, which plays a role in EMT [154, 155]. Moreover, a role of MYC in genomic instability of cancer cells [156-160] has been suggested through MYC induction of ROS [161-164]. A direct effect of MYC on telomere function and thus genomic instability was suggested in 2005 [165].

MYC expression is tightly regulated on the mRNA- and protein-levels. The transcription of *MYC* is controlled through a number of different transcription factors, i.e. CNBP, FBP, TCF [166]. Additionally, the short-lived *MYC* mRNA can be translationally modulated by miRNAs let-7, miR-34, and miR-145 [167-170]. Post-translational modification of MYC protein through phosphorylation at Ser-62 and Thr-58 leads to proteasomal degradation, which leads to a half-life of 15-20 minutes [171-175]. Mutations in the aforementioned phosphorylation sites are observed in Burkitt's lymphoma and result in a stabilized protein contributing to tumorigenesis [173, 174, 176].

MYC regulates transcription of genes through binding to a DNA binding motif known as the MYC E-box with the sequence 5'-CACGTG-3' [177]. Stimulation of proliferation leads to increasing MYC levels and occupation of E-boxes. However, genome wide mapping of MYC binding sites have found that MYC targets require additional factors, like E2F, for their expression [178].

3.2 MYCN in neuroblastoma

MYCN is a member of the MYC oncogene family, which was identified in 1983 and was found to have coding regions homologous to *MYC*, comprising long 5'- and 3'- untranslated regions (UTR) [179, 180], and gene products characterized by conserved regions for protein-protein- and DNA-protein-interactions [181].

MYCN-mediated promotion of cell cycle progression and proliferation through the repression of anti-proliferative factors like Dickkopf-1 and CDKL5 has been described recently [182, 183]. *MYCN* knock-in experiments showed that *MYCN* has the capacity to rescue embryonic lethality in *MYC* knockout mice [148]. Furthermore, compensation of *MYC* and *MYCN* for each other was shown in mouse embryonic stem cells with homozygous deletion for *MYC* or *MYCN* [184-186]. However, a central role for *MYCN* in the development of the central nervous system was shown in *MYCN* null embryos with up-regulation of *MYC*, which showed hindbrain abnormalities [187].

MYCN expression is tissue specific and highest in the kidney, hindbrain, and forebrain of newborn mice. *MYC* expression is more generalized and not restricted to early developmental stages [188].

As reviewed in by Huang and Weiss [189], in neuroblastoma MYCN was found to be down-regulated in differentiating neuroblastoma cells [190-193] and a direct involvement of MYCN in the induction of differentiation pathways and the maintenance of pluripotency was demonstrated [194-198]. *MYCN* amplification is a potent indicator for unfavorable outcome in neuroblastoma patients [61, 145]. Additionally, high *MYCN* levels are strongly associated with invasive behavior and metastasis [199-201]. MYCN has direct effects on adhesion factors by regulation of integrins α1 and β1 [202, 203], in the transcriptional regulation of focal adhesion kinase (FAK) [204], and on miR-9, a micro RNA regulated by MYCN, which promotes EMT by suppressing E-cadherin [154].

A role of MYCN in the immune system of neuroblastoma patients with *MYCN* amplified tumors was shown through the finding of significantly decreased bone marrow natural killer T (NKT) cells compared to patients with tumors without *MYCN* amplification [205]. This is supported by mouse experiments showing an inverse correlation of high MYCN levels with decrease in the ability of NKT cell attraction [205]. Furthermore, amplification of *MYCN* is associated with high vascularity and a loss of the angiogenesis inhibitors Activin A, leukemia inhibitory factor (LIF), and interleukin 6 (IL-6) [206] in response to *MYCN* expression, as well as an induction of the pro-angiogenic factors angiogenin and vascular endothelial growth factor (VEGF) [207] was shown in different studies.

Up-regulation of the pluripotency genes *KLF2*, *KLF4*, and *LIN28B* in response to *MYCN* expression was shown [196] and evidence of a critical role for MYCN in the activation of self-renewal and pluripotency genes and through the inhibition of differentiation pathways [208] has been reported in several studies. Neuroblastomas with *MYCN* amplification are characterized by chemoresistance, which can be explained by the up-regulation of p53 and MDM2 in response to *MYCN*-expression. It has been observed that the response of *MYCN* amplified tumors to chemotherapy is often short-lived and tumors eventually reestablish as therapy-resistant disease [209, 210]. A chemotherapy-induced feed-forward-loop between MYCN and MDM2 through inactivating mutations of p53 has been suggested as the underlying cause for therapy-resistance in *MYCN*-amplified neuroblastomas [189]. Moreover, *NTRK2*-expression has also been associated with therapy-resistance and TrkB/NTRK2 has been shown to be able to up-regulate *MYCN* mRNA [104, 211]. Contrastingly, expression of

NTRK1 is repressed by *MYCN* through the recruitment of HDAC1to the *NTRK1* promotor, resulting in a repressed chromatin state [212].

3.3 MYCN as a therapeutic target

Studies researching therapies for *MYCN*-amplified tumors range from targeting *MYCN* directly by RNA interference and antisense oligonucleotides [195, 213] to targeting *MYCN* mRNA regulators, MYCN protein stability, inducing differentiation or p53-induced apoptosis, and targeting epigenetic reader proteins. Targeting MYCN directly is difficult due to the structure of MYCN consisting of two extended alpha helices and a lack of binding sites for small molecule inhibitors [213].

Induction of differentiation in neuroblastoma has been achieved through the use of retinoic acid, phenylacetate, and nitric oxide [192, 214, 215]. In addition to inducing differentiation, inhibiting anchorage independence and cell growth, MYCN levels were decreased also. Destabilizing MYCN protein through the promotion of MYCN targeting for ubiquitination and degradation by the proteasome [216-218] is attempted through the use of PI3K/mTOR inhibitors blocking a PI3K-induced inhibitory phosphorylation on GSK-3β [219]. Since MYCN silences tumor suppressor genes by recruitment of DNA methyltransferases and up-regulation of HDAC, class I and II HDAC inhibitors like Trichostatin A are evaluated in neuroblastoma mice models and were found to restore the expression of the differentiation factor TG2 [220]. Furthermore, neuroblastoma cell lines harboring a *MYCN*-amplification are more sensitive to MDM2 antagonists (Nutlin-3 and MI63) than *MYCN*-non-amplified cell lines [221]. This might be explained by the ability of MDM2 to bind the 3'UTR of *MYCN* stabilizing its mRNA, and inhibition of MDM2 resulting in destabilization on the mRNA level. BET bromodomain inhibitors like JQ1 are researched in an attempt to interfere with MYCN-mediated promotion of transcription through inhibition of BRD2-4 (members of the bromodomain and extraterminal (BET) subfamily). BRD2-4 are binding partners of chromatin-remodeling complexes (SWI/SNF) and the positive transcriptional elongation factor complex (PTEFB) [222]. JQ1 was shown to increase overall survival in mice and decrease expression of MYCN [223]. A blocking effect on MYC targets and MYC was also demonstrated in the MYC-dependent malignancy multiple myeloma [222].

3.4 TrkA/NTRK1 and MYCN are crucial determinants of neuroblastoma prognosis

A substantial number of NBs carry *MYCN* amplification and this is inversely correlated to TrkA/NTRK1 expression (Figure 10). While *MYCN* amplification is the most powerful single indicator of poor outcome in neuroblastoma, high expression of TrkA/NTRK1 characterizes the patient group with excellent outcome.

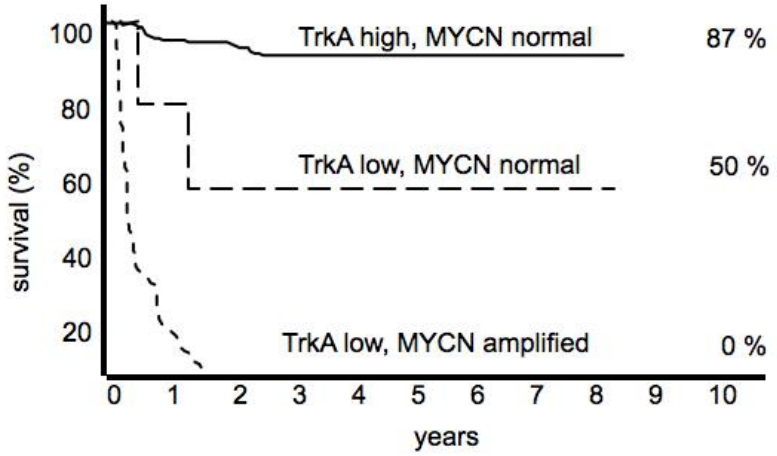

Figure 10: Expression of TrkA/NTRK1 strongly correlates with the five-year cumulative-suvival rate.
High expression of TrkA/NTRK1 in the absence of *MYCN* amplification leads to a cumulative 5-year survival of 87% (n = 62). Tumors with normal MYCN copy number and low levels of TrkA/NTRK1 expression (n=4) are associated with a significantly worse survival of only 50% (p= 0.03) compared to the group with high TrkA/NTRK1 expression. Most patients with tumors that showed MYCN amplification and low TrkA/NTRK1 levels died within two years (adapted from Yamashiro et al., 1997 [224]).

MYCN also has a causative role in neuroblastoma tumorigenesis as demonstrated in both mice and zebrafish [225, 226]. These intriguing observations have motivated many research groups to investigate down-stream effectors of MYCN and TrkA/NTRK1 and to define therapeutic applications from those results. Among other key features, MYCN has been involved in protein synthesis [227] and progression through the cell cycle [228]. While MYCN itself is a poor drug target, inhibition of MYCN interaction partners such as Aurora A or even transcriptional regulators of *MYCN*, most prominently Brd4, showed promising results in preclinical models of MYCN-dependent neuroblastoma [223, 229]. Thus, indirect interference with MYCN functions is a promising approach for the most aggressive subtype of neuroblastoma.

On the other end of the clinical spectrum, high levels of TrkA/NTRK1 expression are found in differentiating tumors with excellent patient prognosis. Functional links between TrkA/NTRK1 expression, differentiation and inhibition of angiogenesis *in vitro* have been demonstrated by different research groups [230, 231]. Moreover, TrkA/NTRK1 expression potentially contributes to suppression of the tumor immune escape [232]. Most recently, we suggested that TrkA/NTRK1-mediated tumor-host interaction could account for the more benign phenotype of low-stage neuroblastomas in a combined *in vitro/ in vivo* approach [102]. Taken together, TrkA/NTRK1 expression contributes to a less aggressive phenotype of NB at various functional levels.

The interplay of MYCN and TrkA/NTRK1 is best understood in one direction only: MYCN can negatively regulate TrkA/NTRK1 functions by transcriptional repression of the *NTRK1/TrkA* promotor in cooperation with HDACs and Miz-1 [212]. Interestingly, little is known how TrkA/NTRK1 signaling might in turn regulate MYCN.

3.5 Down-stream factors of TrkA/NTRK1 in MYCN biology

Down-stream signaling pathways of TrkA/NTRK1 in neuroblastoma cells have been analyzed using high-throughput profiling techniques on the mRNA and protein levels [231, 233]. It has been proposed that TrkA/NTRK1 controls differentiation via the RAS/MAPK/ERK pathway, while the PI3K/ Akt pathway was reportedly crucial in mediating survival [234] reviewed in Schramm et al., Cancer Lett, 2005).

In general, oncogenic activation of receptor tyrosine kinases (RTKs) is discussed as a mechanism to stabilize MYCN by PI3K / Akt signaling involving the mTOR complex as well as GSK3β (glycogen synthase 3β, reviewed in [235] and [236]). Akt inactivates GSK3β by phosphorylation and thus prevents MYCN phosphorylation at T58, which is a signal for subsequent proteasomal degradation of MYCN [237]. Recently, an examination of signaling pathways downstream of PI3K / Akt in head and neck cancers by Shigeishi et al. [238] interestingly revealed an inhibitory function of CD44 to prevent phosphorylation of GSK3β. They demonstrated that active GSK3β was associated with reduced expression of stem cell markers Oct4, Sox2, and Nanog, and an induction of the differentiation factors Calgranulin B and Involucrin. In neuroblastoma cells, Duffy et al. presented evidence that GSK3β may additionally mediate regulation of *MYCN* mRNA levels. Inhibition of GSK3β by BIO-acetoxime or LiCl reduced cell viability by destabilization of *MYCN* mRNA even in cell lines derived from high-risk *MYCN*-amplified tumors [239].

4 Goals of the project

This project aimed to evaluate the effects of short-term *TrkA/NTRK1* expression in neuroblastoma cells with respect to DNA damage repair and to interaction with the *MYCN* oncogene. Previously published results showing a higher DNA repair capacity of TrkA/NTRK1-over-expressing cell lines via the up-regulation of XRCC4 [126] provided the basis for the analyses of the effects of short-term TrkA/NTRK1 signaling on the DNA repair capacity of neuroblastoma cells after ionizing radiation. Specifically, we were interested in the effect of *TrkA/NTRK1*-expression on DNA repair kinetics and dose response after irradiation with X-rays. How does *TrkA/NTRK1*-expression contribute to the DNA damage response? Does TrkA/NTRK1-signaling result in the up-regulation of DSB repair factors in NHEJ, A-EJ or HRR? Does active TrkA/NTRK1 in neuroblastoma cell lines alter checkpoint activation in response to ionizing radiation? How does inhibition of repair mediators influence cell viability in correlation with TrkA/NTRK1?

The mutually exclusive expression of TrkA/NTRK1 and MYCN in neuroblastoma, which result in striking differences in patient outcome, motivated us to investigate the interaction of TrkA/NTRK1 and MYCN on the molecular level. Gene expression analysis was employed to identify other factors correlated with TrkA/NTRK1- and anti-correlated with MYCN expression in primary neuroblastomas. Thereby, the cell surface glycoprotein CD44 was identified to be associated with TrkA/NTRK1-expression, and anti-correlated with high MYCN levels. The possibility of a central role for TrkA/NTRK1 signaling pathways and CD44 expression affecting MYCN levels was sought to be analyzed in *MYCN*-amplified and –non-amplified neuroblastoma cell lines.

The following questions should be addressed: What is the phenotype of MYCN-amplified cell lines following ectopic expression of TrkA/NTRK1? Does TrkA/NTRK1 have an effect on protein levels of MYCN protein in *MYCN*-amplified cell lines? How does TrkA/NTRK1 confer its effect on MYCN in terms of signaling pathways?

Materials and Methods

5 Materials

5.1 Chemicals, solutions and enzymes

Chemicals were obtained from Carl Roth or Sigma-Aldrich, unless indicated otherwise.

Table 2: Chemicals

Product	**Company**
2-Mercaptoethanol	Sigma Aldrich
4,6 diamidino-2-phenylindole (DAPI)	Roth
Aqua ad iniectabilia	B. Braun
Blasticidine	Invitrogen
Bromphenole blue	Serva
Colcemid (L-6221)	Biochrom AG
Coomassie Brilliant Blue R 250	Serva
Complete Protease Inhibitor Cocktail	Roche
Crystal Violet	AppliChem
ECL Prime	GE Healthcare
Entellan	Merck
Ethanol	Riedel-de Haën®
Ethidium Bromide	Roth
FCS	PAA Laboratories GmbH, PAN Biotech
G418	Roth
Giemsa stain	Carl Roth GmbH & Co.
Glacial Acetic Acid	Carl Roth GmbH & Co.
Glycine	Sigma Aldrich
HCl	Roth
Human β-NGF	R&D Systems
InCert Agarose	Biorad
Isopropanol	Sigma Aldrich
Isotone	Beckman Coulter
Methanol	Sigma Aldrich
Milk Powder	Roth
Mowiol 4-88	Roth
MyTaq HS Red Mix	Bioline

NaOH	Roth
Nitrocellulose Protran®	Whatman GmbH
NP-40	Fluka
Orange G	Chroma-Gesellschaft
Paraformaldehyd 4,5%	Morphisto
PBS (Phosphate Buffered Saline) (1x & 10x)	Gibco
Penicillin/ Streptomycin	Gibco
peqGold Universal Agarose	PeqLab
Ponceau S	Serva
RLT-Puffer	Qiagen
RPMI1640	Gibco
SeaKem LE Agarose	Lonza
SDS (Sodium Dodecyl Sulfate)	Gerbu
Sorenson's buffer (10582–013)	Gibco, Invitrogen
TEMED (N,N,N',N'-Tetramethylethylendiamin)	Serva
Tetracycline	Sigma Aldrich
Tris	Roth
Tris-HCl	Roth
Tritan x-100	Merck Millipore
Trypsin/ EDTA (0,05%)	Gibco
Tween20	Roth
Whatman Paper	Whatman GmbH

5.2 Buffers and media

Table 3: Buffers and media

Buffer	**Components**
Blocking Buffer (Western Blot)	5 % milk powder in TBS Buffer
Blocking Buffer (Immunohistochemistry)	3% BSA and 0.2 M Glycine in PBS
DNA-sample buffer (5x)	5 ml Glycerine + 0.2 ml 50x TAE + 0.01 g Orange G, ad 10 ml H_2O
FACS Buffer	1 x PBS + 2 % (v/v) FCS + 2 mM EDTA
Laemmli Buffer	1 % Bromophenole blue + 10 % Glycerine + 2 % SDS + 50 mM Tris-HCl (pH 6.8) + 10 % 2-Mercaptoethanol

PBS	136 mM NaCl + 2.68 mM KCl + 8.09 mM Na_2HPO_4 * $2H_2O$ + 1.47 mM KH_2PO_4
Ponceau S	1 % Ponceau S in 5 % acetic acid
Ripa Buffer	50 mM Tris-HCl (pH 7.4) + 150 mM NaCl + 0.1% SDS + 1% NP-40 + 1% TritonX-100 + Protease Inhibitor Cocktail
RPMIcomplete	RPMI1640 + 10 % FCS + 100 U/ml Penicillin + 0,1 mg/ml Streptomycine
Running Buffer (10x)	250 mM Tris + 1,92 M Glycine + 1 % SDS
Running Gel Buffer (4x) (pH 8,8)	1.5 M + 0.4 % SDS, ad 500 ml H_2O
TBS Buffer (10x)	0.5 M Tris-HCl + 1.5 M NaCl, pH adjusted to 7.5 with HCl
Transfer Buffer (10x)	250 mM Tris + 1.92 M Glycine, adjust pH to 8.3 with HCl
Stacking Gel Buffer (4x) (pH 6.8)	0.5 M Tris + 0.4% SDS, ad 250 ml H_2O
Washing Buffer (Western Blot)	0.1 % Tween20 in 1x TBS

5.3 Enzymes and commercially available kits

Table 4: Enzymes and commercially available kits

Kit	**Company**
Amersham™ ECL Prime Western Blotting Detection Reagent	GE Healthcare
Cell Proliferation ELISA, BrdU (colorimetric)	Roche
High Pure RNA Isolation Kit	Roche
Proteinase K	Fluka
RNAse A	TaKaRa
RNAse H	New England BioLabs
RNeasy Mini Kit	Qiagen
Transcriptor First Strand cDNA Synthesis Kit	Roche

5.4 SDS PAGE

Table 5: Running gel

Gel Concentration	10 %	12 %
Aqua dest (ml)	8.4	7
Acrylamid (30%) (ml)	6.6	8
Running Gel Buffer	5	5
Ammoniumpersulfate (10%) (µl)	200	200
TEMED (µl)	20	20

Table 6: Stacking gel

Gel Concentration	4 %
Aqua dest (ml)	2.48
Acrylamid (30%) (ml)	0.52
Stacking Gel Buffer	1
Ammoniumpersulfate (10 %) (µl)	40
TEMED (µl)	4

5.5 Immunohistochemical detection of CD44

Table 7: Solutions for IHC detection of CD44

Solution	**Components**
Fixing solution	4% paraformaldehyde in PBS
Blocking solution	3% BSA and 0.2 M Glycine in PBS
DAPI staining solution	250 ng/ml 4,6 diamidino-2-phenylindole in PBS

5.6 Pulsed-field gel electrophoresis (PFGE)

Table 8: Buffers for PFGE

Buffer	**Components**
Lysis Buffer	10 mM Tris, 100 mM EDTA, 50 mM NaCl, 2% *N*-laurylsarcosine, 0.2 mg/ml Protease
Washing Buffer	10 mM Tris, 100 mM EDTA, 50 mM NaCl
0.5×TBE	45 mM Tris, pH 8.2, 45 mM boric acid, 1 mM EDTA

5.7 Proliferation assays

Table 9: Buffers used in proliferation assays

Solution	**Components**
Staining Solution for clonogenic assays	1% Crystal violet in 70% Ethanol
MTT Solution	0.18 mM MTT in PBS
MTT Solubilization Solution	10% Triton-X, 90% Isopropanol, 0.8% HCL 37%

5.8 DNA Repair assays

5.8.1 53BP1-assay

Table 10: Solutions and buffers used in γH2AX-assay and 53BP1-assay

Solution	**Components**
Fixing agent	4% paraformaldehyde in PBS
Permeabilization	0.2% Triton + 1% BSA in PBS
Blocking Buffer	3% BSA and 0.2 M Glycine in PBS
Washing Buffer I	PBS with 1% BSA
Antibody Buffer I	% BSA + 0.5% Tween20 in PBS
Antibody Buffer II	0.5% goat serum in PBS
Washing Buffer II	1% BSA + 0.5% Tween20 in PBS
DAPI Staining Solution	250 ng/ml 4,6 diamidino-2-phenylindole (DAPI) in PBS

5.8.2 Chromosome translocation assay

Table 11: Solutions and buffers used in translocation assay

Solution	Components
Carnoy's Fixative	75% Methanol, 25% glacial acetic acid
Staining solution	2.5 ml Giemsa stain in 50 ml Sorenson' s Buffer

5.9 Oligonucleotides for quantitative real-time PCR

Table 12: Primer for quantitative real-time PCR

Oligonucleotide	Primersequence 5' → 3' or Order No.
CD44 sen	QT00073549 (Qiagen)
CD44 rev	
GAPDH sen	CCACCCATGGCAAATTCCATGGCA
GAPDH rev	TCTAGACGGCAGGTCAGGTCCACC
MYCN sen	QT00201404 (Qiagen)
MYCN rev	
TrkA codop sen	TCGAAAATCAGCAGCACC
TrkA codop rev	GCCACAAATCTCAGTCCA

5.10 Antibodies

5.10.1 Antibodies for western blot

Table 13: Primary antibodies for WB

Antibody	Source	Dilution	Manufacturer
Actin	Mouse	1:5000	Sigma Aldrich
AKT	Rabbit	1:1000	Cell Signaling
p-AKT	Rabbit	1:1000	Cell Signaling
Caspase 3	Rabbit	1:1000	Cell Signaling
CD44	Mouse	1:1000	Cell Signaling
Chk1	Rabbit	1:1000	Cell Signaling
p-Chk1	Rabbit	1:1000	Cell Signaling
GAPDH	Mouse	1:2000	Millipore
γ-H2AX	Mouse	1:200	Upstate
Ku70	Rabbit	1:1000	Cell Signaling
Ku80	Rabbit	1:1000	Cell Signaling
Mre11	Rabbit	1:1000	Cell Signaling
N-Myc	Rabbit	1:1000	Cell Signaling
PARP1	Mouse	1:1000	Santa Cruz
p21	Rabbit	1:1000	Cell Signaling
TrkA	Rabbit	1:1000	Cell Signaling
p-TrkA	Rabbit	1:1000	Cell Signaling
WRN	Mouse	1:1000	Cell signaling
XRCC1	Rabbit	1:1000	Cell Signaling
XRCC4	Rabbit	1:1000	AbD Serotec

Table 14: Secondary antibodies for WB

Antibody	Source	Dilution	Manufacturer
α-rabbit HRP-conjugated	goat	1:5000	GE Healthcare
α -mouse HRP-conjugated	goat	1:5000	GE Healthcare

5.10.2 Antibodies for immunological methods

Table 15: Primary antibodies for FACS

Epitope	Fluorophore	Clone	Manufacturer
CD44	PE	G44-26	BD Pharmingen™
H3pS10	none	n/a	Abcam

Fluorochrome	Abbreviation	Absorption (nm)	Emission (nm)
R-Phycoerythrin	PE	488	575

Table 16: Secondary antibodies for FACS

Epitope	Fluorophore	Manufacturer	Dilution
Rabbit	Alexa-Fluor® 488	Life Technologies	1:2000

5.10.3 Antibodies for immunohistochemical methods

Table 17: Primary antibodies for IHC

Epitope	Source	Clone	Manufacturer	Dilution
CD44	Mouse	156-3C11	Cell Signaling	1:50
53BP1	Rabbit	n/a	Cell Signaling	1:100

Table 18: Secondary antibodies for IHC

Epitope	Fluorophore	Manufacturer	Dilution
Rabbit	Alexa-Fluor® 488	Life Technologies	1:2000

5.11 Size and molecular weight-markers

5.11.1 DNA Size marker

100 bp DNA ladder (Invitrogen)
GeneRuler 1 kb DNA Ladder (Fermentas)

5.11.2 Protein molecular weight marker

Precision Plus Protein™ Kaleidoscope™ Standards (Biorad)

5.12 Cell lines

Three different neuroblastoma cell lines were used in this project.

(1) SH-SY5Y – Human neuroblastoma cell line originating from the bone marrow of a 4-year-old female child. This cell line does not show endogenous Trk/NTRK-receptor expression, which is why it was used for transfection with a vector with conditional Trk/NTRK-expression to study its immediate and long-term effects on neuroblastoma cells.
(2) IMR5 – Human neuroblastoma cell line. This cell line was chosen to study the interplay of TrkA/NTRK1-signaling and high MYCN expression, since this cell line carries a *MYCN* amplification.
(3) NGP – Human neuroblastoma cell line originating from lung metastases of a 2 ½-year-old male child. This cell line also carries a *MYCN* amplification and was therefore chosen for transfection with a vector for conditional TrkA/NTRK1-expression to study the interaction of TrkA/NTRK1 and MYCN.

The human neuroblastoma cell lines SH-SY5Y (SY5Y) and IMR5 were used to generate a tet-conditional TrkA/NTRK1 expressing cellular systems [232]. Human *TrkA/NTRK1* cDNA was cloned into the pT-Rex-DEST30 vector (Invitrogen, Carlsbad, CA) by electroporation.

Cells were then transfected with the vector carrying the tetracycline repressor gene, pcDNA6/TR (Invitrogen). Single-clones were selected by limiting dilution in blasticidine- and G418-containing medium.

As part of this PhD-project, a TrkA/NTRK1-inducible cell line of the human neuroblastoma cell line NGP was generated in the same manner.

5.13 Plasmids

The Gateway® pT-Rex™-DEST30 Vector system was used to create all the above-mentioned cell lines with tetracycline-inducible *TrkA/NTRK1*-expression. The pcDNA^{TM}6/TR was used to transfect cells with the tetracycline repressor gene.

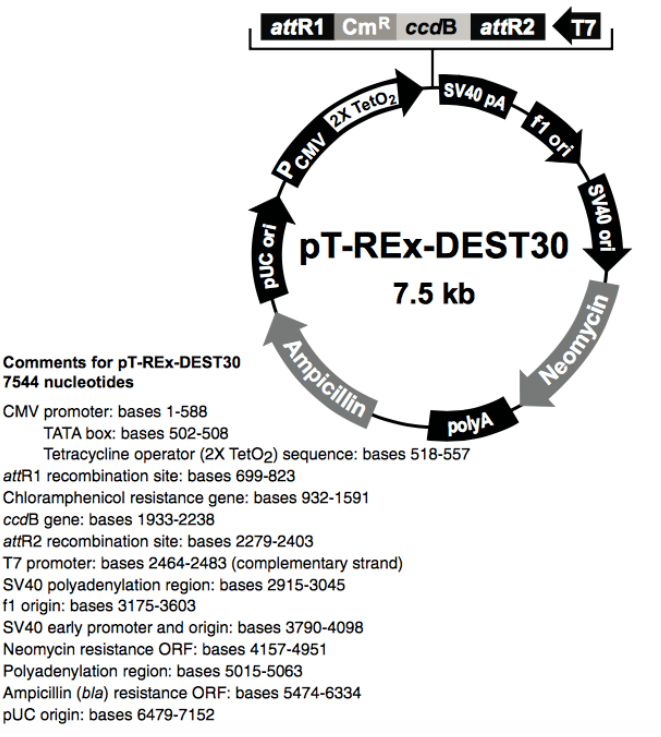

Figure 13: The pT-REx-DEST30 vector used in the generation of cell lines with tetracycline-inducible TrkA Expression.

(adapted from https://tools.lifetechnologies.com/content/sfs/manuals/ptrexdest_man.pdf)

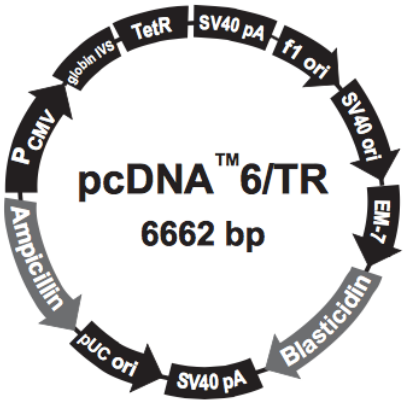

Comments for pcDNA™6/TR
6662 nucleotides

CMV promoter: bases 232-819
Rabbit β-globin intron II (IVS): bases 1028-1600
TetR gene: bases 1684-2340
SV40 early polyadenylation sequence: bases 2346-2477
f1 origin: bases 2897-3325
SV40 promoter and origin: bases 3335-3675
EM-7 promoter: bases 3715-3781
Blasticidin resistance gene: bases 3782-4180
SV40 early polyadenylation sequence: bases 4338-4468
pUC origin: bases 4851-5521
bla promoter: bases 6521-6625 (complementary strand)
Ampicillin (*bla*) resistance gene: bases 5666-6526 (complementary strand)

Figure 14: The pcDNATM6/TR vector carrying the tetracycline repressor gene.
(adapted from https://tools.lifetechnologies.com/content/sfs/manuals/pcdna6tr_man.pdf)

5.14 Instruments

Table 19: Instruments

Instrument	**Company**
Allegra™ X-22R Centrifuge	Beckman Coulter
Axioplan	Zeiss
BioDocAnalyze	Biometra
Blockthermostat TCR 100	Carl Roth
C1000® Thermal Cycler	BioRad
Centrifuge 5415C	Eppendorf
Centrifuge 5415D	Eppendorf
Cytomics FC500 CXP	Beckmann Coulter
EL800 Universal Micorplate Reader	Bio-Tek Instruments
Fluorimager Typhoon	GE-Healthcare
Gel Chamber	PeqLab

HERAcell 150i	Thermo Scientific
HERAsafe	Heraeus Instruments
Incubator	Heraeus Instruments
MicroPorator	Peqlab
Microscop (Motic AE31)	Motic
Mini-PROTEAN Tetra Cell, Biorad	Biorad
Mini Trans-Blot Cell	Biorad
NanoDrop ND-1000 Spectrophotometer	Peqlab
pH-Meter	WTW
PowerPac200 Power Supply	BioRad
Shaker	Köttermann
StepOnePlus™ Real-Time PCR System	Applied Biosystems
UviChemi Chemiluminescence System	Biometra
UviTec	Biometra
Scale (Explorer)	OHAUS
Waterbath	GFL
XCell SureLock™ Mini-Cell Electrophoresis System	Invitrogen
X-ray machine	GE- Healthcare
Axioplan Microscope	Zeiss
ZI Coulter Particle Counter	Beckmann Coulter

5.15 Consumables

Table 20: Consumables

Product	**Company**
10 cm Cell Culture Dish	Greiner BioOne
60 mm Cell Culture Dish	Greiner BioOne
Cryo Tubes	Carl Roth, Simport
FACS Tubes	Greiner BioOne
Filter Tips	TipOne
Parafilm	Pechinery
Pasteur Pipettes	Brand

PCR Tubes	Axygen
Pipettes (2ml, 5 ml, 10 ml, 25 ml)	Greiner BioOne
Pipette Tips (10 µl, 200 µl, 1000 µl)	Sarstedt
Reaction Tubes (0.2 ml, 0.5ml, 1.5 ml, 2 ml)	Eppendorf
Ritips® (0.5 ml, 2.5ml, 5 ml)	Ritter
Tubes (15 ml, 50 ml)	Greiner BioOne
Cell Culture Flasks (25 cm^2, 75 cm^2, 175 cm^2)	Beyer/Corning
Cell Culture Plates (6-well, 12-well, 24-well, 48-well, 96-well)	Greiner BioOne, Starlab

5.16 Software

Table 21: Software

Software	**Version**
Excel (Mac 2011)	14.1.0
EndNote	X7
FlowJo	vX.0.7
GraphPad Prism	5.0
ImageJ	1.47v
Image-Quant	5.0
Keynote'09	5.1.1
Numbers	3.5.2
Pages	5.5.2
Pixelmator	3.3.1 Limestone
PowerPoint (Mac 2011)	14.1
Word (Mac 2011)	14.1.0

6. Methods

6.1 Cell culture

6.1.1 Cultivation and passaging of cells

The human neuroblastoma cell lines SY5Y, NGP and IMR5 were maintained in sterile conditions in an atmosphere of 5% CO_2 in RPMI1640 supplemented with 10% FCS and 5% Penicillin/ Streptavidin. SY5Y transfectants SY5Y-, NGP- and IMR5-TR were maintained in the same medium with additional supplementation of 7.5 µg/ml Blasticidine. In addition to 7.5 µg/ml Blasticidine, the medium for SY5Y-, NGP- and IMR5-TR TrkA also contained 250 µg/ml G418. Cells were split at 80% confluency by removing the culture medium and washing cells with phosphate buffered saline. Cells were trypsinized with 0.05% Trypsin + 0.02% EDTA for 5 min at 37°C. The proteolytic activity of trypsin detaches cells from the culture dish, while EDTA builds complexes with bivalent cations, interfering with cell-cell-cohesion. Subsequently, cells were pelleted by centrifuging for 5 min at 300x g. The cell pellet was then re-suspended in 1 ml of medium and 500 µl of the cell suspension were added to fresh medium for further cultivation.

6.1.2 Freezing and re-cultivation of cells

Cells were frozen at low passages at a density of 2.5 x 10^6 cells in 1 ml FCS + 10% DMSO. The addition of DMSO prevents the formation of ice crystals and, therefore, cell damage. Cryo tubes were stored in liquid nitrogen until re-cultivation. For reactivation, cells were washed in phosphate buffered saline to remove all DMSO, centrifuged at 300x g for 5 min and seeded in 12 ml of medium.

6.1.3 Cell counting

Cells were harvested by adding trypsin after removing the medium and washing the monolayer in phosphate buffered saline. The reaction was stopped by the addition of cell culture medium containing FCS. 100 µl of cell suspension were added to 10 ml of Isotone buffer. Cells were counted using a ZI Coulter Particle Counter (Beckman Coulter).

6.1.4 Generation of transgenic cell lines

Cells were transfected with the tetracycline-inducible pT-Rex™-DEST30 vector (Invitrogen) carrying the codon-optimized human *TrkA/NTRK1* cDNA. Additionally, cell lines were

transfected with the pcDNA™6/TR vector (Invitrogen) harboring the gene for the tetracycline repressor.

Cells were transfected by electroporation using a MicroPorator (Peqlab) and applying one pulse of 1200 V and 50 ms to 10 µl of cells and 0.5 µg of plasmid. After electroporation, cells were cultivated in RPMI1640 + 10% FCS for 24 h. Subsequently, selection was started using RPMI1640 + 10 % FCS + 7.5 µg/ml Blasticidine for control cell lines containing the pcDNA™6/TR vector. Cell clones transfected with the pcDNA™6/TR vector and the pT-Rex™-DEST30 vector containing the human *TrkA/NTRK1* cDNA additionally received G418 (250 µg/ml). Surviving clones were grown and re-seeded into 48-, 24, 12- and 6-well plates. Cells were then treated with tetracycline for 24 hours to induce TrkA/NTRK1-expression. Induction of *TrkA/NTRK1* was verified by real-time PCR following RNA isolation and cDNA synthesis.

6.2 Molecular biology techniques

6.2.1 RNA purification

RNA was isolated using the RNeasy® Mini Kit (Qiagen). After removing the medium and washing the monolayer in phosphate buffered saline, cells were lysed in 600 µl RLT-Buffer + 1% 2-mercaptoethanol. The suspension was transferred into reaction tubes and centrifuged for 5 min at maximum speed. Subsequently, the supernatant was decanted into a new tube and 600µl ethanol were added before transferring the solution into columns. Subsequent steps were carried out according to the protocol provided by the manufacturer.

6.2.2 cDNA synthesis

cDNA synthesis was performed using the Transcriptor First Strand cDNA Synthesis Kit (Roche) and the conditions described in Table 22.

Table 22: cDNA synthesis

25µl reaction for cDNA synthesis	Volumes	Conditions
RNA	1 µg/µl	65°C, 10 min
H_2O	10 µl	
Random Primer	2 µl	

Addition of mastermix		
RT Buffer	4 µl	25°C, 10 min
RNAse Inhibitor	5 µl	55°C, 30 min
DNTP Mix	2 µl	
Reverse Transcriptase	0.5 µl	85°C, 5 min
Addition of RNAse H (3 U/µl)	1 µl	37°C, 20 min

The reaction was run in a C1000Thermal Cycler (Biorad).

6.2.3 Measurement of RNA and cDNA-concentration

The concentration of RNA- and cDNA-samples was measured using the ND-1000 Spectrophotometer (NanoDrop®). The optical density (OD) of nucleic acids at their absorption maximum of 260 nm will be 1 at a concentration of 50 µg/ml for DNA and 40 µg/ml for RNA. The purity of the sample was evaluated by an additional OD-measurement at 280 nm, which is the absorption maximum of proteins. For a sample with a high level of purity the quotient of OD260/OD280 should be between 1.8 and 2.0.

6.2.4 Quantitative real-time PCR

The Polymerase Chain Reaction (PCR) is a method used to amplify specific DNA fragments [240]. A typical reaction contains dNTP-Mix (dATP, dTTP, dCTP und dGTP), specific 5'- und 3' primers, PCR buffer and the appropriate polymerase as well as the DNA-template. The advantage of the quantitative real-time PCR over a classical PCR is that the amplification of the target sequence can be quantified in real-time. Fluorescent dyes, i.e. SYBR Green intercalate into the DNA so that an increase of DNA target sequence correlates with an increase of fluorescent signals, which is measured during each amplification cycle. The Ct-value, which is measured during the exponential phase of the experiment, refers to the threshold value, at which the fluorescence measurement rises above the background fluorescence. The Ct-value is determined for each sample and allows quantitative comparison of different samples. In addition to the target sequences, the Ct-value was also determined for a housekeeping gene such as *GAPDH* or *β-Actin*, to allow for relative comparison of cDNA-quantities.

The quantification of cDNA was calculated using the 2-ΔΔCt-method. The difference between Ct-values of the target gene and the reference gene is used for normalization of Ct-values and gives ΔCt. The ΔCt-value is then normalized to a determined sample, which gives ΔΔCt. The 'fold change'-value is calculated using the formula $2^{-\Delta\Delta Ct}$. This value is then used for quantitative comparison of samples.

Cells were treated with 1 µg/µl tetracycline and 100 ng/µl human β-NGF for 72 hours. Cultivation and treatment of cells and all real-time PCRs for *TrkA/NTRK1* and *MYCN* quantification were performed in our group. RNA isolation, cDNA synthesis and quantification of *CD44* levels by real-time PCR were performed by Alexandra Schütze from the group of Prof. Dr. J. Fischer (HHU Düsseldorf).

The reaction was performed according to the conditions described in Table 23.

Table 23: RT-qPCR for *TrkA/NTRK1*, *CD44*, *MYCN* and *GAPDH*

20 µl RT-qPCR reaction	**Volumes**	**Conditions: *GAPDH/ TrkA***	
cDNA (100 ng)	1 µl	95°C, 20 min	
Primer sen (5 pm)	1µl	95°C, 3 min	40 cycles
Primer rev (5 pm)	1µl		
Fast SYBR Green PCR Master	10 µl	60°C, 30 min	
ddH_2O	7 µl		

The reactions were run in a StepOnePlus™ Real-Time PCR System (Applied Biosystems).

6.2.5 Generation of protein lysates

After trypsinization cells were washed in cold phosphate buffered saline and centrifuged at 1200 rpm for 5 min. The resulting cell pellet was re-suspended in 50-200 µl RIPA buffer, depending on the size of the pellet. The samples were incubated on ice for 20 min and subsequently centrifuged at 1200 rpm for 20 min. The supernatant was transferred into a new 1.5 ml tube and samples were stored at -80°C.

6.2.6 Measurement of protein concentration by Bradford assay

Protein concentration was determined using the Bradford assay [241]. The assay is a spectroscopic method based on the absorbance shift form 465 nm to 595 nm of Coomassie Brilliant Blue G-250 in the presence of protein. A calibration curve with known concentrations of BSA was established at the beginning of each experiment. The BSA- stock solution (10 mg/ml) was diluted 1:20 and the following dilutions were prepared as a basis for the calibration curve:

Table 24: Calibration for Bradford assay

BSA (µg)	0	1	3	5	7	9	10
BSA (µl)	0	2	6	10	14	18	20
H_2O (µl)	50	48	44	40	36	32	30

The samples for the calibration curve were mixed with 950 µl Bradford-Reagent after having been diluted 1:5 in H_2O. After 5 min incubation, samples were measured at 595 nm using a BioPhotometer (Eppendorf). Extinction values were correlated with the known protein-concentration of each sample to deduct the calibration curve.

Subsequently, 2 µl of protein samples with unknown concentration were added to 48 µl of H_2O and incubated with 950 µl of Bradford-Reagent for 5 min before measuring the extinction at 595 nm. The calibration curve was then used to establish the concentration for each sample.

6.2.7 SDS-polyacrylamide-gelelectrophoresis (SDS-PAGE)

SDS-PAGE is a technique used to separate proteins according to their size and was performed based on the protocol described by Shapiro et al. [242], with modifications as described below.

After measuring the protein concentration, 40 µg of protein were added to 4x Laemmli sample buffer, containing 1% β-mercaptoethanol, which dissolves disulfide bonds and causes denaturation of proteins. SDS-anions, which are also a component of Laemmli-buffer, neutralize protein charge by binding positive amino acid tails and thus allowing for size-based separation of proteins in an acrylamide gel. Larger proteins will cross the gel at slower rates than smaller proteins in an electric field. Protein size is compared to a standard with marked bands at specific kDa-values.

The solution was restored to 20 µl with RIPA buffer (Table 3) before incubation for 5 min at 100°C. Gels were cast according to the protocol in 5.4 and used immediately or after storage at 4°C for up to 3 days. After removing the combs from the gels, all wells were washed with electrophoresis buffer. Subsequently, protein samples and 7 µl of a pre-stained protein marker were loaded onto the gel. The gel was run at 120 V for about 60-90 min in a Mini-PROTEAN Tetra Cell (Biorad).

6.2.8 Western blot and immunological detection of proteins

Western Blotting is a technique used to transfer proteins onto a membrane allowing for immunological detection of proteins of interest through specific antibody binding. Primary antibodies are incubated on the membrane and bind to their specific antigen on the target protein. Secondary antibodies are used to visualize the specific antibody-antigen-complex by utilizing an enzyme that catalyzes a chemiluminescence reaction after addition of a substrate.
The experiment was performed based on established protocols [243], with the following modifications: nitrocellulose membranes, Whatman paper and blotting sponges were soaked in transfer buffer and placed into blotting cassettes before assembling the transfer chamber (Mini Trans-Blot Cell, Biorad). Proteins were transferred at 40V and room temperature for 1 hour or at 70 mA and 4°C over night. After blotting, the membranes were stained in Ponceau S to evaluate the protein transfer before being washed and incubated in 5% milk in TBS or 5% BSA in TBS for 45 min to prevent non-specific antibody-binding. The membranes were incubated with the primary antibody diluted in 5% milk in TBS at 4°C over night. Before applying the secondary antibody, membranes were washed in TBST three times for 10 min. The membranes were then incubated with the HRP-coupled secondary antibodies for 1 hour at room temperature, followed by washing in TBST three times for 10 minutes. For detection of protein bands, membranes were incubated in Amersham^{TM} ECL Prime Western Blotting Reagent (Enhanced Chemiluminescence) for 1 min. Detection of protein signals was performed using the UVIchemi chemiluminescence system (Biometra).

6.2.9 Cell proliferation assay

Proliferative capacity of the *MYCN*-amplified cell lines was evaluated after induction of TrkA/NTRK1-expression. NGP-TR, NGP-TR TrkA, IMR5-TR and IMR5-TR TrkA were seeded at a density of 50000 cells/ well in a 12-well dish and treated with 1 µg/ml tetracycline and 100 ng/ml human β-NGF. Cells were incubated at 37°C, 5% CO_2 for 72 hours and

subsequently harvested by trypsinization. Cells were counted using a Neubauer Chamber or a ZI Coulter Particle Counter (Beckman Coulter) by adding 100 µl of the cell suspension to 10 ml of Isotone Buffer.

6.2.10 Colony formation assay

The colony formation assay [244] is used to evaluate the clonogenic growth of single cells. A population of cells is seeded on a sufficiently large surface and incubated until colonies of approx. 50 cells can be seen under a microscope. Colonies are fixed in 70% Ethanol for 1h at room temperature before staining in 1% crystal violet for 5 min. The cells are washed in water until only the colonies are stained and subsequently left to dry. The plating efficiency (PE) is calculated by dividing the colony count by the number of cells seeded at the start of the experiment.

Colony formation capacity of cells was evaluated by seeding 600 cells per well into a 6-well dish and evaluated in the presence or absence of TrkA/NTRK1-signaling. SY5Y-TR, SY5Y-TR TrkA, IMR5-TR, IMR5-TR TrkA, NGP-TR and NGP-TR TrkA were treated with 1 µg/ml tetracycline and 100ng/ml human β-NGF for 72 hours, or were left untreated. Cells were incubated at 37°C and 5% CO_2 for 9 days or until colonies consisted of 50 colonies and then fixed in 70% Ethanol.

6.2.11 Flow cytometry

Flow cytometry [245] allows for characterization of cells in terms of cell size, granularity, structure, surface molecules, DNA content and intracellular proteins. Forward scatter (FSC) and side scatter (SSC) are used to evaluate size, granularity and structure, while antibodies are used to characterize surface molecules and intracellular components. Fluorescent dyes, which are directly coupled to primary antibodies or utilized by secondary antibodies, are detected during analyses and signals are analyzed using the appropriate software.

SY5Y-TR, SY5Y-TR TrkA, IMR5-TR, IMR5-TR TrkA, NGP-TR and NGP-TR TrkA were treated with tetracycline (1 µg/ml) and human β-NGF (100 ng/ml) for 72 hours. Cells were harvested by trypsinization and 100 µl of the cell suspension were collected into each well of a 96-well plate. After centrifugation at 300x g for 5 min at 4°C, the supernatant was discarded and cells were re-suspended in 100 µl of antibody solution. Samples were incubated on ice for 10 minutes in the absence of light, before washing in FACS buffer and centrifuging (300x g, 4°C, 5 min). Cells were then re-suspended in 200 µl of FACS buffer and transferred into

FACS tubes. Presence of surface molecules was analyzed using a BD LSR II Cytometer and CellQuest Software.

6.2.12 Immunohistochemistry

Immunohistochemical detection of CD44 expression was performed using NGP-TR and NGP-TR TrkA cells without or after treatment with 1 µg/ml tetracycline and 100 ng/ml human β-NGF and were grown on cover glasses (∅ =18 mm) in 12-well plates at a density of 50000 cells per well. After 72 hours cells were fixed with 4% paraformaldehyde in PBS for 20 min and then washed with PBS (3x 5min). A blocking solution containing 3% BSA and 0.2 M glycine in PBS was used to block unspecific binding sites. This experiment was performed in cooperation between our group and the group of Prof. Dr. J. Fischer (HHU Düsseldorf), After one hour of incubation in blocking solution, cells were incubated with the primary antibody anti-CD□□ (1:100 in PBS) over night at 4°C. Cells were washed in PBS (3x 5min) before applying the secondary antibody (α-mouse Alexa Fluor® 488-labeled (Invitrogen); 1:2000 in PBS) for 1h. Cover glasses were then washed in PBS (4x 15 min), with the third wash supplemented by 250 ng/ml 4,6 diamidino-2-phenylindole (DAPI) in PBS. Cover glasses were mounted using Mowiol 4-88 (Roth). Analysis of CD44-expression was performed using a Zeiss Axioplan Microscope.

6.3 Radiation biology techniques

6.3.1 Radiation exposure

Irradiation of cells was carried out using an X-ray machine (GE- Healthcare) operated at 320 kV, 10 mA with a 1.65 mm Al filter (effective photon energy approximately 90 kV), at a distance of 50 cm and a dose rate of ~1.3 Gy/min. Dosimetry was performed with a chemical dosimeter, which was used to calibrate an infield ionization monitor. Cells were irradiated in T25 or T75 flasks with closed caps to avoid cell stress through low CO_2 and returned to the incubator immediately after exposure to IR.

6.3.2 Pulsed-field gel electrophoresis (PFGE)

Pulsed-field gel electrophoresis is used to separate large DNA fragments by applying an alternating voltage gradient [246].

1×10^6 cells were pre-treated for 48h with 1 µg/ml tetracycline and 100ng/ml human beta-NGF (R&D Systems), and irradiated at different doses for repair kinetics and dose response

evaluation. After irradiation, cells were returned to the incubator at 37°C for different repair time intervals. Cells were then harvested by trypsinization and embedded in 0.5% Agarose (InCert Agarose, Bio-Rad) growth medium at a final concentration of 1×10^6 cells/ml. Cells were lysed for 18 h at 50°C in lysis buffer. Cell plugs were then placed into washing buffer for 1h and treated for 1h with 0.1 mg/ml RNAase A at 37°C. Induction and repair of double strand breaks were evaluated by asymmetric field inversion gel electrophoresis (AFIGE). AFIGE was carried out in 0.5% gels of SeaKem LE Agarose (Lonza) containing 0.5 µg/ml ethidium bromide, and were run in 0.5×TBE at 8°C for 40h. Electric field cycles of 50 V (1.25 V/cm) for 900 s in the forward direction alternated with cycles of 200 V (5.0 V/cm) for 75 s in reverse direction. Gels were scanned using a fluorimager (Typhoon, GE-Healthcare) and analyzed with Image-Quant (GE-Healthcare). The fraction of DNA released (FDR) from the well into the lane is a measure of double-strand breaks present. FDR measured in non-irradiated samples was subtracted from FDR measured in samples exposed to IR.

To facilitate the inter-comparison of results obtained in correlation to TrkA/NTRK1-signaling, repair kinetics are not presented as FDR versus time, but as dose equivalent (Deq) *versus* time. Deq is calculated from FDR using dose response curves as described in 7.2.1.

6.3.3 Cell cycle analysis by PI and H3pS10 staining

Propidium iodide (PI) intercalation into DNA can be used as a surrogate marker to determine cell cycle distribution by FACS [247]. FSC and SSC inform about the cell size and granularity. They allow for distinguishing cell doublets or triplets vs. single cells with double DNA content in S- or G_2-phase. Furthermore, phospho-Histone 3 staining is a marker for mitotic cells and is performed to evaluate the induction of the G_2 checkpoint. FACS/PI analysis was performed in the lab of Prof. Dr. George Iliakis, with supervision and instruction provided by Dr. Aashish Soni, and the experimental setup based on the standard protocols for PI- [248] and H3pS10-staining [249], modified as described in the following text.

SY5Y-TR and SY5Y-TR TrkA cells were seeded in 6-well dishes in the presence and absence of tetracycline (1 µg/ml) and human β-NGF (100 ng/ml) for various time points. Cells were trypsinized and added to previously collected supernatant containing floating cells. After centrifugation, cell pellets were washed in phosphate buffered saline, resuspended in 300 µl PBS and fixed in 700 µl ice-cold ethanol (70%). After 60 min of incubation on ice, cells were re-suspended in 1 ml 0.25% Triton X-100 in phosphate buffered saline and incubated on ice for 10 minutes. Cells were then centrifuged, the pellet was re-suspended in 500 µl PBS + 1% bovine serum albumin (BSA) and incubated at RT for 30 minutes. Samples were incubated

for 1h in 150µl of a 1:5000 dilution (in PBST) of a polyclonal antibody specific for H3pS10 (Abcam). After washing with PBS, cells were incubated with the secondary antibody (AlexaFluor 488, Invitrogen) diluted 1:300 in PBST for 1 hour at RT. Cells were washed again and then treated with 10µg/ml propidium iodide and subsequently analyzed in a flow cytometer (Gallios, Beckman Coulter). Positive staining for H3pS10 was used as a surrogate marker for the fraction of cells at metaphase (mitotic index).

6.3.4 MTT assay

MTT assay was employed to evaluate the proliferative capacity of irradiated (2 Gy) cells in correlation to TrkA/NTRK1-signaling. The assay was performed based on established protocols [250], with the exact conditions as described below.

SY5Y-TR and SY5Y-TR TrkA were seeded on 96-well plates in triplicates (10000 cells per well) and treated with tetracycline (1 µg/ml) and / or human β-NGF (100ng/ml). The same set was additionally treated with a PARP inhibitor, Olaparib (3 µM). Cells were cultivated up to 96 hours with replicates taken for determination of cell numbers at 24-hour intervals. For this purpose cells were treated with 0.18 mM MTT and incubated for 3 hours. Afterwards, cells were solubilized (10% SDS + 0.6% glacial acetic acid in DMSO) and O.D. values at 590 nm were quantified using the EL800 Universal Microplate Reader (Bio-Tek Instruments).

6.3.5 53BP1-assay

The p53 binding protein, 53BP1, is recruited to DNA double-strand breaks (DSB) and can be used to visualize both DSBs and their repair. Following irradiation and the formation of DSBs, the DNA repair process starts with the recruitment of proteins involved in DSB repair, including 53BP1. These foci can be visualized by specific antibodies and fluorescence microscopy. The number of 53BP1 foci diminishes as DSB repair progresses, so that the kinetics of DNA repair can be analyzed by quantifying foci at different time points post-IR.

SY5Y-TR and SY5Y-TR TrkA cells were seeded into 12-well plates at a density of 50000 cells per well, after placing sterile cover slides (∅ =18 mm) into each well. Cells were treated with 1 µg/ml tetracycline and 100 ng/ml human β-NGF for 24 hours before being irradiated with 2 Gy. DNA repair was stopped at 1h, 4h and 24h after irradiation by fixing cells with 4% paraformaldehyde in PBS for 10 min. Cells were washed 3 x with PBS and subsequently permeabilized with 0.2% Triton + 1% BSA in PBS for 10 min. Cells were then washed again with 1% BSA in PBS (2x 5min) and then incubated in blocking solution (3% BSA and 0.2 M

Glycine in PBS) for 1h to block unspecific binding sites. The primary antibody was diluted 1:200 in 1% BSA + 0.5% Tween20 in PBS and left on the cells over night at 4°C. Cells were washed in 1% BSA + 0.5% Tween20 in PBS before applying the secondary antibody (α-mouse Alexa Fluor® 488-labeled (Invitrogen) at a dilution of 1:2000 in 0.5% goat serum in PBS) for 1h. Cells were washed three times in PBS and once in PBS + 250 ng/ml 4,6 diamidino-2-phenylindole (DAPI). After drying, cover glasses were mounted using Mowiol 4-88 (Roth) and analyzed using a Zeiss Axioplan microscope equipped with a high magnification objective 63 x). Thirty nuclei were analyzed for 53BP1-foci by visual inspection.

6.3.6 Chromosome translocation assay

A chromosome translocation assay was used to evaluate the contribution of TrkA/NTRK1 to DNA repair mechanisms by quantifying chromosome breaks, gaps and translocations after irradiation with 2 Gy in the presence and absence of TrkA/NTRK1-signaling. The protocol employed for cytogenetic analysis in cells irradiated in G_2 is a modification of a protocol that has been extensively used previously [251].

Cells were seeded in T25 flasks at a density of 1 x 10^6 cells and treated with 1 µg/ml tetracycline and 100 ng/ml human β-NGF for 72 hours. Exponentially growing cells were exposed to 2 Gy X-rays and were allowed to repair for 4 h at 37°C. Cells were treated with 0.1 µg/ml Colcemid (L-6221, Biochrom AG) for 1 h to accumulate cells at metaphase. Cells were then harvested at the respective time point. After trypsinization, cells were treated in hypotonic solution (75 mM KCl) for 10 min at room temperature (RT) and fixed in Carnoy's fixative (25% glacial acetic acid, 75% methanol) three times. After fixing, cells were spread on clean glass slides and stained with 3% Giemsa stain in Sorenson's buffer. Standard criteria were used for scoring metaphases. Bright field microscopy (Olympus, Vanox-T, Japan) and a MetaSystems station (Altlussheim, Germany) with a microscope (AxioImagerZ2, Zeiss) and automated image capture and analysis capabilities were used for scoring chromosome aberrations. Chromosome breaks and gaps, as well as chromatid or chromosome translocations were considered during scoring.

6.3.7 Premature chromosome condensation

To analyze chromosome damage prior to metaphase in cells still in interphase, exponentially growing cells (SY5Y-TR, SY5Y-TR TrkA with and without treatment with 1 µg/ml and 100 ng/ml) were exposed to 2 Gy X-rays and allowed to repair at 37°C for 4 h. A total of 100 nM calyculin-A was subsequently added for 15 min to induce premature condensed chromosomes (PCC) before processing for cytogenetic analysis. The time of calyculin-A treatment is integrated in the calculation of the repair time. After trypsinization, cells were incubated in hypotonic solution (75 mM KCl) for 10 min at room temperature (RT) and subsequently fixed in Carnoy's fixative (25% glacial acetic acid, 75% methanol) three times. After fixing, cells were spread on clean glass slides and stained with 3% Giemsa stain in Sorenson's buffer. Cells with PCCs were prepared as described for metaphase analysis. The protocol employed for cytogenetic analysis is a modification of a protocol that has been extensively used previously [251].

6.4 Data Analysis

6.4.1 Statistics

Statistical test including t-test or ANOVA were done using GraphPad Prism 5.0 Software. Error bars shown represent the standard deviation (STDEV). Significant differences between two groups were designated ***: $p < 0.001$, **: $p < 0.001$-0.01, *: $p = 0.01$-0.05

6.4.2 Image processing

All images were processed using Pixelmator, Version 3.3.1.

Results

7. DSB repair capacity of TrkA/NTRK1-over-expressing SY5Y neuroblastoma cells

7.1 Inducible expression of TrkA/NTRK1 in the neuroblastoma cell line SY5Y

In order to study immediate effects of TrA/NTRK1-signaling in the SY5Y neuroblastoma cell line, a conditional system (generated by Dr. S. Lindner, UK Essen) was analyzed for tetracycline-inducible expression of TrkA/NTRK1 on the mRNA- and protein levels (Figure 15).

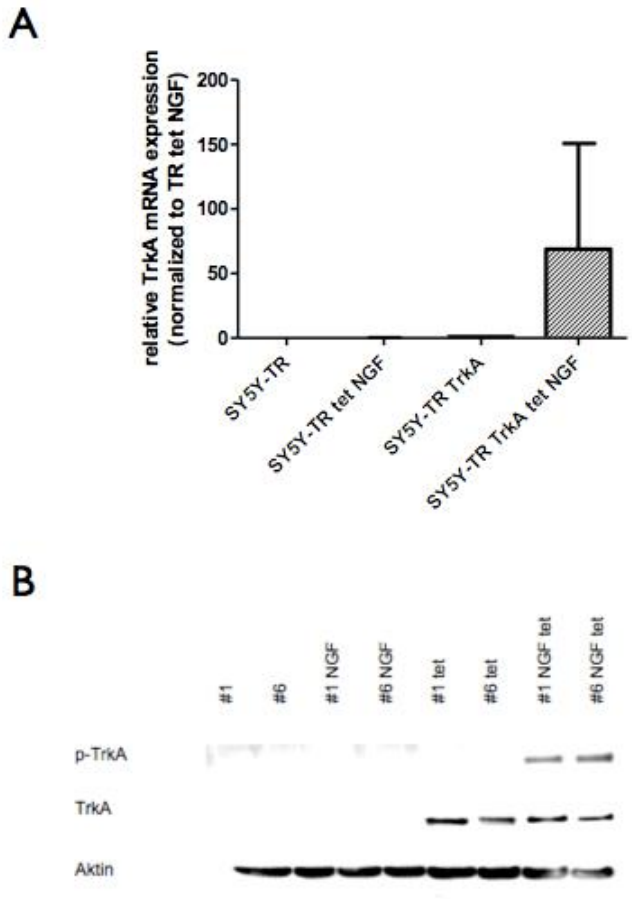

Figure 15: Validation of inducible TrkA/NTRK1-expression in SY5Y neuroblastoma cells.
TrkA/NTRK1 mRNA-levels were up-regulated after treatment with tetracycline + NGF in SY5Y neuroblastoma cells carrying a plasmid with a codon-optimized TrkA/NTRK1-gene under the control of a tet-repressor (n=2). Contrastingly, *TrkA/NTRK1* mRNA-levels are unaltered by tetracycline + NGF in the vector control TR, which only codes for the tet-repressor (Figure 15A). TrkA/NTRK1 protein levels are shown in two different SY5Y-TR TrkA clones (#1 and #6). Expression of TrkA/NTRK1 was limited to tetracycline-treated samples and not detectable in untreated or NGF-treated cells. Moreover, phosphorylation of TrkA/NTRK1 was only achieved by addition of the specific TrkA/NTRK1 ligand, NGF, in the presence of tetracycline (Figure 15B).

Induction of TrkA/NTRK1 could be shown on both the mRNA- and protein-level in response to tetracycline (Figure 15A). Receptor phosphorylation and activation was observed only after treatment with the ligand nerve growth factor (NGF; Figure 15B) enabling us to analyze the effects of TrkA/NTRK1 signaling under defined conditions.

7.2 Impact of TrkA/NTRK1-signaling on dose response and DNA repair kinetics

Previous experiments with stably TrkA/NTRK1 -expressing SY5Y cells showed differences in DNA repair kinetics and DNA repair capacity between TrkA/NTRK1 -positive and TrkA/NTRK1 -negative cells [126]. Here the effects of short-term TrkA/NTRK1-signaling on the ability of cells to repair DSBs were analyzed. The DNA repair capacity and dose response of cell lines can be determined by different means *in vitro.* Since methodological and biological factors can influence the results of radiation-based experiments different assays were employed to determine the role of short-acting TrkA/NTRK1-signaling in the DNA damage response of neuroblastoma cells.

7.2.1 TrkA/NTRK1-expressing cells show slower initiation of DNA repair post-IR

High doses of irradiation induce fragmention of cellular DNA and allow for analysis of DNA repair capacity and repair kinetics associated with high numbers of DSBs. The control cell line SY5Y-TR and the tet-inducible TrkA/NTRK1-transfectant were left untreated or incubated with tetracycline and NGF for 48 hours prior to irradiation. Dose response curves for the induction of double strand breaks were established by exposing cells to increasing doses of X-rays (10, 20 and 30 Gy) and determining the fragmentation of DNA by gel electrophoresis. Cells were embedded in agarose prior to irradiation to avoid any DNA repair. Ethidium bromide stained gels allow for quantification of fractions of DNA released (FDR) into the lane and plotting this value as a function of irradiation dose (Figure 16). As expected, the FDR increases with the irradiation dose in all four analyzed samples. At 10 Gy, the FDR value is between 10 and 15% in all cell lines and increases to around 50% at a dose of 30 Gy. While the SY5Y-TR TrkA transfectant with and without induction of TrkA/NTRK1 (green and yellow symbols) shows slightly higher FDR values at all doses, differences in dose response between the four cell lines are not significant.

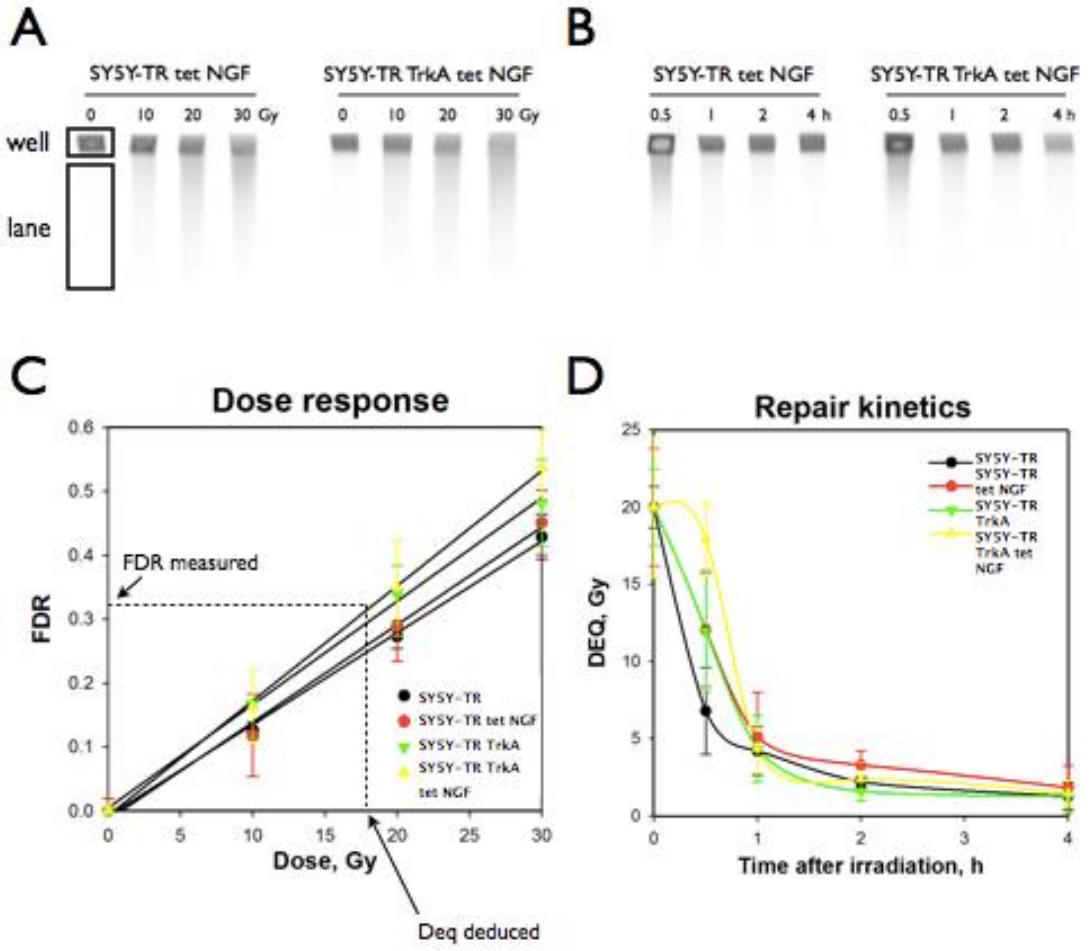

Figure 16: Dose response and repair kinetics as evaluated by PFGE.

Dose response of SY5Y cells with and without expression and activation of TrkA/NTRK1 is shown in FDR (fraction of DNA released from the well into the lane) as a function of IR dose. PFGE gels show electrophoresis of DNA samples for dose response (A) and repair kinetics (B) for SY5Y-TR +/- tet NGF (left) and SY5Y-TR TrkA +/- tet NGF (right). The dose response curves show the highest FDR for the TrkA-positive SY5Y transfectant at 10, 20 and 30 Gy (C). DNA repair kinetics of SY5Y-TR TrkA cells show a slower initial start of DNA repair (yellow curve, D). Results of three technical replicates were used to calculate the indicated means and standard deviations.

The DNA repair kinetics were established by irradiation of all samples with 20 Gy to induce initial fragmentation of DNA and incubation of cells under physiological conditions for 0.5h, 1h, 2h or 4h to allow for repair of the induced DSBs. Cells were then embedded in agarose and the FDR in repaired lanes was measured for each time point. However, repair kinetics are affected by cells being in different phases of the cell cycle. In order to correct for those differences, the repair kinetics are plotted as Deq versus time, rather than FDR vs. time. Deq is the equivalent dose of fragments released from the well (FDR) after each repair time

interval (see dotted line in Figure 16C). The FDR measured for each sample was converted to Deq by using the previously established dose response curve for each condition. Since the linear increase of FDR with irradiation dose corresponds to the linear increase of DSBs with irradiation dose, the Deq deduced from the FDR can serve as a measure of remaining DSBs at each time point. The resulting DNA repair kinetics are shown in Figure 16D. At t= 0.5h post-IR TrkA/NTRK1-expressing cells show the highest Deq of all four samples. However, while DNA repair starts delayed in these cells, the repair of damage is synchronous to the kinetics in the three TrkA/NTRK1-negative controls at the time points of 1, 2 and 4h post-irradiation.

7.2.2 TrkA/NTRK1-expression significantly increases residual damage 24h after IR

Accumulation of the p53-binding protein 53BP1 is a marker for DNA double-strand breaks, as 53BP1 becomes hyper-phosphorylated in response to DNA strand breaks and relocates to DSB sites early in the DNA damage-signaling pathway. SY5Y-TR and SY5Y-TR TrkA were irradiated with 1 Gy after being treated with 1 µg/ml tetracycline and 100 ng/ml human β-NGF for 24 hours or were left untreated. The 53BP1-foci were quantified at 0h, 1h, 5h and 24 hours after irradiation by counting the number of foci in 30 nuclei per sample. At t = 0 the number of 53BP1-foci served as a background value indicating the general amount of DSBs in the absence of DNA damaging agents (Figure 17A). This value ranged between 0.5 and 0.8 foci in the four samples. At 1h post-IR, SY5Y-TR TrkA showed on average 15.7 foci per nuclei, which is comparable to SY5Y-TR tet NGF (15.9 foci/ nuclei). TrkA/NTRK1-induction and activation (= SY5Y-TR TrkA tet NGF) resulted in 13 foci per nuclei, which is significantly lower than the number of foci in the control treated cells without TrkA/NTRK1 expression (SY5Y-TR tet NGF, t-test, p= 0.002). Over the course of the next 4 hours foci numbers were reduced as DNA damage repair progressed. The TrkA/NTRK1-expressing SY5Y cells had the least number of residual 53BP1-foci (n= 4), which is significantly less than those counted in the control cells, SY5Y-TR tet NGF (n= 7.9). Numbers of foci for non-induced SY5Y-TR TrkA were comparable to those of the control cell line SY5Y-TR (n= 5.2 and 5.9 on average, respectively).

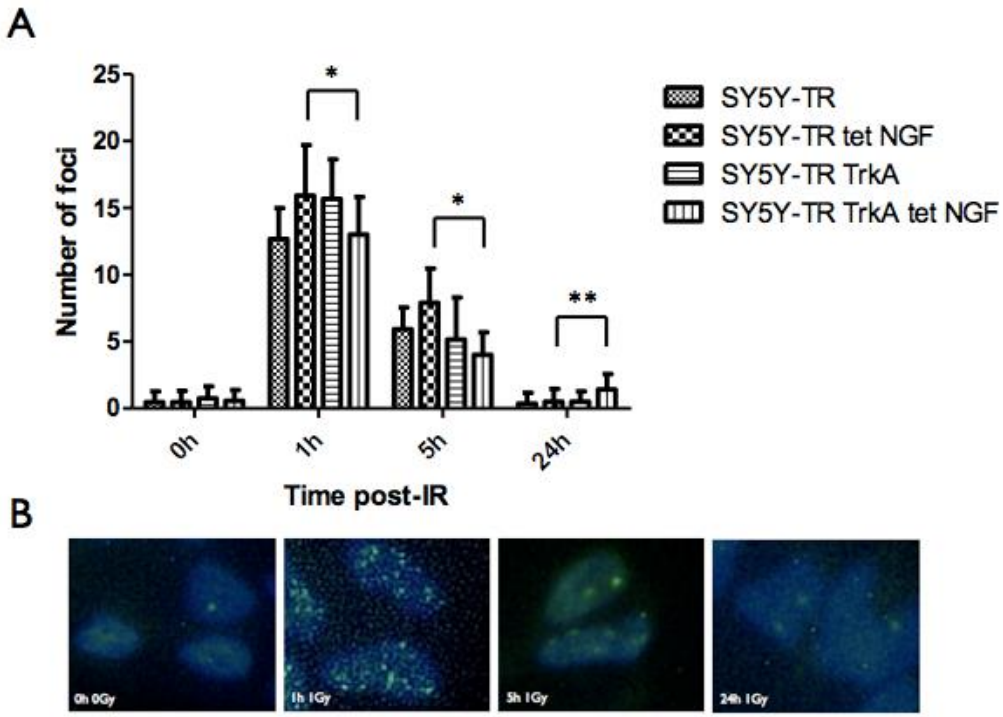

Figure 17: Analysis of DSB repair capacity as a function of TrkA/NTRK1 expression and activation evaluated by 53BP1-Assay.

The number of DNA double-strand breaks following irradiation with 1 Gray was quantified in the SY5Y transfectants SY5Y-TR and SY5Y-TR TrkA with and without tetracycline + NGF treatment. **(A)** Quantification of 53BP1-foci: Quantified values are represented as the median of the number of 53BP1-foci in 30 nuclei per sample (t-test, **: p <0.001-0.01, *: p = 0.01-0.05, +STDEV; values are given to include the standard deviation of foci quantified in 30 nuclei per sample). **(B)** DAPI-stained nuclei with 53BP1-foci of SY5Y-TR TrkA at 0 hours, 1 hour, 5 hours and 24 hours post-irradiation.

The number of foci was again quantified at 24 hours post-IR to determine residual DNA damage in any of the four samples. In TrkA/NTRK1-negative cell lines (SY5Y-TR, SY5Y-TR tet NGF, SY5Y-TR TrkA) 53BP1 foci were back to baseline levels (0.4/ 0.5/ 0.5, respectively), whereas the TrkA/NTRK1-positive nuclei showed significantly more residual foci compared to control cells, SY5Y-TR tet NGF (n= 1.4, paired t-test, p=0.0012).

7.2.3 TrkA/NTRK1-expression does not quantitatively affect IR-induced chromosomal aberrations

Since TrkA/NTRK1-expression has been associated with genomic integrity in both primary neuroblastomas and cellular *in vitro* systems, Giemsa staining of metaphase chromosomes

was performed to quantify the numbers of chromosomal aberrations and translocations in neuroblastoma cells with and without expression of TrkA/NTRK1.

SY5Y-TR +/- tet NGF and SY5Y-TR TrkA +/- tet NGF were irradiated with 1 Gy and incubated for 4 hours at 37°C to allow for DSB repair potentially resulting in translocations. Cells were treated with colcemid for 1 hour to block cells just about to reach metaphase. Giemsa staining allowed for quantitation of fifteen metaphases per sample by bright-field microscopy. Numbers of translocations were scored separately from unrepaired chromosomal aberrations to consider partial, but defective repair in the development of translocations (Figure 18).

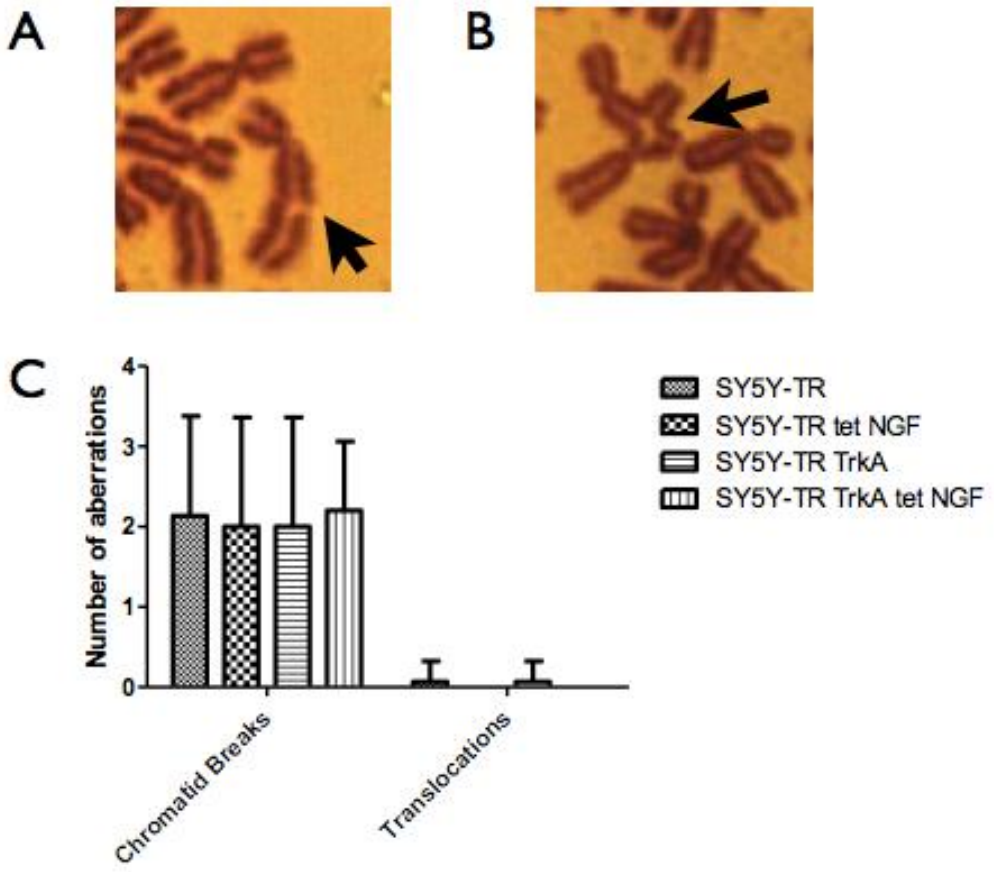

Figure 18: Translocation assay for quantification of chromosomal aberrations does not reveal a role for TrkA/NTRK1

The ability of SY5Y cells to repair chromosome breaks after irradiation with 1 Gy was evaluated 4h post-IR in cells with and without expression and activation of TrkA/NTRK1. Chromatid breaks (A, arrow) indicating absence of repair were scored separately from translocations (B, arrow), which indicate a defective form of repair whereas breaks represent no repair. No significant differences were observed between the samples analyzed (C). Only 2 translocations were found in all metaphases. Error bars represent the standard deviation of values quantified in 15 metaphases per sample in one single experiment.

While chromosomal aberrations were readily detectable in TrkA/NTRK1-negative samples due to high numbers of metaphases, scoring was difficult in preparations from SY5Y-TR TrkA tet NGF since only a very small fraction of cells could be blocked in metaphase. In order to overcome this limitation, analysis of chromosome damage prior to metaphase via premature chromosome condensation (PCC) was evaluated as an alternative method enabling analysis of chromosomes still in interphase. However, SY5Y cells were extremely sensitive to calyculin-A with even very short treatment times resulting in cell death and calyculin-A reduction to tolerated doses failing to produce completely condensed chromosomes.

7.3 Expression of NHEJ factors is not significantly altered by TrkA/NTRK1 expression

Up-regulation of the NHEJ-factor XRCC4 has been demonstrated in stably TrkA/NTRK1-expressing SY5Y cells, and was correlated with an increased NHEJ capacity and altered DNA repair kinetics compared to SY5Y cells lacking TrkA/NTRK1-signaling [126]. Protein expression of key factors involved in NHEJ or A-EJ was analyzed in differentially treated SY5Y transfectants. SY5Y-TR and SY5Y-TR TrkA were treated with tetracycline and NGF (tet NGF) or left untreated, and exposed to X-rays at a dose of 20 Gy. Only SY5Y-TR TrkA tet NGF cells expressed TrkA/NTRK1 in irradiated and non-irradiated samples (Figure 19A). Expression of the NHEJ-factors XRCC4, Ku80 (Figure 19A) and Ku70 (Figure 19B) were not altered by TrkA/NTRK1-expression in irradiated or non-irradiated cells. Furthermore, A-EJ factors WRN and MRE11 were expressed at similar levels irrespective of the TrkA/NTRK1-status of the cells (Figure 19B). Protein levels of the apoptosis-related cysteine protease (Caspase 3), and p21, the mediator of p53-induced growth arrest, were analyzed to visualize a potential effect of TrkA/NTRK1-signaling on the induction of irradiation-induced cell death. However, both Caspase 3- and p21-levels were unchanged by activation of TrkA/NTRK1.

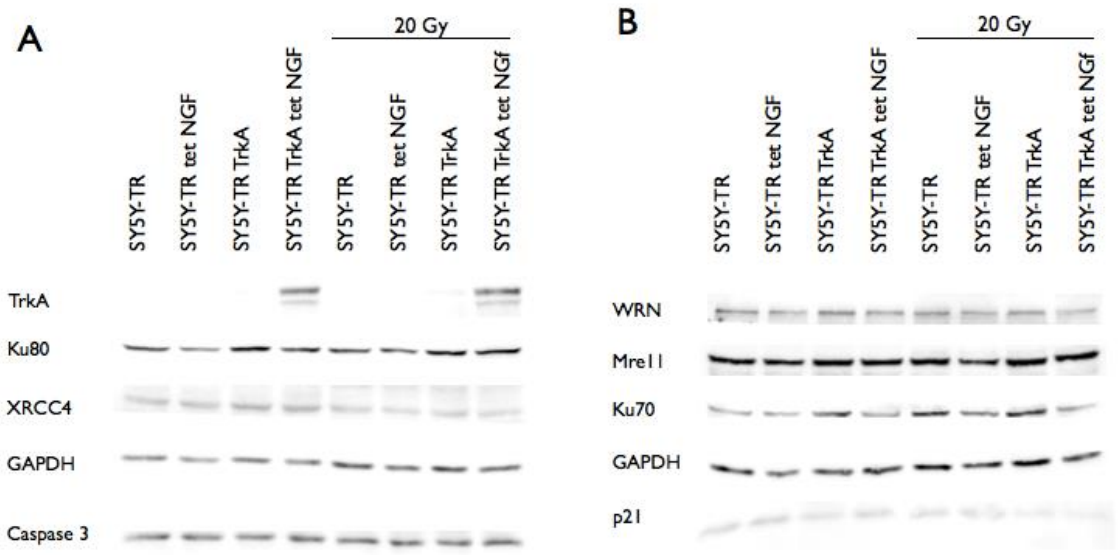

Figure 19: Protein expression of DNA repair factors in SY5Y transfectants

Differentially treated SY5Y transfectants were subjected to 20 Gy of X-rays in order to analyze a potential role of TrkA/NTRK1 in the expression of DNA damage response factors. While TrkA/NTRK1 expression is limited to conditional TrkA/NTRK1-transfectants treated with tetracycline and NGF, protein levels of NHEJ-factors (XRCC4, Ku80 and Ku70) and A-EJ factors (WRN and MRE11) as well as the apoptosis mediator Caspase 3 and the cell cycle regulator p21 are unaffected by TrkA/NTRK1-signaling.

In contrast to previous findings in stably TrkA/NTRK1-expressing SY5Y cells, no up-regulation of XRCC4 was observed in response to short-term TrkA/NTRK1-signaling for 24 hours. Furthermore, expression of other NHEJ factors was unchanged irrespective of TrkA/NTRK1-signaling.

7.4 TrkA/NTRK1-expression is implicated in the up-regulation of PARP1

While TrkA/NTRK1 did not alter protein levels of the A-EJ factors MRE11 and WRN, protein levels of PARP1 were found to be up-regulated in response to TrkA/NTRK1-expression. Two different SY5Y-TR TrkA clones (#1 and #6) were differentially treated with NGF and/or tetracycline (Figure 20).

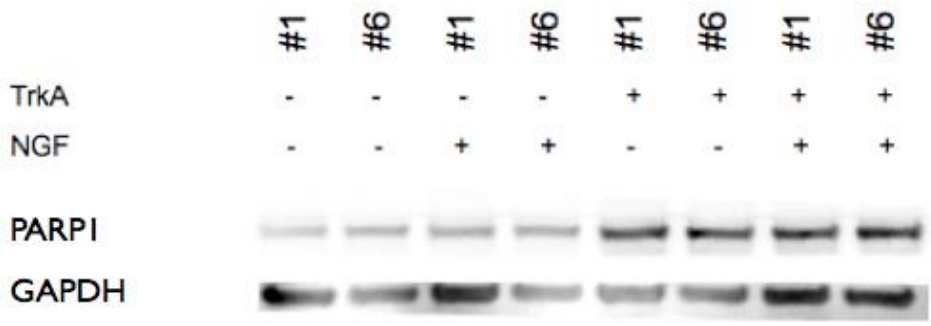

Figure 20: PARP1 is differentially expressed in conditional SY5Y-TR TrkA transfectants with and without induction of *TrkA/NTRK1*-expression.

Protein expression of PARP1 was analyzed in two different TrkA/NTRK1-transfectants with conditional expression of TrkA/NTRK1 (#1 and #6). Samples were left untreated (lanes 1 and 2) or differentially treated with only NGF (lane 3 and 4), only tetracycline (lanes 5 and 6), or tetracycline and NGF (lanes 7 and 8). Levels of PARP1 are up-regulated only in samples that were treated with tetracycline or tetracycline + NGF (lanes 5-8) compared to untreated or NGF-treated cells.

PARP1 expression was shown in all samples, but induction of *TrkA/NTRK1*-expression by tetracycline was associated with a stronger PARP1 signal compared to non-induced cells. However, up-regulation of PARP1 could not be consistently reproduced in every experiment, which may be explained by cell cycle-dependent fluctuations of PARP1-levels.

7.4.1 Olaparib reduces PARP1 protein levels in TrkA/NTRK1-positive cells post-IR

The role of TrkA/NTRK1 in the regulation of PARP1 was further analyzed by treating cells with the PARP1 inhibitor Olaparib. PARP1 is involved in DNA double-strand break repair as part of the A-EJ and in the base excision repair (BER) of single-stranded DNA breaks. PARP1 inhibition results in the accumulation of DNA single-strand breaks and increases the risk for DSBs.

To analyze the potential role of TrkA/NTRK1 in the regulation of PARP1 SY5Y-TR and –TR TrkA cells were differentially treated with tetracycline and NGF for 48 hours and with 3 µM Olaparib for 24 hours prior to irradiation with 20 Gy. Protein levels of WRN, PARP1, Chk1, GAPDH and Caspase 3 were evaluated at 30 minutes post-IR (Figure 21).

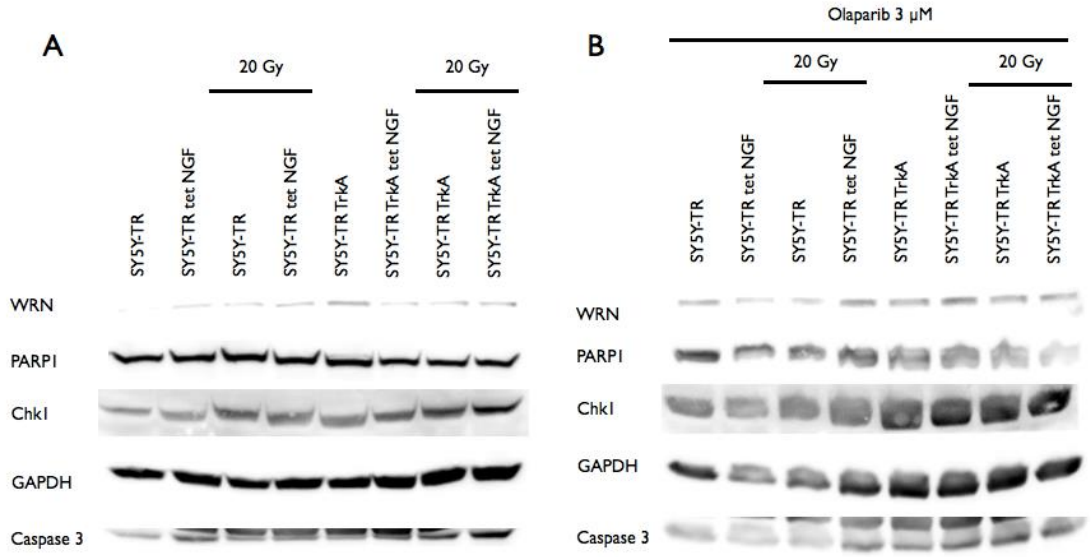

Figure 21: Expression of DNA damage response factors in cells treated with Olaparib

Protein levels of the A-EJ factors WRN and PARP1 were analyzed in TrkA/NTRK1-positive and –negative cells with and without irradiation (A) and PARP1-inhibition by Olaparib (B). In this experiment, PARP1 levels were not altered in response to TrkA/NTRK1-expression in the absence of Olaparib (A). Irradiation of PARP1-inhibited cells shows down-regulation of PARP1 in irradiated TrkA/NTRK1-positve SY5Y cells (B). Expression of WRN, Chk1 and Caspase 3 was not affected by Olaparib treatment.

While protein levels stay unchanged in Olaparib-treated vector control cells (SY5Y-TR +/- tet NGF), TrkA/NTRK1 transfectants display lower PARP1 levels after irradiation with 20 Gy, especially after induction and activation of TrkA/NTRK1 by tetracycline and NGF (Figure 21B). Interestingly, PARP1 cleavage product was not detected in irradiated or non-irradiated samples. Furthermore, Olaparib treatment led to a down-regulation of XRCC1 in all samples irrespective of TrkA/NTRK1-signaling (Figure 22B).

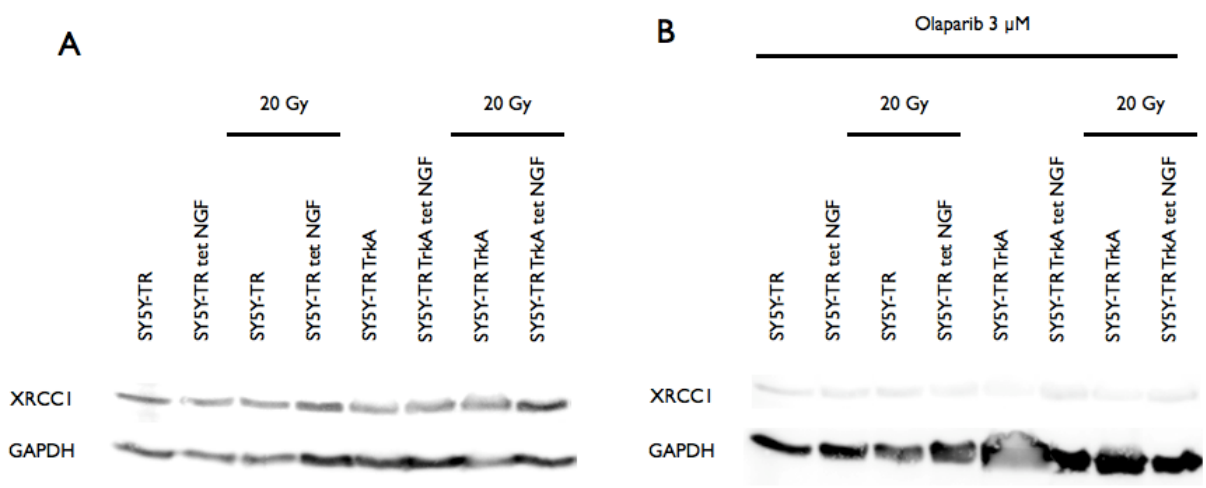

Figure 22: XRCC1 is down-regulated in response to Olaparib treatment

Expression of the A-EJ factor XRCC1 was analyzed in cells treated with Olaparib and subjected to 20 Gy of X-rays. PARP1 inhibition leads to a down-regulation of XRCC1 in all samples irrespective of TrkA/NTRK1-signaling and irradiation dose.

Down-regulation of XRCC1 by PARP1 inhibition is in line with published data analyzing the role of PARP1 in the recruitment and the assembly of subnuclear XRCC1 foci during SSB repair [252]. Even though PARP1 levels were down-regulated only in TrkA/NTRK1-activated SY5Y cells, the down-stream effect of XRCC1-down-regulation of Olaparib treatment was visible in all cell lines irrespective of TrkA/NTRK1-signaling.

7.4.2 TrkA/NTRK1-expressing SY5Y cells are less sensitive to Olaparib

Cell viability after irradiation was evaluated by MTT assay. The assay was performed using SY5Y-TR and SY5Y-TR TrkA with and without 24 hours of tet + NGF treatment before irradiation with 2 Gy (0 Gy for controls). O.D. values were determined in 24h intervals post-IR for 96 hours. Cell viability of SY5Y-transfectants is shown in Figure 23A and B. Optical density values increased at each time point ranging from 0.2 at 24 hours to 0.7 at 96h in SY5Y-TR and SY5Y-TR tet NGF. The O.D. values for the conditional TrkA/NTRK1-transfectants were slightly lower with the maximum O.D. value at 96 hours after the start of the experiment at around 0.5. Contrastingly, irradiation with 2 Gy resulted in a very low metabolic activity of irradiated SY5Y-transfectants. While cell viability of TrkA/NTRK1-positive samples was reduced compared to controls in non-irradiated samples, TrkA/NTRK1-signaling leads to a significant increase in viability at 48 hours post-irradiation with 2 Gy (t-test $p=0.0208$).

Sensitization of SY5Y-TR and SY5Y-TR TrkA to X-rays by Olaparib was analyzed

accordingly. Cells were differentially treated with tetracycline and NGF for 48 hours and with 3 µM Olaparib, a dose frequently described for *in vitro* experiments in the literature, for 24 hours prior to irradiation with 2 Gy. Olaparib treatment reduced cell viability in the presence and absence of irradiation compared to the untreated controls (Figure 23C,D).

However, TrkA/NTRK1-expression showed a protective effect against Olaparib toxicity in non-irradiated and irradiated cells. TrkA/NTRK1-positive SY5Y cells show significantly higher O.D. values after 48h ($p=0.002$), 72h ($p=0.0001$), and 96h ($p=0.0001$) after the start of the experiment in non-irradiated cells. Cell viability of vector control cells decreases steeply between the 24h and 48h time points, while the measured O.D. values of TrkA/NTRK1-transfectants with and without TrkA/NTRK1-activation show almost no decrease in cell viability until the last time point at 96 hours. Furthermore, TrkA/NTRK1-activated cells do not show an apoptotic effect of Olaparib with even slightly increasing O.D. values at time points 24h and 48h compared to 0h.

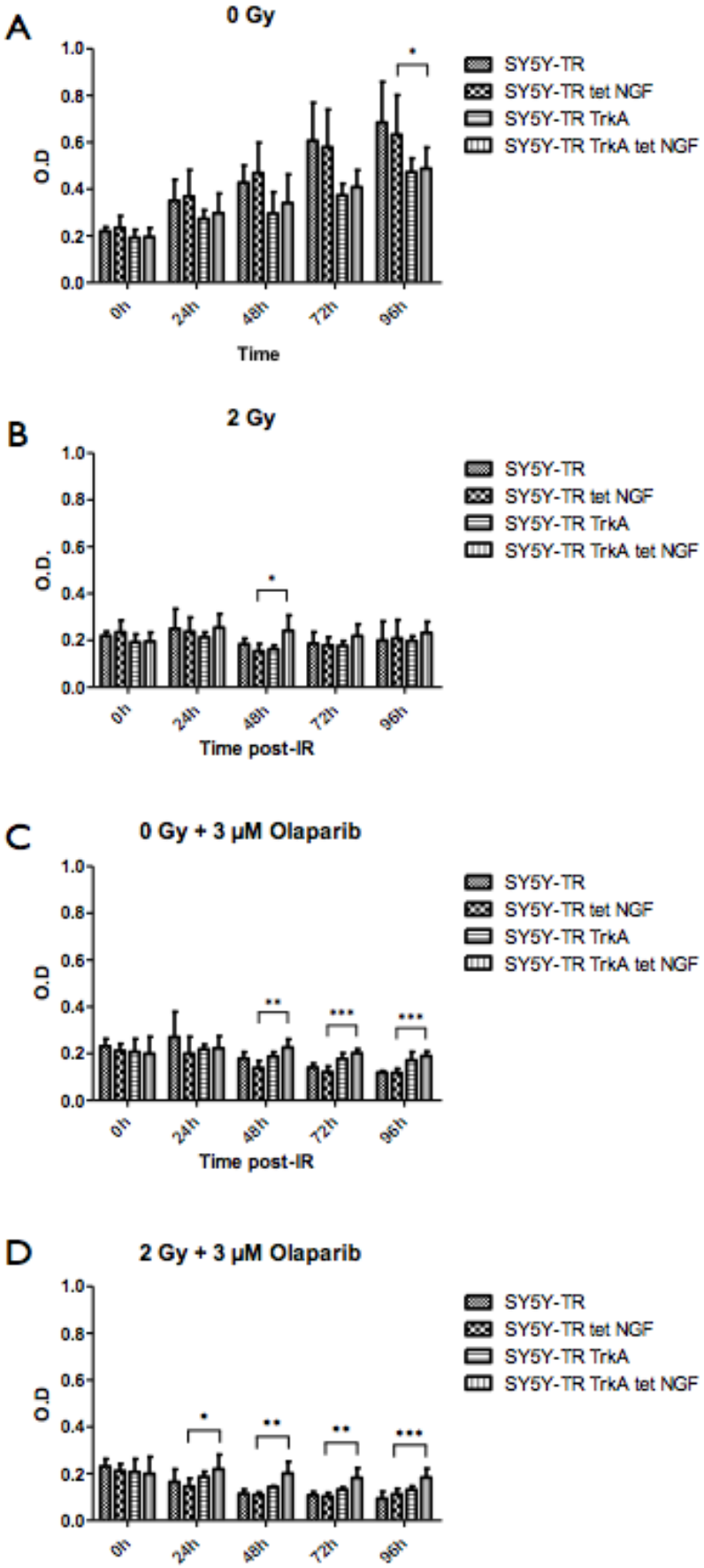
A
0 Gy
O.D
Time
SY5Y-TR
SY5Y-TR tet NGF
SY5Y-TR TrkA
SY5Y-TR TrkA tet NGF
B
2 Gy
O.D.
Time post-IR
C
0 Gy + 3 µM Olaparib
D
2 Gy + 3 µM Olaparib
0h
24h
48h
72h
96h

Figure 23: Cell Viability in response to PARP1-Inhibition by Olaparib

The metabolic activity of SY5Y cells with and without active TrkA/NTRK1-signaling was evaluated by MTT assay. SY5Y-TR +/- tet NGF showed higher viability at all time points compared to SY5Y-TR TrkA +/- tet NGF. (A). Viability of cells after irradiation with 2 Gy is visibly reduced with stagnating O.D. values at around 0.2 over the course of the 96-hour experiment. Viability was significantly higher in TrkA/NTRK1-positive cells at 48 hours post-IR (B). PARP1-inhibition leads to decreasing O.D. values in TrkA/NTRK1-negative vector controls after 72 hours of Olaparib treatment (24h time point), while cell viability of TrkA/NTRK1-positive cells is significantly better compared to SY5Y-TR tet NGF (C) Olaparib-treatment in combination with irradiation resulted in decreased viability of cell lines without TrkA/NTRK1-expression. SY5Y-TR TrkA tet NGF showed significantly higher O.D. values at all time points post-IR. Results of triplicate measurements from three independent experiments were used to calculate the indicated means and standard deviations (paired t-test, ***: $p < 0.001$, **: $p < 0.001$-0.01, *: $p = 0.01$-0.05).

The protective effect of TrkA/NTRK1-signaling against Olaparib toxicity was even more pronounced in irradiated SY5Y cells (Figure 23D). O.D. values of TrkA/NTRK1-negative cell lines are decreased at every time point after the addition of 3 µM Olaparib at 0 hours, signifying a decline in cell viability. Contrastingly, treatment with tetracycline and human β-NGF renders SY5Y-TR TrkA cells significantly more viable compared to cells without TrkA/NTRK1-expression at all time points post-IR.

7.5 TrkA/NTRK1-expression induces a G_2-checkpoint defect in SY5Y cells

Flow cytometric analyses of the cell cycle distribution of SY5Y transfectants were performed after exposing cells to IR. IR results in readily detectable cell cycle arrest and accumulation of cells at cell cycle checkpoints in G_1, S, and G_2 phases. Analysis of cells irradiated in G_2-phase was performed by evaluating the levels of H3pS10 to differentiate mitotic cells from cells in G_2-phase in the four differentially tetracycline- and NGF-treated samples. Striking differences in the mitotic indices (MI) were revealed for TrkA/NTRK1-positive and TrkA/NTRK1-negative SY5Y cells after irradiation with 1 Gy (Figure 24). A reduction in the fraction of mitotic cells from 1.6% before irradiation to 0.1% and 0.2 at 1h and 4 h, respectively, indicated an intact G_2-checkpoint in control cells in response to 1 Gy-IR. Contrastingly, TrkA/NTRK1-positive cells demonstrated a defect in the early G_2 checkpoint by displaying higher fractions of mitotic cells following IR, as the fraction of mitotic cells decreased from 0.95% to 0.55% at 1h and to 0.48% 4h post-IR, respectively.

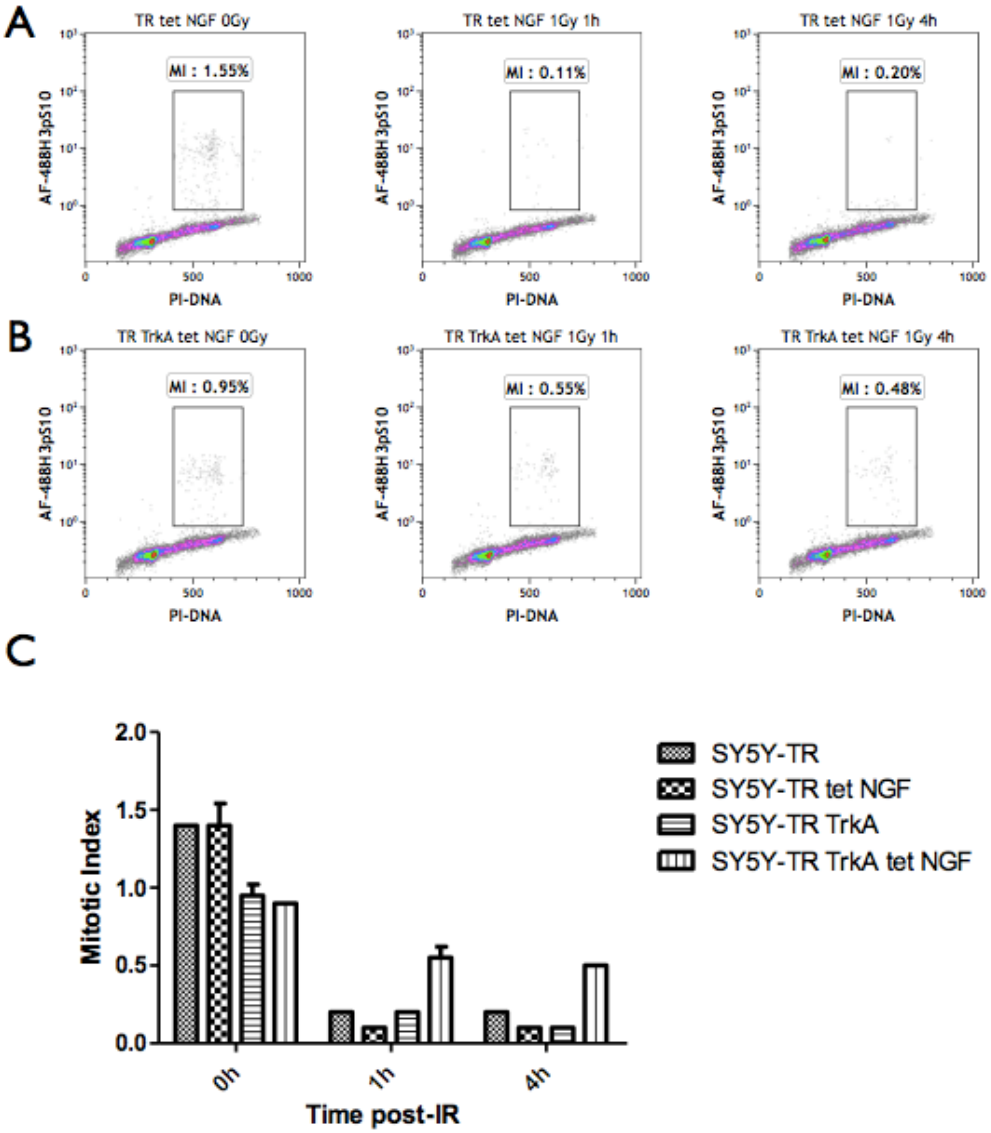

Figure 24: Mitotic Indices of SY5Y transfectants after irradiation with 1 Gy

The mitotic indices (MI) of SY5Y transfectants was analyzed by H3pS10 staining. Histograms of SY5Y-TR tet NGF cells with gated H3pS10-fraction are shown at 0h, 1h and 4h after irradiation with 1 Gy (A). The mitotic index of TrkA/NTRK1-positive cells at 1h and 4h post-IR was reduced by only 50%, while IR resulted in a 70-80% reduction in TrkA/NTRK1-negative cells (A, B). Mitotic fractions were determined in two independent experiments and error bars represent the standard deviation (C).

Interestingly, the defect in G_2-checkpoint was visible only in tetracycline + NGF-treated TrkA/NTRK1 transfectants, while the same cell line displays an IR-response in line with an intact G_2-checkpoint in the absence of NGF. This suggests that the G_2-checkpoint defect is a direct consequence of active TrkA/NTRK1-signaling.

In order to evaluate a possible dose-dependence of the defect in the early G2-checkpoint, mitotic indices were analyzed in the same experimental set-up after 4 Gy-IR (Figure 25).

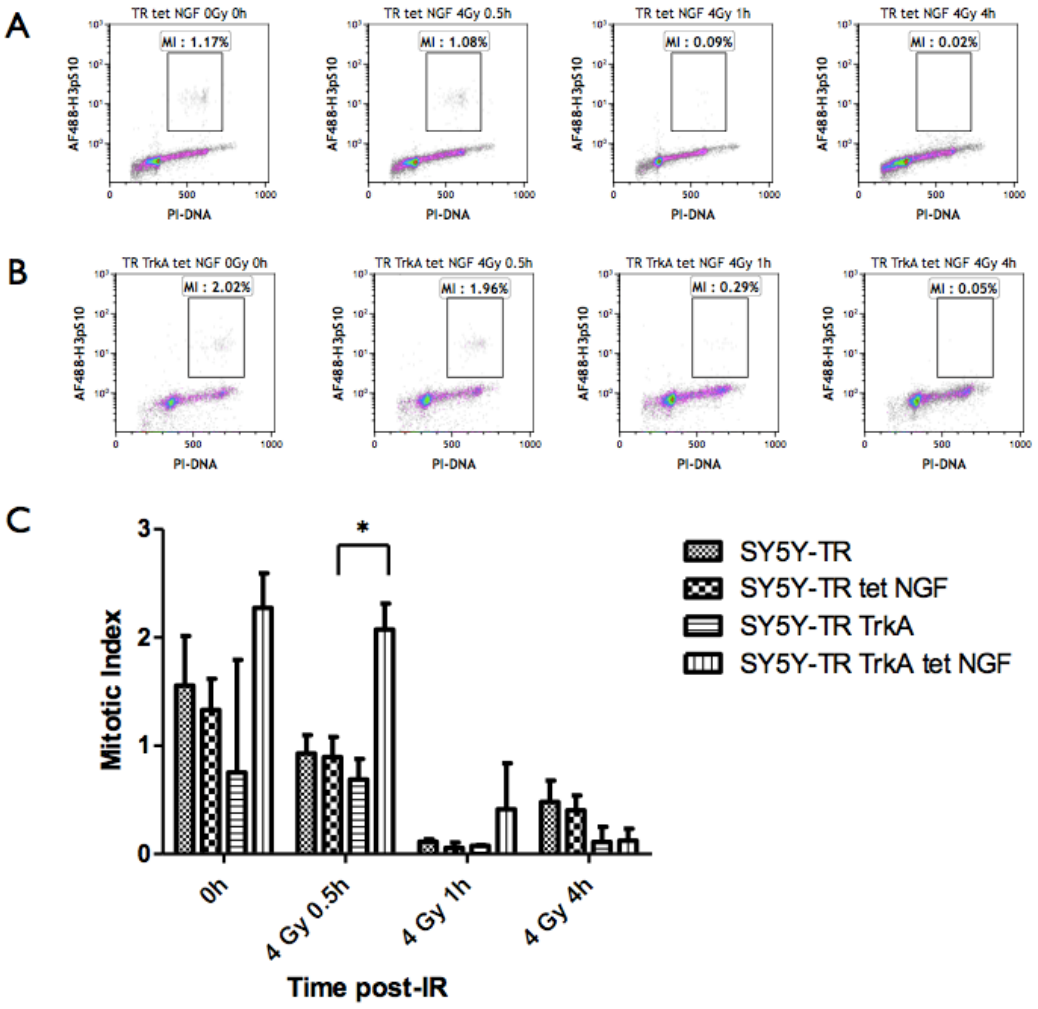

Figure 25: Mitotic Indices of SY5Y transfectants after irradiation with 4 Gy

The mitotic fraction of SY5Y cells with and without expression of TrkA/NTRK1 was analyzed by determining the phosphorylation status at Serine 10 of Histone H3. Histograms of SY5Y-TR tet NGF cells stained with H3pS10 are shown. Inserts indicate cells positively staining for H3pS10 at 0h, 0.5h, 1h and 4h after irradiation with 4 Gy (A). The mitotic index (MI) was higher for TrkA/NTRK1-positive cells (B) at all time points, except at 4 hours post-IR. SY5Y cells with active TrkA/NTRK1-signaling had a higher fraction of mitotic cells and this reached statistical significance at 0.5h post-4 Gy-IR (paired t-test, p=0.029). Mitotic fractions were determined in three independent experiments and error bars represent the standard deviation (C).

Mitotic indices of cells post 4 Gy-IR also pointed to a defective G_2-checkpoint in TrkA/NTRK1-positive cells. TrkA/NTRK1-positive SY5Y cells had a significantly higher proportion of mitotic cells compared to controls (SY5Y-TR tet NGF) at 30 min post-4 Gy-IR (t-test, p=0.029), while TrkA/NTRK1-negative cell lines had an intact G_2-checkpoint indicated by a decrease in the mitotic fraction of cells. At 1h post-IR, TrkA/NTRK1-negative cells showed an almost complete regression of mitotic cells (0.09%) corresponding to an

intact G_2-checkpoint, while TrkA/NTRK1-positive cells still had elevated numbers of mitotic cells (0.3%). Four hours after irradiation with 4 Gy, SY5Y-TR and SY5Y-TR tet NGF showed already increasing numbers of mitotic cells hinting at recovery after G_2-checkpoint induction (Figure 25C), while at this time point TrkA/NTRK1-positive cells have virtually no cells in mitosis (MI= 0.05%). In order to analyze the G_2-checkpoint response of cells irradiated during the S-phase of the cell cycle, PI-staining was employed after 1 and 4 Gy-IR. After 1 Gy-IR less TrkA/NTRK1-positive cells were found in G_2-phase at 0h and 1h post-IR, while no difference was detected between TrkA/NTRK1-positive and TrkA/NTRK1-negative cells at 4h post-IR (Figure 26C).

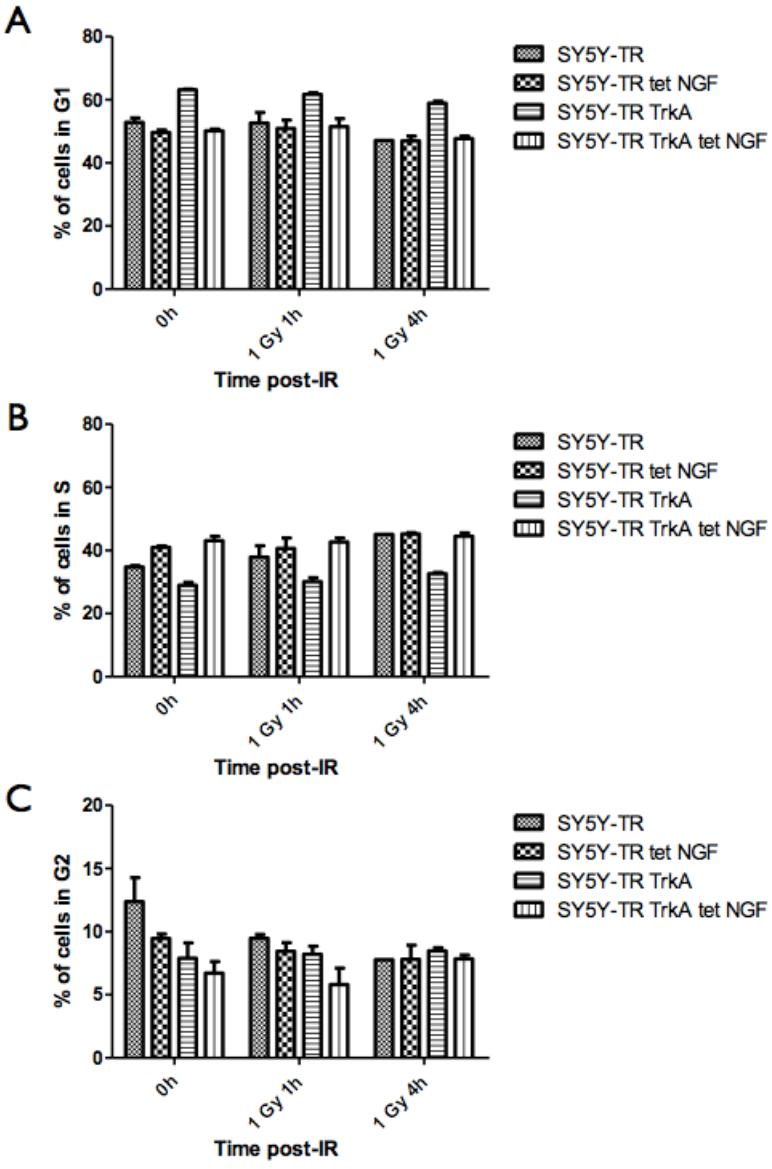

Figure 26: Cell cycle distribution after irradiation with 1 Gy

Cell cycle distribution of irradiated SY5Y transfectants was analyzed at 0h, 1h and 4h post-IR with 1 Gy. SY5Y-TR TrkA cells presented with less cells in G_1- and more cells in S-phase at all time points irrespective of irradiation (A, B). While the fraction of cells in G_2-phase differed between all transfectants at 0h and 1h post-IR, at t= 4h post-IR the fraction of cells in G_2-phase were comparable irrespective of TrkA/NTRK1 status (C). The cell cycle distribution was determined in two independent experiments and error bars represent the standard deviation thereof.

By contrast, TrkA/NTRK1-positive cells had >10 % of cells in G_2-phase at all time points analyzed following 4 Gy-IR (Figure 27), while TrkA/NTRK1-negative cells had very low numbers (<6%) of cells in G_2-phase at 0h, 0.5h and 1h post-IR, and a complete absence of cells in G_2-phase at 4h post-IR.

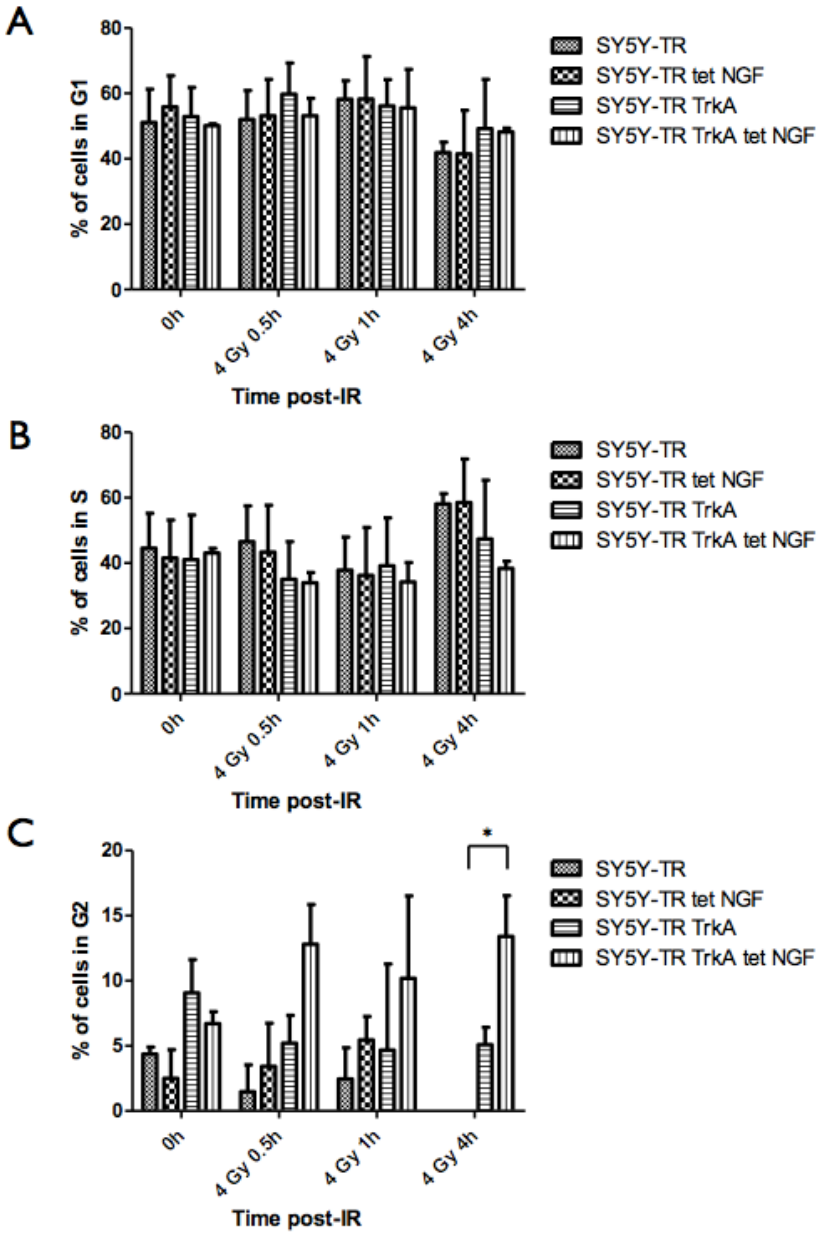

Figure 27: Cell cycle distribution after irradiation with 4 Gy

Cell cycle distribution of irradiated SY5Y transfectants was analyzed using PI staining at 0h, 0.5h, 1h and 4h post-IR with 4 Gy. While distribution of cells in G_1- and S-phase were similar for all conditions, TrkA/NTRK1-expressing SY5Y presented with more cells in G_2-phase, which was significant at 4h after 4 Gy-IR, when SY5Y TR and SY5Y-TR tet NGF cells completely lacked G_2-phase. The cell cycle distribution was determined in three independent experiments and error bars represent the standard deviation (*: p = 0.01-0.05).

The data gained from the PI-staining complements the analysis of MIs by confirming the hypothesized G_2-checkpoint deficiency in TrkA/NTRK1-positive SY5Y cells. Analysis of cells irradiated during G_2-phase as monitored by H3pS10 staining allowed for discriminating mitotic cells from S-phase cells. The data showed significantly elevated numbers of mitotic

cells in TrkA/NTRK1-positive cells compared to TrkA/NTRK1-negative sample at both 1 and 4 Gy-IR. The analysis of cell cycle distribution by PI-staining of the DNA content confirmed the elevated numbers of cells in G_2-phase in TrkA/NTRK1-positive cells upon TrkA/NTRK1-activation after 4 Gy-IR.

8. TrkA/NTRK1-expression in *MYCN*-amplified neuroblastoma cell lines

MYCN-amplification and TrkA/NTRK1-over-expression are mutually exclusive in neuroblastoma. Amplification of *MYCN* is the single most devastating prognostic factor in neuroblastoma outcome. Contrastingly, *TrkA/NTRK1*-expression is associated with a very good prognosis with many patients not receiving any treatment at all. Furthermore, in neuroblastomas with normal *MYCN* expression elevated TrkA/NTRK1 levels can improve the 5-year cumulative survival rate by 37% [224]. In order to elucidate the underlying causes for these two factors being anti-correlated and associated with opposing outcomes, we have analyzed gene expression data from primary neuroblastomas for other genes that are anti-correlated with *MYCN* mRNA expression (Figure 28).

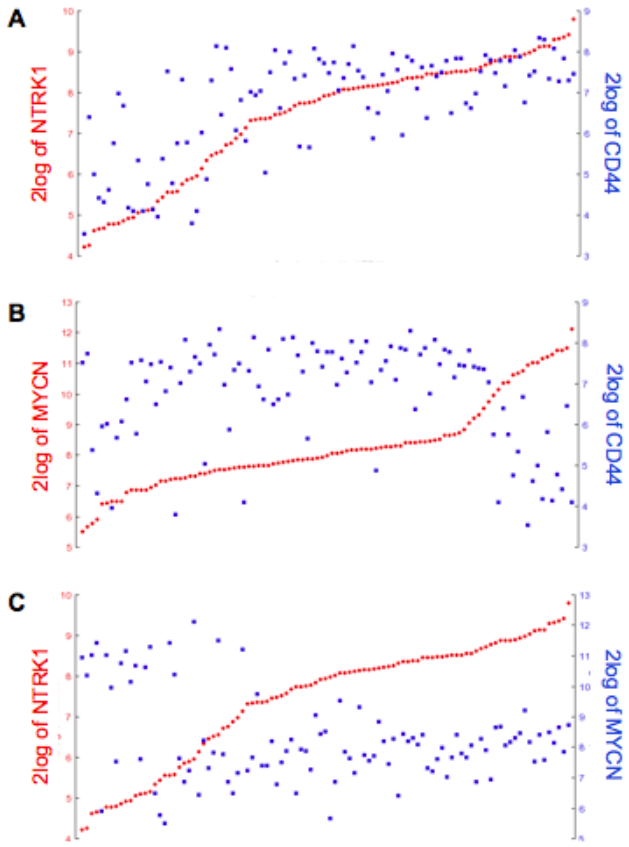

Figure 28: Pairwise correlation of mRNA expression for *TrkA/NTRK1*, *CD44* and *MYCN*.
Gene expression data are derived from a previously published data set using primary NBs (n=113, GSE32664, [253, 254]). Each circle represents an expression value of the indicated gene in one tumor. Expression levels of *CD44* mRNA were significantly correlated with *TrkA/NTRK1* in primary NBs (A, $p=6.2e^{-18}$). Contrastingly, *MYCN* mRNA levels are highest in tumors with low *CD44*- (B, $p=1.3e^{-4}$) or *TrkA/NTRK1*- (C, $p=1.6e^{-4}$) expression and the inverse correlation is also significant.

An additional factor that has been shown to be anti-correlated with *MYCN* and associated with disease outcome in neuroblastoma is the cell surface glycoprotein *CD44*. Microarray-based analysis of primary neuroblastomas confirmed these findings for our own patient cohort *in vivo* [253]. A search for TrkA/NTRK1-correlated genes revealed that tumors with high levels of TrkA/NTRK1 also expressed CD44 at high levels (Figure 28A). In contrast, expression of *MYCN* is inversely correlated with both *CD44*- (Figure 28B) and *TrkA/NTRK1*-expression (Figure 28C).

8. 1 TrkA/NTRK1 activation induces CD44 expression in vitro

Expression of *CD44* mRNA was analyzed in response to expression of TrkA/NTRK1 in our conditional SY5Y model system. SY5Y-TR TrkA transfectants were left untreated or subjected to 48 hours of tetracycline treatment followed by 24 hours of both tetracycline- and NGF-treatment to ensure both TrkA/NTRK1 expression and activation. Up-regulation of *CD44* mRNA could only be demonstrated for TrkA/NTRK1-expressing cells upon TrkA/NTRK1-activation by NGF suggesting that CD44 is a downstream target of TrkA/NTRK1 (Figure 29).

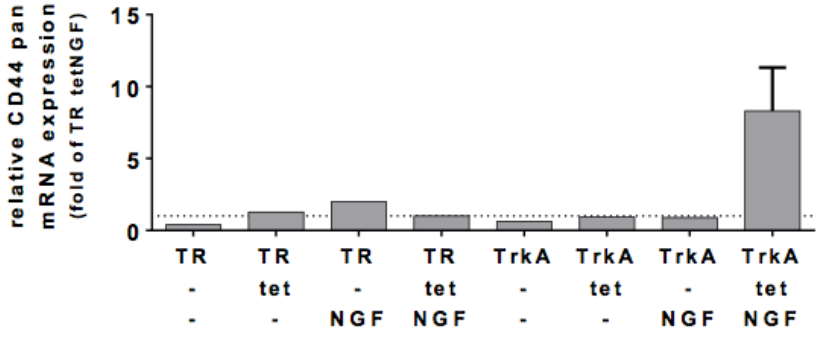

Figure 29: Expression of *CD44* mRNA as analyzed by real-time PCR.

CD44 mRNA levels were determined in SY5Y neuroblastoma cell lines, which were either transfected with a control vector (TR) or genetically engineered to express TrkA/NTRK1 (TrkA) upon treatment with NGF, tetracycline (tet), or both as indicated. Expression values of pan-*CD44* were normalized to the control SY5Y-TR tet NGF (dotted line). Real-time PCR for *CD44* was done by A. Schütze (HHU Düsseldorf). Values were determined in 4 independent experiments and error bars represent the standard deviation.

Expression of CD44 protein was subsequently analyzed by immunohistochemistry and FACS analysis. SY5Y-TR and SY5Y-TR TrkA cells were left untreated or treated with NGF + tetracycline for 24 hours before analysis by fluorescence microscopy (Figure 30A-D). Again,

CD44 expression could be observed in SY5Y cells with activated TrkA/NTRK1 (Figure 30D). Further up-regulation of CD44 on the cell surface was demonstrated by FACS analysis after combined treatment with tetracycline + NGF for 48 and 72 hours (Figure 30E).

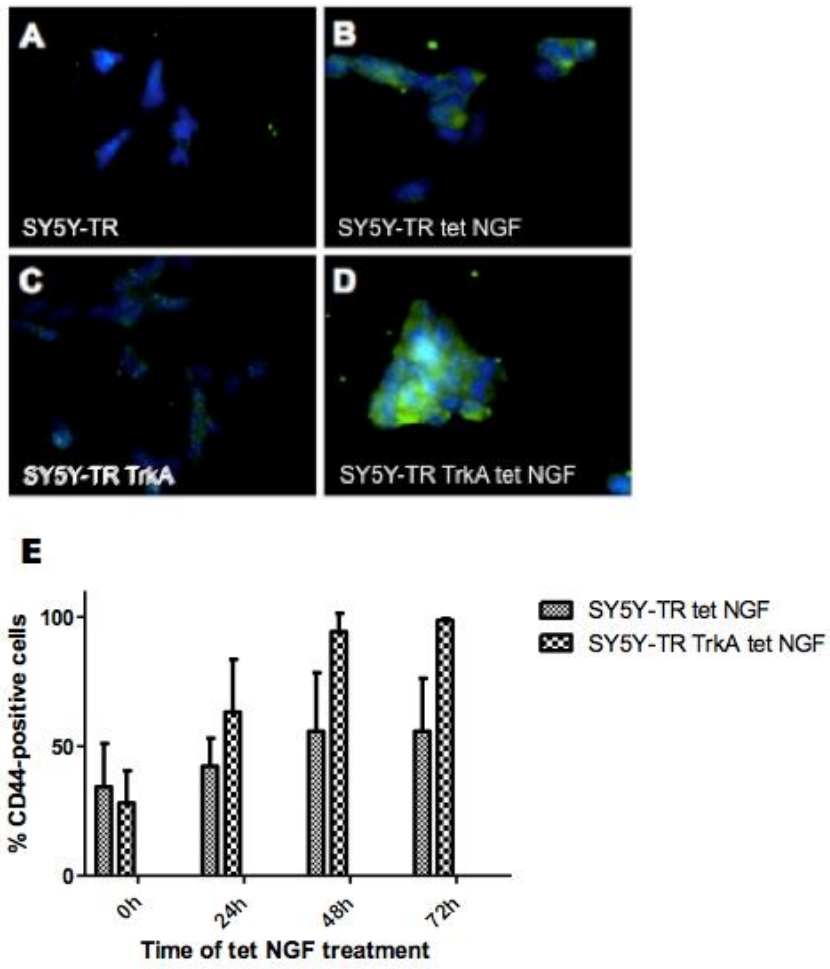

Figure 30: Protein expression of CD44 as shown by immunohistochemistry and FACS analysis.
Up-regulation of CD44 on the cell surface was demonstrated in SY5Y with expression and activation of TrkA/NTRK1 (D) in comparison to SY5Y-TR TrkA cells without *TrkA/NTRK1*-induction (C), untreated (A) and tetracycline + NGF-treated (B) control cell line SY5Y-TR (IHC for CD44 was done by A. Schütze (HHU Düsseldorf). FACS-analysis of CD44-expression demonstrated TrkA/NTRK1-dependent up-regulation of CD44 that increased over time (E). Percentages of CD44-protein levels were determined in three independent experiments and error bars represent the standard deviation thereof.

As SY5Y neuroblastoma cells are diploid for *MYCN*, we also wanted to provide a cellular model system to analyze TrkA/NTRK1-MYCN interactions in the context of *MYCN*-amplification. For this purpose, we incorporated the already established *MYCN*-amplified neuroblastoma cell line IMR5 (generated and provided by Dr. S Lindner and Dr. S. Schulte

from the group of Prof. J.H. Schulte, UK Essen), and independently raised a second TrkA/NTRK1-expressing *MYCN*-amplified cell line, NGP, which are both also devoid of endogenous TrkA/NTRK1. The identical expression cassette system as used for SY5Y cells was chosen to express TrkA/NTRK1 in NGP and IMR5 cells.

8.2 Conditional TrkA/NTRK1-expression in *MYCN*-amplified neuroblastoma cell lines

Conditional expression of TrkA/NTRK1 in response to tetracycline was verified by real-time PCR for both NGP and IMR5 cells. Vector control and TrkA/NTRK1-transfectants were left untreated or treated with 1 µg/ml tetracycline and 100ng/ml human β-NGF for 72 hours.
NGP-TR cells were TrkA/NTRK1-negative both in the absence or presence of tetracycline. NGP-TR TrkA cells expressed TrkA/NTRK1 mRNA in the absence of tetracycline, but expression could be significantly increased (p=0.02) by tet NGF treatment (Figure 31A). Levels of TrkA/NTRK1 mRNA are very low in IMR5 vector controls and the untreated TrkA-transfectant. Treatment with tetracycline and NGF increased TrkA/NTRK1-expression only in the cells harboring the plasmid with human *TrkA/NTRK1* cDNA (Figure 31B).

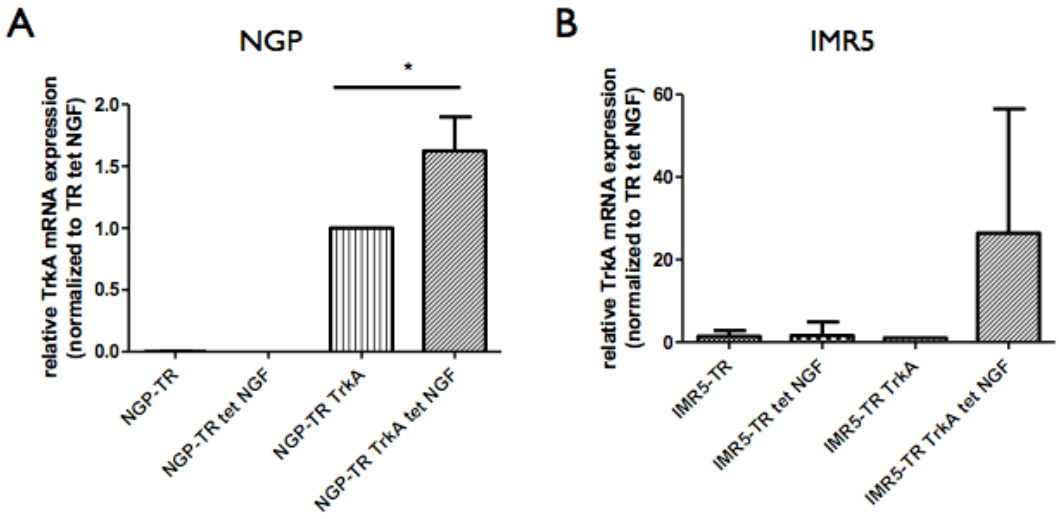

Figure 31: Conditional expression of TrkA/NTRK1 in the MYCN-amplified Cell lines, NGP and IMR5
Up-regulation of *TrkA/NTRK1* mRNA in response to tetracycline was established for both MYCN-amplified neuroblastoma cell lines, NGP and IMR5. A significant increase in *TrkA/NTRK1* mRNA levels was demonstrated in tetracycline-treated NGP-TR TrkA cells compared to the untreated control. *TrkA/NTRK1* levels are not detectable in the vector controls (NGP-TR) of this cell line (A). IMR5 cells showed up-regulated *TrkA/NTRK1* mRNA in tetracycline-treated TrkA/NTRK1-transfectants only, while the untreated, transfected control and both vector controls show only very low *TrkA/NTRK1*-expression (B). Values were determined by triplicate measurements in four independent experiments (paired t-test, *: $p < 0.05$).

MYCN-amplified cell lines were then tested for tetracycline-induced protein expression of TrkA/NTRK1 (Figure 32). Western Blot of protein lysates from differentially treated vector controls and TrkA/NTRK1-transfectants revealed TrkA/NTRK1 staining in NGP-TR TrkA and IMR5-TR TrkA after treatment with NGF and tetracycline, while Vector controls (NGP-TR and IMR5-TR) were TrkA/NTRK1-negative irrespective of treatment with tetracycline and NGF. In line with the mRNA data, low TrkA/NTRK1 expression is present already in non-induced NGP-TR TrkA cells while expression of TrkA/NTRK1 is limited to the tetracycline-treated TrkA-transfectant in IMR5 transfectants (Figure 32).

Figure 32: TrkA/NTRK1 is up-regulated in response to tetracycline treatment in NGP and IMR5 transfectants

TrkA/NTRK1 protein expression of *MYCN*-amplified cell lines engineered for conditional TrkA/NTRK1-expression was evaluated by Western Blot. NGP-TR TrkA and IMR5-TR TrkA show TrkA/NTRK1 protein bands at 140 kDa in response to tetracycline + NGF treatment with low level TrkA/NTRK1 expression also detectable in untreated NGP-TR TrkA cells.

Induction of *CD44* mRNA in response to TrkA/NTRK1-activation was then analyzed in NGP-TR TrkA and IMR5-TR TrkA. The cell lines were left untreated or subjected to treatment with 1 µg/ml tetracycline and 100 ng/ml human β-NGF for 72 hours before harvesting cells and performing RNA isolation and cDNA synthesis. The levels of *CD44* mRNA were then determined in comparison to the vector controls NGP-TR, IMR5-TR and the untreated NGP-TR TrkA and IMR5-TR TrkA cells (Figure 33).

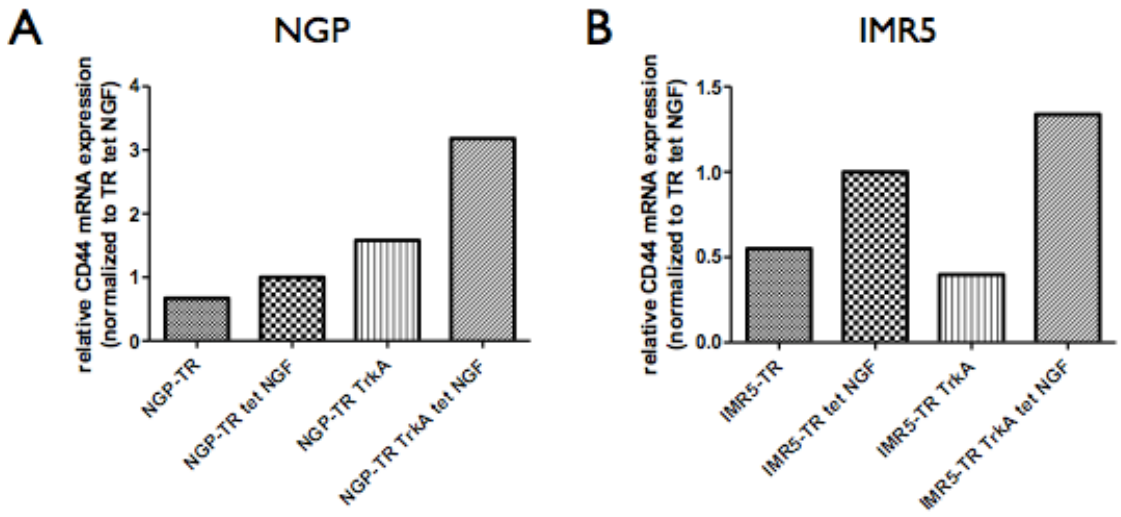

Figure 33: NGP neuroblastoma cells engineered to conditionally express TrkA/NTRK1 upregulate *CD44*
Inducible TrkA/NTRK1 expression in NGP neuroblastoma cells resulted in > 4-fold induction of *CD44* mRNA upon activation of TrkA/NTRK1 (achieved by 24-hour-treatment with tetracycline and NGF). Up-regulation of *CD44* in IMR5- cells was less pronounced, as *CD44* expression also increased two fold upon tet + NGF treatment in control cells (B). Ct-values were determined in triplicates in one experiment and this was performed in cooperation with A.Schütze, HHU Düsseldorf.

Levels of *CD44* mRNA were increased in NGP-TR TrkA cells after induction and activation of TrkA/NTRK1 by tetracycline and human β-NGF compared to the TrkA/NTRK1-negative control cell lines. Additionally, TrkA/NTRK1-transfectants of IMR5 cells also displayed higher levels of *CD44* mRNA in response to activation of TrkA/NTRK1.

8.3 MYCN is down-regulated in NGP and IMR5 with TrkA/NTRK1 over-expression

NGP- and IMR5-derivatives with conditional TrkA/NTRK1-expression were further analyzed to evaluate a possible effects of TrkA/NTRK1-signaling on MYCN expression. MYCN protein levels were therefore determined in NGP and IMR5 cell lines with and without expression of TrkA/NTRK1 (Figure 34). Cells were left untreated or were treated with tetracycline for 72 hours before protein lysates were prepared.

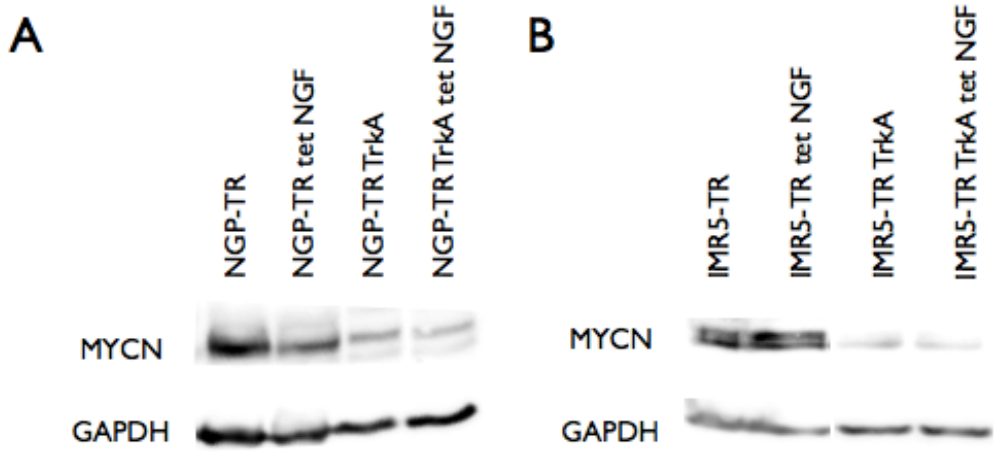

Figure 34: MYCN protein is down-regulated in response to TrkA/NTRK1-signaling

MYCN protein expression was analyzed in the *MYCN*-amplified NGP- and IMR5-transfectants. The vector controls, NGP-TR and IMR5-TR, had high levels of MYCN irrespective of treatment with tetracycline and NGF. Down-regulation of MYCN protein was observed in TrkA/NTRK1-transfectants, especially in response to TrkA/NTRK1-activation (tet NGF) in NGP- (A) and IMR5-TR TrkA (B).

High levels of MYCN protein were detected in *MYCN*-amplified cell lines expressing the control vector only (NGP-TR and IMR5-TR) with and without tet NGF-treatment. TrkA/NTRK1-transfectants of both cell lines presented with reduced MYCN protein levels in comparison to the vector controls. Further reduction of MYCN was detected upon tetracycline-induction and activation of TrkA/NTRK1 by human β-NGF.

8.4 Proliferation of *MYCN*-amplified neuroblastoma cells with TrkA/NTRK1-signaling is decreased *in vitro*

In order to further analyze the effect of TrkA/NTRK1-signaling in *MYCN*-amplified cell lines, proliferation of NGP- and IMR5-transfectants was evaluated in the presence and absence of TrkA/NTRK1 expression. Cells were seeded in 12-well dishes at a density of 50000 cells per well and differentially treated with 1 µg/ml tetracycline and 100 ng/ml human β-NGF at the time of seeding. The assay was stopped after 72 hours and cell numbers were determined by counting (Figure 35).

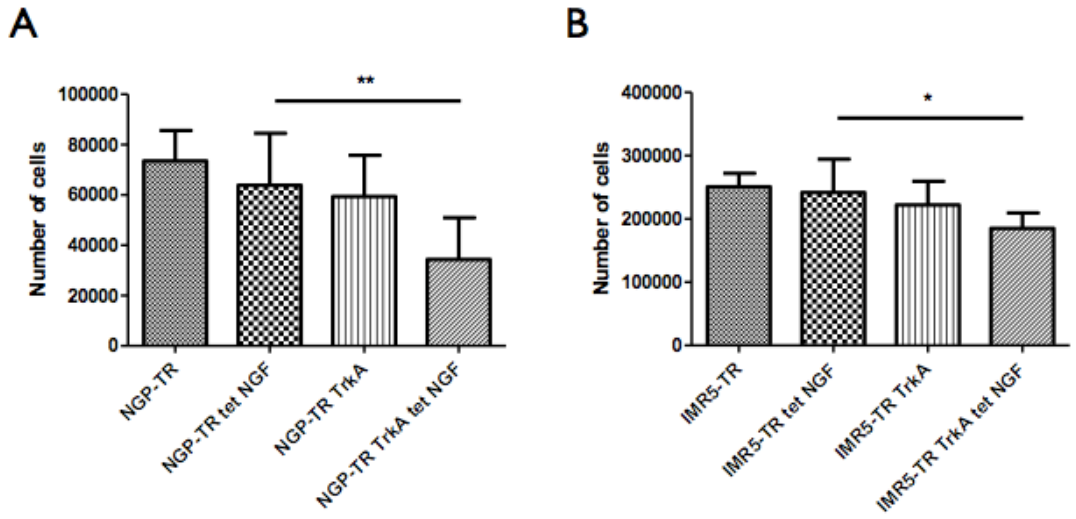

Figure 35: Proliferation of *MYCN*-amplified neuroblastoma cell lines is decreased in the presence of TrkA/NTRK1-signaling

Proliferation rates of NGP- and IMR5-transfectants were evaluated in cells with and without active TrkA/NTRK1 signaling. NGP-TR TrkA cells showed significantly lower cell numbers after 72h of treatment with tetracycline and NGF compared to the vector control cell line with the same treatment (n=5) (A). Proliferation of TrkA/NTRK1-negative IMR5 cells was higher compared to the cells with induction of TrkA/NTRK1. A direct comparison between IMR5-TR tet NGF and IMR5-TR TrkA tet NGF revealed significantly decreased cell numbers in response to TrkA/NTRK1-expression (n=3) (B). Significant differences were determined by a paired t-test and error bars represent the standard deviation of all measurements. Experiments were performed in cooperation with A. Schütze, HHU Düsseldorf.

Active TrkA/NTRK1-signaling led to a reduction of cell proliferation in NGP- and IMR5-transfectants. Numbers of the three TrkA/NTRK1-negative NGP vector control cells increased over time (Figure 35A), while TrkA/NTRK1-positive NGP cells showed significantly lower proliferation rates compared to NGP-TR tet NGF ($p = 0.0085$). Proliferation dropped significantly in TrkA/NTRK1-expressing IMR5 transfectants compared to the vector control cell line IMR5-TR receiving the same treatment (tet NGF, ($p = 0.02$) Figure 35B).

8.5 Clonogenic survival of NGP and IMR5 is reduced in TrkA/NTRK1-over-expressing subclones

MYCN-amplification in neuroblastoma is associated with aggressive disease and poor prognosis, while simultaneous expression of TrkA/NTRK1 and MYCN in primary neuroblastoma resulted in significantly better 5-year cumulative survival rate in *MYCN*-amplified tumors (Figure 10, [224]). Clonogenic survival was evaluated to determine the

impact of TrkA/NTRK1 on the ability of a *MYCN*-amplified neuroblastoma cells to form colonies. Cells were seeded at a density of 600 cells in a 6-well dish and were differentially treated with tetracycline and NGF at the time of seeding. Dishes were incubated at 37°C until colonies consisted of at least 50 cells. Colony numbers were determined by Crystal Violet-staining and the plating efficiency was calculated by dividing colony numbers by the number of cells seeded at the beginning of the experiment (Figure 36).

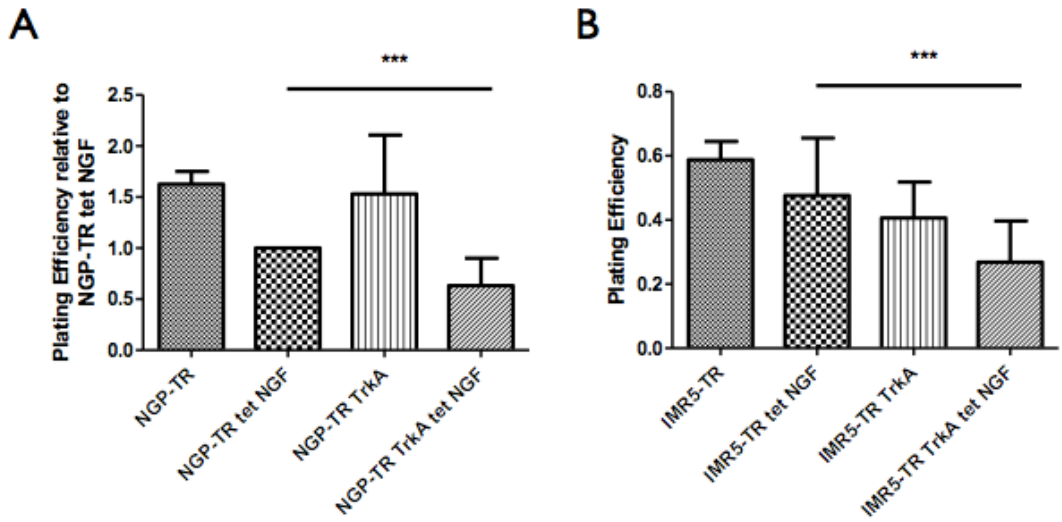

Figure 36: TrkA/NTRK1-activation reduced clonogenic survival of *MYCN*-amplified neuroblastoma cell lines

The ability to form colonies was evaluated in *MYCN*-amplified cell lines with and without active TrkA/NTRK1-signaling. NGP-TR TrkA cells showed a significantly decreased clonogenic survival after treatment with tetracycline and NGF in comparison to the vector control cells that received the same treatment ($p < 0.0001$) (A). Furthermore, the ability to form colonies was also significantly reduced in TrkA/NTRK1-expressing IMR5 cells compared to the respective vector control ($p = 0.0001$) (B). Plating efficiencies were determined in triplicate in 3 independent experiments. A paired t-test was used to calculate significance for differences. Values are plotted +/- standard deviation.

Plating efficiency of NGP transfectants was evaluated in relation to NGP-TR tet NGF, since plating efficiencies varied between experimental rounds. While the plating efficiency of NGP-TR and NPG-TR TrkA were very similar, treatment with tetracycline and NGF was associated with a decrease in clonogenic survival in both transfectants. However, colony formation in NGP-TR TrkA tet NGF was significantly reduced in comparison to NGP-TR tet NGF ($p<0.0001$, Figure 36A). In line with the findings in NGP cells, TrkA/NTRK1-expression causes a significant decrease in clonogenic survival compared to the tetracycline- and NGF-treated vector control in IMR5 cells, too (Figure 36B).

Taken together, these experiments demonstrated CD44 up-regulation can be achieved by expression and activation of TrkA/NTRK1, even in a cellular background with high MYCN levels. Furthermore, TrkA/NTRK1-overexpression in *MYCN*-amplified neuroblastoma cell lines resulted in a decrease in MYCN protein levels and coincided with a reduction in proliferation and clonogenic survival of otherwise rapidly growing cells.

Discussion and Outlook

9. The role of TrkA/NTRK1 in the DNA damage response of neuroblastoma cells

High ectopic expression of TrkA/NTRK1 in neuroblastoma cells causes auto-phosphorylation and thereby auto-activation of TrkA/NTRK1. TrkA/NTRK1-signaling induces differentiation or apoptosis in the presence or absence of its specific ligand human β-NGF, respectively, which leads to a reduction in cell viability and proliferation, and puts selective pressure on TrkA/NTRK1-expressing cells. To overcome this limitation of stably TrkA/NTRK1-expressing cells, an inducible TrkA/NTRK1-expressing system was generated. This project aimed to evaluate the consequences of short-term expression of TrkA/NTRK1 in neuroblastoma cells using tet-conditional cellular systems.

Previous results have suggested a possible role of TrkA/NTRK1-expression in the DNA damage response of neuroblastoma cell lines in stably TrkA/NTRK1-expressing SY5Y neuroblastoma cells [126]. To further elucidate the impact of TrkA/NTRK1 in the DNA damage response, a tetracycline conditional vector system was used to evaluate immediate effects of TrkA/NTRK1-expression in SY5Y neuroblastoma cells regarding DNA repair kinetics, expression of DSB repair factors, and cell viability after ionizing radiation.

9.1 TrkA/NTRK1 expression alters IR dose response and DNA repair kinetics

DNA repair kinetics were evaluated using pulsed-field gel electrophoresis (PFGE) and 53BP1-assay. For the PFGE-assay cells were irradiated at high doses of 20 Gy to induce fragmentation of DNA. PFGE-analyses of SY5Y cells showed the highest values for the fraction of DNA released into the well (FDR) at all doses (10, 20 and 30 Gy) for TrkA/NTRK1-expressing cells, corresponding to a higher level of DNA fragmentation. Furthermore, at 0.5h after irradiation TrkA/NTRK1-positive cells were slower to repair fragmented DNA, suggesting a delayed induction of DNA repair compared to the TrkA/NTRK1-negative control cell lines. The limitations in using high doses of irradiation to generate DSBs are the risk of inducing cell death and thereby causing secondary double-strand breaks. Furthermore, pulsed-field gel electrophoresis is generally used to separate very large fragments of DNA in the range of several hundred kilo base pairs (kbp), but IR may also produce clustered double-strand breaks resulting in small DNA fragments that are missed in PFGE leading to an underestimation of the amount of total DSB generated [255].To compensate for these limitations, assays based on radiation-induced foci (RIF) formation were additionally employed to analyze DNA-repair kinetics of TrkA/NTRK1-positive and

TrkA/NTRK1-negative SY5Y cells at low doses of irradiation (1 Gy). RIF-based assays take advantage of the accumulation of proteins involved in the DNA damage response at DSB sites. Immunofluorescence imaging allows for quantitation of RIF at very low doses of irradiation, serving as a very sensitive assay determining DNA repair capacity and kinetics. Here, the mediator protein 53BP1 was used as a surrogate marker for double-strand breaks in SY5Y neuroblastoma transfectants. The numbers of 53BP1-foci were quantified at 0h, 1h, 5h and 24 hours after irradiation with 1 Gy. All four SY5Y transfectants showed an appropriate DNA damage response by maximum 53BP1-foci appearance at 0.5h post-IR. However, the number of 53BP1-foci was significantly smaller in tet NGF-treated TrkA/NTRK1-transfectants compared to the vector control with the same treatment. Decay of most of the 53BP1-foci is observed at 5h after irradiation until foci numbers are at background levels 24h post-IR. Interestingly, only TrkA/NTRK1-expressing SY5Y cells presented with a significantly higher amount of residual 53BP1 foci suggesting a less effective or erroneous DNA damage response.

The significantly smaller numbers of 53BP1-foci observed in TrkA/NTRK1-expressing cells early after IR may correspond to a delay in the DNA damage response, which is corroborated by a delay in the initiation of DNA repair observed in PFGE. Here, TrkA/NTRK1-positive cells showed a higher degree of DNA fragmentation at 0.5h-post IR compared to TrkA/NTRK1-negative cells. If TrkA/NTRK1-expression caused a compromised initial DNA damage response, signaling inducing DNA repair would also be expected to be impaired. At the end point of the 53BP1-assay, TrkA/NTRK1-positive cells had a significantly higher amount of residual foci (n=1.4) compared to TrkA/NTRK1-negative cells (n=0.5). This might suggest a less efficient DNA repair in response to TrkA/NTRK1-expression, but it has to be considered, that 53BP1-foci are also associated with replicative stress.

Double-strand breaks are precursors of chromosomal translocations and the main repair pathways for the processing of DSBs are NHEJ and homologous recombination repair (HRR). Our previously published data showing up-regulation of the C-NHEJ-factor XRCC4 in stably TrkA/NTRK1-overexpressing SY5Y cells [126] was thought be linked to the previously described association of TrkA/NTRK1-expression and genomic integrity observed *in vivo* and *in vitro*. The analysis of manifest chromosomal aberrations such as translocations and chromosome breaks serves to evaluate short-term TrkA/NTRK1-signaling in the maintenance of genomic integrity in response to IR. While chromosomal aberrations such as chromatid breaks (CB) may be classified as unrepaired DNA damage, translocations have been formed

through defective processing of DNA breakage ends. A translocation assay scoring metaphase chromosomes for chromatid breaks and chromosomal translocations after 4h post-1 Gy-IR did not reveal significant variations in the numbers of chromosomal aberrations between TrkA/NTRK1-positive and TrkA/NTRK1-negative SY5Y cells. The number of translocations was overall very low, with only two translocations present in all 60 metaphases analyzed. Chromatid breaks were found at similar frequency in TrkA/NTRK1-negative and TrkA/NTRK1-positive cells. This is in line with the results gained from the PFGE and 53BP1-assays: while the initial DNA damage response was slower as deduced from the PFGE-assay, DNA repair was identical in all cell lines at later time points and resulted in the same reduction in DNA fragmentation. This corresponds to the genomic integrity observed in the chromosome translocation assay at 4h post-IR and suggests that TrkA/NTRK1-signaling does not affect robustness of the DNA repair capacity in SY5Y cells.

9.2 TrkA/NTRK1 confers resistance to the PARP1-Inhibitor Olaparib

PARP1 expression was found to be up-regulated in TrkA/NTRK1-positive cells in experiments addressing the impact of TrkA/NTRK1-signaling on protein levels of DSB repair factors. However, PARP1 up-regulation was not consistently reproducible in TrkA/NTRK1-positive cells. In order to evaluate a role for TrkA/NTRK1 in regulating PARP1, cell viability of TrkA/NTRK1-positive and –negative SY5Y cells was analyzed with and without treatment with the PARP-Inhibitor Olaparib. Additionally, cells were subjected to irradiation with 2 Gy or left un-irradiated to analyze the effect of PARP-inhibition after IR.

Cell viability was reduced in all transfectants in response to irradiation and/ or treatment with Olaparib. However, TrkA/NTRK1-expression rescued SY5Y cells from Olaparib-induced cell killing compared to TrkA/NTRK1-negative controls. Furthermore, while TrkA/NTRK1-expression conferred a significant survival advantage only 48 hours after irradiation, protection against Olaparib and elevated cell viability was observed for TrkA/NTRK1-expressing cells at all time points post-IR. Interestingly, XRCC1-levels were decreased in response to Olaparib treatment (3µM) in irradiated (20 Gy) and non-irradiated cells irrespective of TrkA/NTRK1-expression or IR. A possible explanation for increased cell viability of TrkA/NTRK1-positive cells post-IR could be that PARP1 up-regulation improves DNA repair capacity, thus conferring resistance to DNA-damaging agents such as ionizing radiation. However, DNA repair capacity was not found to be enhanced in PFGE and 53BP1 assays in response to TrkA/NTRK1 expression. PARP1 over-expression has been associated

with resistance to Olaparib in breast cancer [256]. Additionally, over-expression of other drug targets such as the methotrexate target DHFR (sarcoma), and the imatinib target BCR-ABL (leukemia) have resulted in increased concentrations of drug necessary to effectively inhibit the target [257, 258]. To answer the question if up-regulation of PARP1 leads to the observed Olaparib-resistance, it would be necessary to analyze PARP1-levels in (apparently) Olaparib-resistant cells.

However, other factors could also be causing the observed phenoytpe in response to TrkA/NTRK1-expression.PARP1 also has a role in checkpoint activation through binding to $p21^{waf/cip1}$ [259] and a role for PARP1 in cell cycle regulation has been proposed as PARP1-deficient cells present with a prolonged G_2/M-arrest [260] and the necessity for PARylation during cell cycle progression into mitosis [261]. Interestingly, PARP1 has been identified as a CHFR binding protein through a poly(ADP-ribose)-binding zinc finger (PBZ) motif [262] and it was suggested that silencing of CHFR could result in the over-expression of PARP1, thereby inducing checkpoint deregulation. In the same study, a direct interaction of PARP1 and CHFR was observed in the CHFR-mediated ubiquitination of PARP1 to induce a cell cycle arrest by reducing PARP1 levels below the threshold needed for mitosis [262]. Up-regulation of PARP1 in response to TrkA/NTRK1 could therefore be linked to a higher resistance to Olaparib as observed in higher cell viability of treated cells, or be caused by a PARP1-over-expression-mediated deregulation of cell cycle progression. Further research would be necessary to elucidate the fluctuating PARP1-levels in TrkA/NTRK1-expressing cells and determine the underlying causes for the resistance to Olaparib.

9.3 TrkA/NTRK1-overexpression in SY5Y cells results in a defective G_2-checkpoint

Cell cycle analysis was employed to evaluate the checkpoint response of TrkA/NTRK1-positive and TrkA/NTRK1-negative SY5Y cells after irradiation with 1 and 4 Gy. Analysis of the G_2-checkpoint through staining of the mitotic marker H3pS10 showed abnormally high mitotic indices of TrkA/NTRK1-positive cells. All TrkA/NTRK1-negative cell lines showed an intact G_2-checkpoint indicated by reduction of H3pS10-positive cells to almost 0% at 1h post-IR. Contrastingly, tetracycline + NGF-treatment of TrkA/NTRK1-transfectants led to elevated numbers of mitotic cells upon irradiation, suggesting a deficient G_2-checkpoint in response to TrkA/NTRK1-overexpression.

Significantly increased levels of mitotic cells in TrkA/NTRK1-positive transfectants were seen after 1 and 4 Gy-IR. While cells with an intact G_2-checkpoint display a reduction in mitotic cells already at 30 minutes post-IR, and a complete lack of cells in G2-phase at 1h post-IR, TrkA/NTRK1 positive cells showed only a 50% reduction in mitotic cells. Interestingly, this was restricted to TrkA/NTRK1 expressing cells upon activation of TrkA/NTRK1 by NGF. This suggests that the initiation of the early G_2-arrest is defective only as a direct response to TrkA/NTRK1 activation and hints at a role for TrkA/NTRK1 in the initial DNA damage response.

Propidium iodide staining was employed to analyze the cell cycle distribution in all phases and revealed higher proportions of cells in G_2-phase in TrkA/NTRK1-expressing cells compared to control cell lines at 4 Gy-post-IR. However, at 1 Gy post-IR percentages of cells in G_2-phase were not increased in response to TrkA/NTRK1-expression even though a G_2-checkpoint defect was visible through altered MIs at 1 Gy in these cells. A possible explanation for this is that it is not possible to discriminate between cells in G_2-phase and mitotic cells by PI staining. At a dose of 1 Gy, induction of an immediate cell cycle arrest causes no TrkA/NTRK1-dependent difference in the fraction of cells in G2-phase. However, differences in mitotic cells can be seen in response to TrkA/NTRK1-expression through H3pS10-staining. At a relatively high dose of 4 Gy, TrkA/NTRK1-negative cells show an immediate reduction in the total fraction of cells in G_2-phase in line with an intact cell cycle checkpoint. Contrastingly and irrespective of IR dose, TrkA/NTRK1-positive cells retain high mitotic indices indicative of G_2-checkpoint deficiency. An involvement of TrkA/NTRK1 in the regulation of the G_2-checkpoint has not yet been described. However, one of the primary effectors of TrkA/NTRK1-signaling is PI3K [77]. PI3K is a mediator of ATM-activation [263] and thus DNA damage response post-IR. Cell cycle checkpoints consist of the combinatorial signaling of DNA damage response sensors and the regulatory factors of the cell cycle [264]. Arrest in G_2-phase of the cell cycle is controlled by two molecularly distinct checkpoints. The late G_2-checkpoint is ATM-independent, dose-dependent and represents cells that were in earlier phases of the cell cycle (G_1- or S-phase) at the time of irradiation [265]. Contrastingly, another DNA damage induced early checkpoint is dependent on ATM signaling occurs transiently and is dose-independent. The ATM-dependent induction of the G_2-checkpoint is controlled through the Cyclin B-Cdc2 complex, MPF (mitosis-promoting factor). Two kinases, Wee1 and Myt1, phosphorylate Cdc2 to keep it inactive prior to mitosis. Phosphorylation of Wee1 and Cdc25 by Polo-like kinase 1 (Plk1) induces degradation of Wee1 and activates the phosphatase cdc25, thereby inducing the removal of inhibitory

phosphorylation on Cdc2 [266]. A positive feedback loop initiated by a complex consisting of Plk1, Cdc2 and Cdc25 results in the activation of downstream initiators promoting mitosis [266]. During DNA damage response, ATM/Chk1-mediated phosphorylation of CDC25C creates a binding site for 14-3-3 proteins conferring a nuclear export signal. This interferes with de-phosphorylation of Cdc2 and progression to M phase [267]. A role for PI3K in the G_2/M-progression has been suggested through G_2-arrest induction by the PI3K inhibitor LY294002. Furthermore, constitutively active PI3K enabled cells to override the DNA damage-induced G_2/M-checkpoint [268]. The mechanism by which over-activation of PI3K inhibits G_2-arrest may involve PKB-mediated inactivation of Chk1 through phosphorylation at Serine 280, thereby impairing phosphorylation of Cdc25 and preventing inhibition of the Cyclin B1/Cdc2 complex [269]. Additionally, deregulation of the PI3K down-stream effector PKB has been implicated in the mitotic progression of cells despite DNA damage [268]. TrkA/NTRK1-over-expression might therefore result in the observed G_2-checkpoint deficiency through a deregulation of post-IR PI3K- and ATM-signaling.

9.4 Elucidating the role of TrkA/NTRK1 over-expression in G_2-checkpoint deficiency

A role for TrkA/NTRK1 in the G_2-checkpoint regulation has been suggested in this project. The early G_2-checkpoint is ATM-dependent at up to 4h post-IR, but both ATR and Chk1-dependent at later time points. It would therefore be necessary to evaluate the checkpoint response at later time points than 4 hours to elucidate the underlying cause for the TrkA/NTRK1-dependent G_2-checkpoint-deficiency. Levels of PI3K, PKB, Polo-like kinase, and Wee1 may implicate PI3K in the deregulation of the G_2-checkpoint in response to TrkA/NTRK1-expression.

Furthermore, inhibition of TrkA/NTRK1 by Lestaurtinib may be used in G_2-checkpoint analysis by H3pS10-staining to confirm TrkA/NTRK1 as an underlying factor in the observed G_2-checkpoint deficiency in TrkA/NTRK1-positive cells. Additionally, H3pS10-levels in TrkA/NTRK1-positive and –negative cells at higher doses will clarify a dose-dependent or –independent mechanism of the deficient G_2-checkpoint. Evaluation of checkpoint recovery at 6-10 hours post-IR can be employed to analyze the consequences of the observed checkpoint deficiency.

10. The role of TrkA/NTRK1 in the modulation of MYCN protein levels and cell proliferation

A direct negative regulation of TrkA/NTRK1 and the standard isoform of CD44 (CD44S) by MYCN has already been described, but little is known about the molecular processes governing the opposite direction. The second part of this project was therefore aimed at analyzing a possible function of TrkA/NTRK1 in the regulation of MYCN.

10.1 TrkA/NTRK1-signaling induces up-regulation of *CD44* and down-regulation of MYCN

TrkA/NTRK1 over-expression and *MYCN* amplification are mutually exclusive and associated with opposing prognoses in neuroblastoma. TrkA/NTRK1 levels were shown to significantly alter the five-year cumulative survival rate in patients with *MYCN* non-amplified neuroblastoma. An additional factor that has been shown to be associated with disease outcome in neuroblastoma is the cell surface glycoprotein CD44. A microarray-based analysis of primary neuroblastomas confirmed these findings for our own patient cohort *in vivo* [253]. A comparison of *TrkA/NTRK1*- vs. *CD44*-expression shows that tumors with high levels of *TrkA/NTRK1* also express *CD44* at high levels. In contrast, expression of *MYCN* is inversely correlated with both *CD44*- and *TrkA/NTRK1*-expression. Furthermore, loss of expression of the standard isoform of CD44 has been shown to be a significant indicator of unfavorable outcome in neuroblastoma [270-272]. Additionally, transfection of functional CD44 into a cell line with *MYCN* amplification decreased tumorigenicity [273].

In SY5Y neuroblastoma cells engineered to conditionally express TrkA/NTRK1, up-regulation of *CD44* mRNA in response to TrkA/NTRK1-signaling was 8-fold compared to control cell lines. Furthermore, CD44 protein levels were increased by TrkA/NTRK1 expression as revealed by FACS analysis and IHC.

In order to analyze the association of TrkA/NTRK1-signaling with CD44 up-regulation and MYCN anti-correlation, *MYCN*-amplified cell lines were transfected with the same expression cassette already established in SY5Y cells. Expression of *TrkA/NTRK1* mRNA and protein was evaluated in *MYCN*-amplified cell lines to confirm inducible TrkA-expression. Ectopic expression of TrkA/NTRK1 also avoids transcriptional repression of TrkA by MYCN through binding to the endogenous *TrkA/NTRK1* promotor [212]. Up-regulation of *TrkA/NTRK1* mRNA and protein were successfully shown by real-time PCR and

western blot in both NGP- and IMR5-transfectants in response to tetracycline. *CD44* levels were then determined by real-time PCR and were also shown to be elevated in response to induction of TrkA/NTRK1. Most interestingly, down-regulation of MYCN protein was observed in response to TrkA/NTRK1-signaling.

10.2 TrkA/NTRK1 reduces proliferation rates of *MYCN*-amplified cell lines

One of the main goals of this project was to elucidate a possible TrkA/NTRK1-induced MYCN destabilization on the protein level using neuroblastoma model systems. As knockdown of *MYCN* was shown to decrease proliferation rates [274], high expression of TrkA/NTRK1 resulting in the down-regulation of MYCN protein might have a role in thwarting *MYCN*-driven neuroblastoma progression. Indeed, functional analyses of TrkA/NTRK1-signaling showed a decrease in both the proliferation rates over 72 hours and the capacity of colony formation over the course of 9-11 days in TrkA/NTRK1-expressing NGP- and IMR5-transfectants *in vitro*.

Different pathways mainly regulating MYCN protein stability tightly control cellular MYCN levels. Normal cells are characterized by a rapid turnover of MYCN, with phosphorylation at T58 and S62 marking the protein for proteasomal degradation. Stabilization of MYCN and a markedly prolonged half-life of MYCN are frequently observed in MYCN-dependent malignant cells. Of those proteins regulating MYCN phosphorylation, GSK3β might be of interest in the observed TrkA/NTRK1-mediated down-regulation of MYCN as it is a downstream target of both TrkA/NTRK1 and CD44. Recent reports indicated that PI3K/ Akt signaling upon TrkA/NTRK1 activation inhibits GSK3β activity, while a metastasis-associated CD44 variant (CD44v) seemed to stabilize GSK3β functions. A model, in which TrkA/NTRK1 and the standard isoform of CD44 (CD44S) contribute to destabilization of MYCN both on the mRNA and the protein levels is shown in Figure 37.

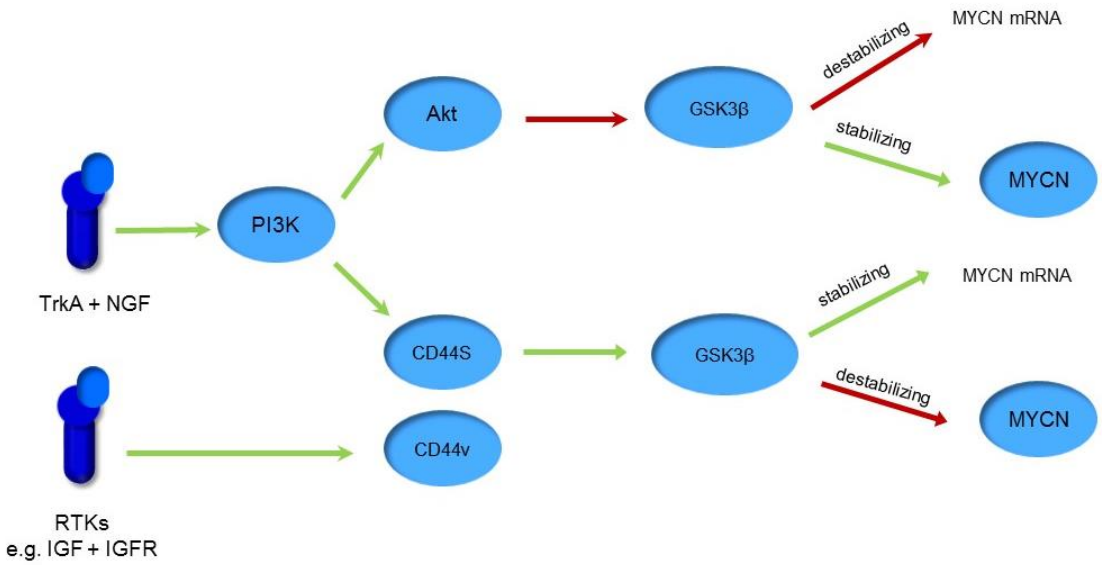

Figure 37: Schematic overview of a possible role of TrkA/NTRK1 in MYCN destabilization via CD44

It was shown that activation of TrkA/NTRK1 by its ligand NGF causes up-regulation of CD44. CD44S has been shown to inhibit phosphorylation of GSK3β, which can in turn induce MYCN phosphorylation at T58 and thus destabilization of MYCN protein. In an alternative route, TrkA/NTRK1-mediated activation of Akt causes phosphorylation and thus inactivation of GSK3β, which stabilizes MYCN protein and destabilizes MYCN mRNA. Oncogenic activation of other RTKs was shown to induce variant CD44 (CD44V), which is associated with aggressive tumor behavior. Green arrows depict activation/stabilization, while red arrows indicate inactivation/destabilization.

Here, TrkA/NTRK1 down-regulates MYCN by 1.) destabilizing *MYCN* mRNA via inhibition of GSK3β through signaling by PI3K and Akt and 2.) destabilizing MYCN protein via inhibitory action of CD44 on the phosphorylation of GSK3β. GSK3β-mediated dual regulation of the stability of *MYCN* mRNA and protein could serve as a safeguard against uncontrolled proliferation as a consequence of high-level expression of MYCN protein, while allowing for quick responses to receptor signaling by modulating *MYCN* mRNA levels. Pharmacological intervention through the use of the Akt inhibitor MK2206, the PI3K inhibitor LY294002, or dual inhibition of PI3K-mTOR-signaling by BEZ-235, could be used to further analyze the convergance of TrkA/NTRK1-CD44-GSK3β-signaling on MYCN stability.

These experiments would serve to further elucidate the TrkA/NTRK1-mediated regulation of MYCN and close the gap to the already known mechanism of *TrkA/NTRK1*-regulation through MYCN.

Summary

Neuroblastoma is the most common extracranial tumor of childhood. It is characterized by extreme courses of the disease ranging from spontaneous regression to rapid progression with infaust outcome. High expression of the receptor tyrosine kinase TrkA/NTRK1 is associated with a favorable outcome in neuroblastoma. TrkA/NTRK1 had been associated with an upregulation of a major factor in non-homologous end-joining (NHEJ), XRCC4, in SY5Y cells stably expressing TrkA/NTRK1. Here, stably transfected SY5Y cells carrying an inducible vector for TrkA/NTRK1 were used to analyze the effect of this neurotrophin receptor on cell viability, checkpoint activation, and the DNA repair capacity of these cells in response to ionizing irradiation.

No differences in DNA repair capacity were found in response to TrkA/NTRK1-expression. However, inducible TrkA/NTRK1 over-expression induced a deficient G_2 checkpoint at both low (1 Gy) and high doses (4 Gy) of ionizing radiation. Furthermore, cell viability was increased in TrkA/NTRK1-positive cells post-IR compared to vector control cells. TrkA/NTRK1-positive cells up-regulated PARP1 and showed significantly increased cell viability compared to TrkA/NTRK1-negative controls after PARP1-inhibition by Olaparib with and without irradiation with 2 Gy.

Amplification of the *MYCN* oncogene is frequently observed in high-stage neuroblastoma, which cannot be treated currently with curative intent. Furthermore, *MYCN* amplification is inversely correlated to expression of both the neurotrophin receptor TrkA/NTRK1 and the cell surface glycoprotein CD44. We have found a direct link between TrkA/NTRK1 and up-regulation of *CD44* using neuroblastoma cells with inducible, ectopic expression of TrkA/NTRK1. CD44 was elevated both on the mRNA and protein level only after induction and activation of TrkA/NTRK1 by its specific ligand, nerve growth factor (NGF). Furthermore, MYCN protein was found down-regulated in response to TrkA/NTRK1-signaling in *MYCN*-amplified transfectants with inducible TrkA/NTRK1-expression. Additionally, proliferation rates and clonogenic survival were significantly decreased in TrkA/NTRK1-positive, *MYCN*-amplified neuroblastoma cell lines.

Taken together, checkpoint deregulation and altered Olaparib response suggest a role for TrkA/NTRK1 in cell cycle regulation and checkpoint control. Furthermore, down-regulation of MYCN in response to TrkA/NTRK1-expression together with decreased clonogenic survival and proliferation of *MYCN*-amplified neuroblastoma cell lines points to an interaction of TrkA/NTRK1 and MYCN, possibly through CD44- and GSK3β-signaling.

Summary

Zusammenfassung

Neuroblastome sind die häufigsten extrakranialen Tumore des Kindesalters. Diese maligne Erkrankung zeichnet sich durch eine extreme Spannweite der Krankheitsverläufe aus, die von spontaner Differenzierung und Tumorregression bis hin zu raschem Progress und infauster Prognose reicht. Hohe Expressionslevel der Rezeptortyrosinkinase TrkA/NTRK1 sind mit einer guten Prognose assoziiert. TrkA/NTRK1-Expression korreliert zudem mit einer höheren Expression des DNA-Reparaturproteins XRCC4 in stabil TrkA/NTRK1-exprimierenden SY5Y Zellen.

Stabil transfizierte SY5Y Zellen mit induzierbarer TrkA/NTRK1-Expression wurden genutzt, um den Effekt dieses Neurotrophin-Rezeptors auf Zellviabilität, Aktivierung von Zellzyklus-*Checkpoints* und die DNA-Reparaturkapazität in der Strahlenantwort zu analysieren. Hierbei konnte kein Einfluss von TrkA/NTRK1 auf die Reparaturkapazität oder die DNA Reparaturkinetik im Zusammenhang mit ionisierender Bestrahlung festgestellt werden. Jedoch wurde gezeigt, dass die Überexpression von TrkA/NTRK1 eine Defizienz im G_2-Kontrollpunkt bei niedrigen (1 Gy) und hohen (4 Gy) Dosen bedingt. Zudem war die Zellviabilität in TrkA/NTRK1-positiven Zellen im Vergleich zu TrkA/NTRK1-negativen Zellen nach Bestrahlung erhöht. TrkA/NTRK1-exprimierende Zellen zeigten außerdem eine signifikant erhöhte Zellviabilität nach PARP1-Inhibition durch Olaparib mit und ohne Bestrahlung mit 2 Gy.

Die häufigste genetische Veränderung beim Neuroblastom, welche nur ein einzelnes Gen betrifft, ist die Amplifikation des *MYCN* Onkogens. Diese definiert auch den aggressivsten Tumor-Subtyp, der mit gegenwärtigen Mitteln nicht kurativ behandelt werden kann. Die MYCN-Amplifikation ist anti-korreliert zur Expression der Rezeptortyrosinkinase TrkA/NTRK1 und des Zelloberflächen-Glykoproteins CD44, die wiederum mit einer günstigen Prognose und spontaner Tumorregression assoziiert sind. Wir konnten einen direkten Zusammenhang zwischen hohen TrkA/NTRK1-Leveln und der Hochregulation von CD44 in Neuroblastomzellen mit induzierbarer TrkA/NTRK1-Expression zeigen. Dabei wurden die *CD44* Spiegel auf mRNA und Proteinebene in Gegenwart und Abwesenheit von aktiviertem TrkA untersucht. Hochregulation von CD44 konnte nur nach TrkA/NTRK1-Aktivierung durch den spezifischen Liganden, Nerve Growth Factor (NGF), gezeigt werden. Zudem ist das MYCN Protein in TrkA/NTRK1-exprimierenden Zellen mit *MYCN*-Amplifikation runterreguliert. Die Proliferationsrate und die Koloniebildungsfähigkeit sind in TrkA/NTRK1-exprimierenden, *MYCN*-amplizierten Neuroblastomzellen signifikant erniedrigt.

Zusammenfassend konnte gezeigt werden, dass eine Deregulation der Zellzyklus-Kontrollpunkte und ein verändertes Ansprechen auf Olaparib- in Einklang mit einer Rolle von TrkA/NTRK1 bei der Zellzykluskontrolle stehen. Eine reduzierte Expression von MYCN-Protein in Abhängigkeit vom TrkA/NTRK1-Status zusammen mit verminderter Koloniebildungsfähigkeit und Zellproliferation in *MYCN*-amplifizierten Neuroblastomzelllinien weist auf eine gegenseitige Interaktion von TrkA/NTRK1 und MYCN hin.

Bibliography

1. Maris, J.M., et al., *Neuroblastoma.* Lancet, 2007. **369**(9579): p. 2106-20.
2. Gatta, G., et al., *Childhood cancer survival in Europe 1999-2007: results of EUROCARE-5--a population-based study.* Lancet Oncol, 2014. **15**(1): p. 35-47.
3. Gurney, J.G., et al., *Infant cancer in the U.S.: histology-specific incidence and trends, 1973 to 1992.* J Pediatr Hematol Oncol, 1997. **19**(5): p. 428-32.
4. Brodeur, G.M., *Neuroblastoma: biological insights into a clinical enigma.* Nat Rev Cancer, 2003. **3**(3): p. 203-16.
5. Diede, S.J., *Spontaneous regression of metastatic cancer: learning from neuroblastoma.* Nat Rev Cancer, 2014. **14**(2): p. 71-2.
6. Matthay, K.K., *Stage 4S neuroblastoma: what makes it special?* J Clin Oncol, 1998. **16**(6): p. 2003-6.
7. Nakagawara, A., *Molecular basis of spontaneous regression of neuroblastoma: role of neurotrophic signals and genetic abnormalities.* Hum Cell, 1998. **11**(3): p. 115-24.
8. Nickerson, H.J., et al., *Favorable biology and outcome of stage IV-S neuroblastoma with supportive care or minimal therapy: a Children's Cancer Group study.* J Clin Oncol, 2000. **18**(3): p. 477-86.
9. Kreissman, S.G., et al., *Purged versus non-purged peripheral blood stem-cell transplantation for high-risk neuroblastoma (COG A3973): a randomised phase 3 trial.* Lancet Oncol, 2013. **14**(10): p. 999-1008.
10. Maris, J.M., *Recent advances in neuroblastoma.* N Engl J Med, 2010. **362**(23): p. 2202-11.
11. Cohn, S.L., et al., *The International Neuroblastoma Risk Group (INRG) classification system: an INRG Task Force report.* J Clin Oncol, 2009. **27**(2): p. 289-97.
12. Mosse, Y.P., et al., *Identification of ALK as a major familial neuroblastoma predisposition gene.* Nature, 2008. **455**(7215): p. 930-5.
13. Mosse, Y.P., et al., *Germline PHOX2B mutation in hereditary neuroblastoma.* Am J Hum Genet, 2004. **75**(4): p. 727-30.
14. Shojaei-Brosseau, T., et al., *Genetic epidemiology of neuroblastoma: a study of 426 cases at the Institut Gustave-Roussy in France.* Pediatr Blood Cancer, 2004. **42**(1): p. 99-105.
15. George, R.E., et al., *Activating mutations in ALK provide a therapeutic target in neuroblastoma.* Nature, 2008. **455**(7215): p. 975-8.
16. Chen, Y., et al., *Oncogenic mutations of ALK kinase in neuroblastoma.* Nature, 2008. **455**(7215): p. 971-4.
17. Janoueix-Lerosey, I., G. Schleiermacher, and O. Delattre, *Molecular pathogenesis of peripheral neuroblastic tumors.* Oncogene, 2010. **29**(11): p. 1566-79.
18. Pugh, T.J., et al., *The genetic landscape of high-risk neuroblastoma.* Nat Genet, 2013. **45**(3): p. 279-84.
19. Cheung, N.K., et al., *Association of age at diagnosis and genetic mutations in patients with neuroblastoma.* JAMA, 2012. **307**(10): p. 1062-71.
20. Sausen, M., et al., *Integrated genomic analyses identify ARID1A and ARID1B alterations in the childhood cancer neuroblastoma.* Nat Genet, 2013. **45**(1): p. 12-7.
21. Molenaar, J.J., et al., *Sequencing of neuroblastoma identifies chromothripsis and defects in neuritogenesis genes.* Nature, 2012. **483**(7391): p. 589-93.
22. Bosse, K.R., et al., *Common variation at BARD1 results in the expression of an oncogenic isoform that influences neuroblastoma susceptibility and oncogenicity.* Cancer Res, 2012. **72**(8): p. 2068-78.
23. Capasso, M., et al., *Common variations in BARD1 influence susceptibility to high-risk neuroblastoma.* Nat Genet, 2009. **41**(6): p. 718-23.

24. Wang, K., et al., *Integrative genomics identifies LMO1 as a neuroblastoma oncogene.* Nature, 2011. **469**(7329): p. 216-20.
25. Nguyen le, B., et al., *Phenotype restricted genome-wide association study using a gene-centric approach identifies three low-risk neuroblastoma susceptibility Loci.* PLoS Genet, 2011. **7**(3): p. e1002026.
26. Diskin, S.J., et al., *Common variation at 6q16 within HACE1 and LIN28B influences susceptibility to neuroblastoma.* Nat Genet, 2012. **44**(10): p. 1126-30.
27. Park, J.R., A. Eggert, and H. Caron, *Neuroblastoma: biology, prognosis, and treatment.* Pediatr Clin North Am, 2008. **55**(1): p. 97-120, x.
28. Simoes-Costa, M. and M.E. Bronner, *Insights into neural crest development and evolution from genomic analysis.* Genome Res, 2013. **23**(7): p. 1069-80.
29. Betancur, P., M. Bronner-Fraser, and T. Sauka-Spengler, *Assembling neural crest regulatory circuits into a gene regulatory network.* Annu Rev Cell Dev Biol, 2010. **26**: p. 581-603.
30. Takahashi, Y., D. Sipp, and H. Enomoto, *Tissue interactions in neural crest cell development and disease.* Science, 2013. **341**(6148): p. 860-3.
31. Beiske, K., et al., *Consensus criteria for sensitive detection of minimal neuroblastoma cells in bone marrow, blood and stem cell preparations by immunocytology and QRT-PCR: recommendations by the International Neuroblastoma Risk Group Task Force.* Br J Cancer, 2009. **100**(10): p. 1627-37.
32. De Preter, K., et al., *Human fetal neuroblast and neuroblastoma transcriptome analysis confirms neuroblast origin and highlights neuroblastoma candidate genes.* Genome Biol, 2006. **7**(9): p. R84.
33. Pei, D., et al., *Distinct neuroblastoma-associated alterations of PHOX2B impair sympathetic neuronal differentiation in zebrafish models.* PLoS Genet, 2013. **9**(6): p. e1003533.
34. Cheung, N.K. and M.A. Dyer, *Neuroblastoma: developmental biology, cancer genomics and immunotherapy.* Nat Rev Cancer, 2013. **13**(6): p. 397-411.
35. Louis, C.U. and J.M. Shohet, *Neuroblastoma: molecular pathogenesis and therapy.* Annu Rev Med, 2015. **66**: p. 49-63.
36. Fredlund, E., et al., *High Myc pathway activity and low stage of neuronal differentiation associate with poor outcome in neuroblastoma.* Proc Natl Acad Sci U S A, 2008. **105**(37): p. 14094-9.
37. Prasad, M.S., T. Sauka-Spengler, and C. LaBonne, *Induction of the neural crest state: control of stem cell attributes by gene regulatory, post-transcriptional and epigenetic interactions.* Dev Biol, 2012. **366**(1): p. 10-21.
38. Mayanil, C.S., *Transcriptional and epigenetic regulation of neural crest induction during neurulation.* Dev Neurosci, 2013. **35**(5): p. 361-72.
39. Beck, B. and C. Blanpain, *Unravelling cancer stem cell potential.* Nat Rev Cancer, 2013. **13**(10): p. 727-38.
40. Howk, C.L., et al., *Genetic Diversity in Normal Cell Populations is the Earliest Stage of Oncogenesis Leading to Intra-Tumor Heterogeneity.* Front Oncol, 2013. **3**: p. 61.
41. Beckwith, J.B. and E.V. Perrin, *In Situ Neuroblastomas: A Contribution to the Natural History of Neural Crest Tumors.* Am J Pathol, 1963. **43**: p. 1089-104.
42. Brodeur, G.M. and R. Bagatell, *Mechanisms of neuroblastoma regression.* Nat Rev Clin Oncol, 2014. **11**(12): p. 704-13.
43. Brodeur, G.M., et al., *International criteria for diagnosis, staging, and response to treatment in patients with neuroblastoma.* J Clin Oncol, 1988. **6**(12): p. 1874-81.
44. Monclair, T., et al., *The International Neuroblastoma Risk Group (INRG) staging system: an INRG Task Force report.* J Clin Oncol, 2009. **27**(2): p. 298-303.

45. Challis, G.B. and H.J. Stam, *The spontaneous regression of cancer. A review of cases from 1900 to 1987.* Acta Oncol, 1990. **29**(5): p. 545-50.
46. Papac, R.J., *Spontaneous regression of cancer: possible mechanisms.* In Vivo, 1998. **12**(6): p. 571-8.
47. D'Angio, G.J., A.E. Evans, and C.E. Koop, *Special pattern of widespread neuroblastoma with a favourable prognosis.* Lancet, 1971. **1**(7708): p. 1046-9.
48. Evans, A.E., G.J. D'Angio, and J. Randolph, *A proposed staging for children with neuroblastoma. Children's cancer study group A.* Cancer, 1971. **27**(2): p. 374-8.
49. Strother, D.R., et al., *Outcome after surgery alone or with restricted use of chemotherapy for patients with low-risk neuroblastoma: results of Children's Oncology Group study P9641.* J Clin Oncol, 2012. **30**(15): p. 1842-8.
50. Rubie, H., et al., *Excellent outcome with reduced treatment in infants with nonmetastatic and unresectable neuroblastoma without MYCN amplification: results of the prospective INES 99.1.* J Clin Oncol, 2011. **29**(4): p. 449-55.
51. Baker, D.L., et al., *Outcome after reduced chemotherapy for intermediate-risk neuroblastoma.* N Engl J Med, 2010. **363**(14): p. 1313-23.
52. Bagatell, R., et al., *Significance of MYCN amplification in international neuroblastoma staging system stage 1 and 2 neuroblastoma: a report from the International Neuroblastoma Risk Group database.* J Clin Oncol, 2009. **27**(3): p. 365-70.
53. Owens, C. and M. Irwin, *Neuroblastoma: the impact of biology and cooperation leading to personalized treatments.* Crit Rev Clin Lab Sci, 2012. **49**(3): p. 85-115.
54. Park, J.R., et al., *Children's Oncology Group's 2013 blueprint for research: neuroblastoma.* Pediatr Blood Cancer, 2013. **60**(6): p. 985-93.
55. Schmidt, M., et al., *The prognostic impact of functional imaging with (123)I-mIBG in patients with stage 4 neuroblastoma >1 year of age on a high-risk treatment protocol: results of the German Neuroblastoma Trial NB97.* Eur J Cancer, 2008. **44**(11): p. 1552-8.
56. Schwab, M., et al., *Amplified DNA with limited homology to myc cellular oncogene is shared by human neuroblastoma cell lines and a neuroblastoma tumour.* Nature, 1983. **305**(5931): p. 245-8.
57. Caron, H., et al., *Allelic loss of chromosome 1p as a predictor of unfavorable outcome in patients with neuroblastoma.* N Engl J Med, 1996. **334**(4): p. 225-30.
58. Srivatsan, E.S., K.L. Ying, and R.C. Seeger, *Deletion of chromosome 11 and of 14q sequences in neuroblastoma.* Genes Chromosomes Cancer, 1993. **7**(1): p. 32-7.
59. Bown, N., et al., *Gain of chromosome arm 17q and adverse outcome in patients with neuroblastoma.* N Engl J Med, 1999. **340**(25): p. 1954-61.
60. Nakagawara, A., et al., *Expression and function of TRK-B and BDNF in human neuroblastomas.* Mol Cell Biol, 1994. **14**(1): p. 759-67.
61. Seeger, R.C., et al., *Association of multiple copies of the N-myc oncogene with rapid progression of neuroblastomas.* N Engl J Med, 1985. **313**(18): p. 1111-6.
62. Kaneko, Y., et al., *Different karyotypic patterns in early and advanced stage neuroblastomas.* Cancer Res, 1987. **47**(1): p. 311-8.
63. Nakagawara, A., et al., *Association between high levels of expression of the TRK gene and favorable outcome in human neuroblastoma.* N Engl J Med, 1993. **328**(12): p. 847-54.
64. Look, A.T., et al., *Cellular DNA content as a predictor of response to chemotherapy in infants with unresectable neuroblastoma.* N Engl J Med, 1984. **311**(4): p. 231-5.
65. Schramm, A., et al., *Next-generation RNA sequencing reveals differential expression of MYCN target genes and suggests the mTOR pathway as a promising therapy target in MYCN-amplified neuroblastoma.* Int J Cancer, 2013. **132**(3): p. E106-15.

66. Eggert, A., et al., *Prognostic and biological role of neurotrophin-receptor TrkA and TrkB in neuroblastoma.* Klin Padiatr, 2000. **212**(4): p. 200-5.
67. Huang, E.J. and L.F. Reichardt, *Trk receptors: roles in neuronal signal transduction.* Annu Rev Biochem, 2003. **72**: p. 609-42.
68. Lewin, G.R. and Y.A. Barde, *Physiology of the neurotrophins.* Annu Rev Neurosci, 1996. **19**: p. 289-317.
69. Huang, E.J. and L.F. Reichardt, *Neurotrophins: roles in neuronal development and function.* Annu Rev Neurosci, 2001. **24**: p. 677-736.
70. Lee, R., et al., *Regulation of cell survival by secreted proneurotrophins.* Science, 2001. **294**(5548): p. 1945-8.
71. Seidah, N.G., et al., *Cellular processing of the neurotrophin precursors of NT3 and BDNF by the mammalian proprotein convertases.* FEBS Lett, 1996. **379**(3): p. 247-50.
72. Teng, H.K., et al., *ProBDNF induces neuronal apoptosis via activation of a receptor complex of p75NTR and sortilin.* J Neurosci, 2005. **25**(22): p. 5455-63.
73. Goldschneider, D. and P. Mehlen, *Dependence receptors: a new paradigm in cell signaling and cancer therapy.* Oncogene, 2010. **29**(13): p. 1865-82.
74. Rabizadeh, S., et al., *Neurotrophin dependence mediated by p75NTR: contrast between rescue by BDNF and NGF.* Cell Death Differ, 1999. **6**(12): p. 1222-7.
75. Lu, B., P.T. Pang, and N.H. Woo, *The yin and yang of neurotrophin action.* Nat Rev Neurosci, 2005. **6**(8): p. 603-14.
76. Skaper, S.D., *The neurotrophin family of neurotrophic factors: an overview.* Methods Mol Biol, 2012. **846**: p. 1-12.
77. Kaplan, D.R. and F.D. Miller, *Neurotrophin signal transduction in the nervous system.* Curr Opin Neurobiol, 2000. **10**(3): p. 381-91.
78. Suzuki, T., et al., *Lack of high-affinity nerve growth factor receptors in aggressive neuroblastomas.* J Natl Cancer Inst, 1993. **85**(5): p. 377-84.
79. Brodeur, G.M., et al., *Trk receptor expression and inhibition in neuroblastomas.* Clin Cancer Res, 2009. **15**(10): p. 3244-50.
80. Ehlers, M.D., et al., *NGF-stimulated retrograde transport of trkA in the mammalian nervous system.* J Cell Biol, 1995. **130**(1): p. 149-56.
81. Grimes, M.L., et al., *Endocytosis of activated TrkA: evidence that nerve growth factor induces formation of signaling endosomes.* J Neurosci, 1996. **16**(24): p. 7950-64.
82. Kuruvilla, R., et al., *A neurotrophin signaling cascade coordinates sympathetic neuron development through differential control of TrkA trafficking and retrograde signaling.* Cell, 2004. **118**(2): p. 243-55.
83. Delcroix, J.D., et al., *NGF signaling in sensory neurons: evidence that early endosomes carry NGF retrograde signals.* Neuron, 2003. **39**(1): p. 69-84.
84. Tsui-Pierchala, B.A. and D.D. Ginty, *Characterization of an NGF-P-TrkA retrograde-signaling complex and age-dependent regulation of TrkA phosphorylation in sympathetic neurons.* J Neurosci, 1999. **19**(19): p. 8207-18.
85. Watson, F.L., et al., *Neurotrophins use the Erk5 pathway to mediate a retrograde survival response.* Nat Neurosci, 2001. **4**(10): p. 981-8.
86. Eggert, A., et al., *Expression of the neurotrophin receptor TrkB is associated with unfavorable outcome in Wilms' tumor.* J Clin Oncol, 2001. **19**(3): p. 689-96.
87. Rutkowski, S., et al., *Prognostic relevance of clinical and biological risk factors in childhood medulloblastoma: results of patients treated in the prospective multicenter trial HIT'91.* Clin Cancer Res, 2007. **13**(9): p. 2651-7.
88. McGregor, L.M., et al., *Roles of trk family neurotrophin receptors in medullary thyroid carcinoma development and progression.* Proc Natl Acad Sci U S A, 1999. **96**(8): p. 4540-5.

89. George, D.J., et al., *Mutational analysis of the TrkA gene in prostate cancer.* Prostate, 1998. **36**(3): p. 172-80.
90. Pflug, B.R., et al., *Expression of a Trk high affinity nerve growth factor receptor in the human prostate.* Endocrinology, 1995. **136**(1): p. 262-8.
91. Dolle, L., et al., *Nerve growth factor overexpression and autocrine loop in breast cancer cells.* Oncogene, 2003. **22**(36): p. 5592-601.
92. Descamps, S., et al., *Expression of nerve growth factor receptors and their prognostic value in human breast cancer.* Cancer Res, 2001. **61**(11): p. 4337-40.
93. Pierotti, M.A., P. Vigneri, and I. Bongarzone, *Rearrangements of RET and NTRK1 tyrosine kinase receptors in papillary thyroid carcinomas.* Recent Results Cancer Res, 1998. **154**: p. 237-47.
94. Greco, A., et al., *Chromosome 1 rearrangements involving the genes TPR and NTRK1 produce structurally different thyroid-specific TRK oncogenes.* Genes Chromosomes Cancer, 1997. **19**(2): p. 112-23.
95. Rubin, B.P., et al., *Congenital mesoblastic nephroma t(12;15) is associated with ETV6-NTRK3 gene fusion: cytogenetic and molecular relationship to congenital (infantile) fibrosarcoma.* Am J Pathol, 1998. **153**(5): p. 1451-8.
96. Knezevich, S.R., et al., *A novel ETV6-NTRK3 gene fusion in congenital fibrosarcoma.* Nat Genet, 1998. **18**(2): p. 184-7.
97. Kogner, P., et al., *Coexpression of messenger RNA for TRK protooncogene and low affinity nerve growth factor receptor in neuroblastoma with favorable prognosis.* Cancer Res, 1993. **53**(9): p. 2044-50.
98. Nakagawara, A., et al., *Inverse relationship between trk expression and N-myc amplification in human neuroblastomas.* Cancer Res, 1992. **52**(5): p. 1364-8.
99. Acheson, A., et al., *A BDNF autocrine loop in adult sensory neurons prevents cell death.* Nature, 1995. **374**(6521): p. 450-3.
100. Nakagawara, A. and G.M. Brodeur, *Role of neurotrophins and their receptors in human neuroblastomas: a primary culture study.* Eur J Cancer, 1997. **33**(12): p. 2050-3.
101. Meitar, D., et al., *Tumor angiogenesis correlates with metastatic disease, N-myc amplification, and poor outcome in human neuroblastoma.* J Clin Oncol, 1996. **14**(2): p. 405-14.
102. Pajtler, K.W., et al., *Neuroblastoma in dialog with its stroma: NTRK1 is a regulator of cellular cross-talk with Schwann cells.* Oncotarget, 2014. **5**(22): p. 11180-92.
103. Matsumoto, K., et al., *Expression of brain-derived neurotrophic factor and p145TrkB affects survival, differentiation, and invasiveness of human neuroblastoma cells.* Cancer Res, 1995. **55**(8): p. 1798-806.
104. Ho, R., et al., *Resistance to chemotherapy mediated by TrkB in neuroblastomas.* Cancer Res, 2002. **62**(22): p. 6462-6.
105. Nakamura, K., et al., *Brain-derived neurotrophic factor activation of TrkB induces vascular endothelial growth factor expression via hypoxia-inducible factor-1alpha in neuroblastoma cells.* Cancer Res, 2006. **66**(8): p. 4249-55.
106. Evans, A.E., et al., *Effect of CEP-751 (KT-6587) on neuroblastoma xenografts expressing TrkB.* Med Pediatr Oncol, 2001. **36**(1): p. 181-4.
107. Evans, A.E., et al., *Antitumor activity of CEP-751 (KT-6587) on human neuroblastoma and medulloblastoma xenografts.* Clin Cancer Res, 1999. **5**(11): p. 3594-602.
108. Iyer, R., et al., *Lestaurtinib enhances the antitumor efficacy of chemotherapy in murine xenograft models of neuroblastoma.* Clin Cancer Res, 2010. **16**(5): p. 1478-85.

109. Iyer, R., et al., *AZ64 inhibits TrkB and enhances the efficacy of chemotherapy and local radiation in neuroblastoma xenografts.* Cancer Chemother Pharmacol, 2012. **70**(3): p. 477-86.
110. Pastink, A., J.C. Eeken, and P.H. Lohman, *Genomic integrity and the repair of double-strand DNA breaks.* Mutat Res, 2001. **480-481**: p. 37-50.
111. Rothkamm, K., et al., *Pathways of DNA double-strand break repair during the mammalian cell cycle.* Mol Cell Biol, 2003. **23**(16): p. 5706-15.
112. Lobrich, M. and P.A. Jeggo, *The impact of a negligent G2/M checkpoint on genomic instability and cancer induction.* Nat Rev Cancer, 2007. **7**(11): p. 861-9.
113. Abner, C.W. and P.J. McKinnon, *The DNA double-strand break response in the nervous system.* DNA Repair (Amst), 2004. **3**(8-9): p. 1141-7.
114. Ochi, T., et al., *DNA repair. PAXX, a paralog of XRCC4 and XLF, interacts with Ku to promote DNA double-strand break repair.* Science, 2015. **347**(6218): p. 185-8.
115. Lieber, M.R., et al., *Mechanism and regulation of human non-homologous DNA end-joining.* Nat Rev Mol Cell Biol, 2003. **4**(9): p. 712-20.
116. Iliakis, G., et al., *Mechanisms of DNA double strand break repair and chromosome aberration formation.* Cytogenet Genome Res, 2004. **104**(1-4): p. 14-20.
117. Ferguson, D.O., et al., *The nonhomologous end-joining pathway of DNA repair is required for genomic stability and the suppression of translocations.* Proc Natl Acad Sci U S A, 2000. **97**(12): p. 6630-3.
118. Kabotyanski, E.B., et al., *Double-strand break repair in Ku86- and XRCC4-deficient cells.* Nucleic Acids Res, 1998. **26**(23): p. 5333-42.
119. Wang, H., et al., *Biochemical evidence for Ku-independent backup pathways of NHEJ.* Nucleic Acids Res, 2003. **31**(18): p. 5377-88.
120. Terzoudi, G.I., et al., *Premature chromosome condensation reveals DNA-PK independent pathways of chromosome break repair.* Int J Oncol, 2008. **33**(4): p. 871-9.
121. Wu, W., et al., *Enhanced use of backup pathways of NHEJ in G2 in Chinese hamster mutant cells with defects in the classical pathway of NHEJ.* Radiat Res, 2008. **170**(4): p. 512-20.
122. Guirouilh-Barbat, J., S. Huck, and B.S. Lopez, *S-phase progression stimulates both the mutagenic KU-independent pathway and mutagenic processing of KU-dependent intermediates, for nonhomologous end joining.* Oncogene, 2008. **27**(12): p. 1726-36.
123. Wu, W., et al., *Repair of radiation induced DNA double strand breaks by backup NHEJ is enhanced in G2.* DNA Repair (Amst), 2008. **7**(2): p. 329-38.
124. Lieber, M.R., *NHEJ and its backup pathways in chromosomal translocations.* Nat Struct Mol Biol, 2010. **17**(4): p. 393-5.
125. Mladenov, E., et al., *DNA double-strand break repair as determinant of cellular radiosensitivity to killing and target in radiation therapy.* Front Oncol, 2013. **3**: p. 113.
126. Schulte, J.H., et al., *Expression of the TrkA or TrkB receptor tyrosine kinase alters the double-strand break (DSB) repair capacity of SY5Y neuroblastoma cells.* DNA Repair (Amst), 2008. **7**(10): p. 1757-64.
127. Carson, C.T., et al., *The Mre11 complex is required for ATM activation and the G2/M checkpoint.* EMBO J, 2003. **22**(24): p. 6610-20.
128. Uziel, T., et al., *Requirement of the MRN complex for ATM activation by DNA damage.* EMBO J, 2003. **22**(20): p. 5612-21.
129. Falck, J., J. Coates, and S.P. Jackson, *Conserved modes of recruitment of ATM, ATR and DNA-PKcs to sites of DNA damage.* Nature, 2005. **434**(7033): p. 605-11.
130. Lavin, M.F., *Ataxia-telangiectasia: from a rare disorder to a paradigm for cell signalling and cancer.* Nat Rev Mol Cell Biol, 2008. **9**(10): p. 759-69.

131. Rogakou, E.P., et al., *DNA double-stranded breaks induce histone H2AX phosphorylation on serine 139.* J Biol Chem, 1998. **273**(10): p. 5858-68.
132. Stucki, M. and S.P. Jackson, *gammaH2AX and MDC1: anchoring the DNA-damage-response machinery to broken chromosomes.* DNA Repair (Amst), 2006. **5**(5): p. 534-43.
133. Fernandez-Capetillo, O., et al., *DNA damage-induced G2-M checkpoint activation by histone H2AX and 53BP1.* Nat Cell Biol, 2002. **4**(12): p. 993-7.
134. Chapman, J.R. and S.P. Jackson, *Phospho-dependent interactions between NBS1 and MDC1 mediate chromatin retention of the MRN complex at sites of DNA damage.* EMBO Rep, 2008. **9**(8): p. 795-801.
135. Hirao, A., et al., *DNA damage-induced activation of p53 by the checkpoint kinase Chk2.* Science, 2000. **287**(5459): p. 1824-7.
136. Matsuoka, S., M. Huang, and S.J. Elledge, *Linkage of ATM to cell cycle regulation by the Chk2 protein kinase.* Science, 1998. **282**(5395): p. 1893-7.
137. Nelson, W.G. and M.B. Kastan, *DNA strand breaks: the DNA template alterations that trigger p53-dependent DNA damage response pathways.* Mol Cell Biol, 1994. **14**(3): p. 1815-23.
138. Lavin, M.F., et al., *Defect in radiation signal transduction in ataxia-telangiectasia.* Int J Radiat Biol, 1994. **66**(6 Suppl): p. S151-6.
139. Byun, T.S., et al., *Functional uncoupling of MCM helicase and DNA polymerase activities activates the ATR-dependent checkpoint.* Genes Dev, 2005. **19**(9): p. 1040-52.
140. Chaturvedi, P., et al., *Mammalian Chk2 is a downstream effector of the ATM-dependent DNA damage checkpoint pathway.* Oncogene, 1999. **18**(28): p. 4047-54.
141. Jazayeri, A., et al., *Mre11-Rad50-Nbs1-dependent processing of DNA breaks generates oligonucleotides that stimulate ATM activity.* EMBO J, 2008. **27**(14): p. 1953-62.
142. Schulte, J.H., et al., *Microarray analysis reveals differential gene expression patterns and regulation of single target genes contributing to the opposing phenotype of TrkA- and TrkB-expressing neuroblastomas.* Oncogene, 2005. **24**(1): p. 165-77.
143. Gossen, M. and H. Bujard, *Tight control of gene expression in mammalian cells by tetracycline-responsive promoters.* Proc Natl Acad Sci U S A, 1992. **89**(12): p. 5547-51.
144. Urlinger, S., et al., *Exploring the sequence space for tetracycline-dependent transcriptional activators: novel mutations yield expanded range and sensitivity.* Proc Natl Acad Sci U S A, 2000. **97**(14): p. 7963-8.
145. Brodeur, G.M., et al., *Amplification of N-myc in untreated human neuroblastomas correlates with advanced disease stage.* Science, 1984. **224**(4653): p. 1121-4.
146. Kohl, N.E., C.E. Gee, and F.W. Alt, *Activated expression of the N-myc gene in human neuroblastomas and related tumors.* Science, 1984. **226**(4680): p. 1335-7.
147. Nau, M.M., et al., *L-myc, a new myc-related gene amplified and expressed in human small cell lung cancer.* Nature, 1985. **318**(6041): p. 69-73.
148. Malynn, B.A., et al., *N-myc can functionally replace c-myc in murine development, cellular growth, and differentiation.* Genes Dev, 2000. **14**(11): p. 1390-9.
149. Shih, C.M., et al., *Association of L-myc polymorphism with lung cancer susceptibility and prognosis in relation to age-selected controls and stratified cases.* Lung Cancer, 2002. **36**(2): p. 125-32.
150. Adams, J.M., et al., *The c-myc oncogene driven by immunoglobulin enhancers induces lymphoid malignancy in transgenic mice.* Nature, 1985. **318**(6046): p. 533-8.

151. Chesi, M., et al., *AID-dependent activation of a MYC transgene induces multiple myeloma in a conditional mouse model of post-germinal center malignancies.* Cancer Cell, 2008. **13**(2): p. 167-80.
152. Leder, A., et al., *Consequences of widespread deregulation of the c-myc gene in transgenic mice: multiple neoplasms and normal development.* Cell, 1986. **45**(4): p. 485-95.
153. Arvanitis, C. and D.W. Felsher, *Conditional transgenic models define how MYC initiates and maintains tumorigenesis.* Semin Cancer Biol, 2006. **16**(4): p. 313-7.
154. Ma, L., et al., *miR-9, a MYC/MYCN-activated microRNA, regulates E-cadherin and cancer metastasis.* Nat Cell Biol, 2010. **12**(3): p. 247-56.
155. Song, L.B., et al., *The polycomb group protein Bmi-1 represses the tumor suppressor PTEN and induces epithelial-mesenchymal transition in human nasopharyngeal epithelial cells.* J Clin Invest, 2009. **119**(12): p. 3626-36.
156. Felsher, D.W. and J.M. Bishop, *Transient excess of MYC activity can elicit genomic instability and tumorigenesis.* Proc Natl Acad Sci U S A, 1999. **96**(7): p. 3940-4.
157. Karlsson, A., et al., *Defective double-strand DNA break repair and chromosomal translocations by MYC overexpression.* Proc Natl Acad Sci U S A, 2003. **100**(17): p. 9974-9.
158. Neiman, P.E., et al., *Genomic instability during Myc-induced lymphomagenesis in the bursa of Fabricius.* Oncogene, 2006. **25**(47): p. 6325-35.
159. Prochownik, E.V., *c-Myc: linking transformation and genomic instability.* Curr Mol Med, 2008. **8**(6): p. 446-58.
160. Ray, S., et al., *MYC can induce DNA breaks in vivo and in vitro independent of reactive oxygen species.* Cancer Res, 2006. **66**(13): p. 6598-605.
161. Egler, R.A., et al., *Regulation of reactive oxygen species, DNA damage, and c-Myc function by peroxiredoxin 1.* Oncogene, 2005. **24**(54): p. 8038-50.
162. Vafa, O., et al., *c-Myc can induce DNA damage, increase reactive oxygen species, and mitigate p53 function: a mechanism for oncogene-induced genetic instability.* Mol Cell, 2002. **9**(5): p. 1031-44.
163. Zhang, H., et al., *HIF-1 inhibits mitochondrial biogenesis and cellular respiration in VHL-deficient renal cell carcinoma by repression of C-MYC activity.* Cancer Cell, 2007. **11**(5): p. 407-20.
164. Gao, P., et al., *HIF-dependent antitumorigenic effect of antioxidants in vivo.* Cancer Cell, 2007. **12**(3): p. 230-8.
165. Louis, S.F., et al., *c-Myc induces chromosomal rearrangements through telomere and chromosome remodeling in the interphase nucleus.* Proc Natl Acad Sci U S A, 2005. **102**(27): p. 9613-8.
166. Levens, D., *You Don't Muck with MYC.* Genes Cancer, 2010. **1**(6): p. 547-554.
167. Cannell, I.G., et al., *p38 MAPK/MK2-mediated induction of miR-34c following DNA damage prevents Myc-dependent DNA replication.* Proc Natl Acad Sci U S A, 2010. **107**(12): p. 5375-80.
168. Kress, T.R., et al., *The MK5/PRAK kinase and Myc form a negative feedback loop that is disrupted during colorectal tumorigenesis.* Mol Cell, 2011. **41**(4): p. 445-57.
169. Kim, H.H., et al., *HuR recruits let-7/RISC to repress c-Myc expression.* Genes Dev, 2009. **23**(15): p. 1743-8.
170. Christoffersen, N.R., et al., *p53-independent upregulation of miR-34a during oncogene-induced senescence represses MYC.* Cell Death Differ, 2010. **17**(2): p. 236-45.
171. Gregory, M.A. and S.R. Hann, *c-Myc proteolysis by the ubiquitin-proteasome pathway: stabilization of c-Myc in Burkitt's lymphoma cells.* Mol Cell Biol, 2000. **20**(7): p. 2423-35.

172. Gregory, M.A., Y. Qi, and S.R. Hann, *Phosphorylation by glycogen synthase kinase-3 controls c-myc proteolysis and subnuclear localization.* J Biol Chem, 2003. **278**(51): p. 51606-12.
173. Salghetti, S.E., S.Y. Kim, and W.P. Tansey, *Destruction of Myc by ubiquitin-mediated proteolysis: cancer-associated and transforming mutations stabilize Myc.* EMBO J, 1999. **18**(3): p. 717-26.
174. Thomas, L.R. and W.P. Tansey, *Proteolytic control of the oncoprotein transcription factor Myc.* Adv Cancer Res, 2011. **110**: p. 77-106.
175. Popov, N., et al., *The ubiquitin-specific protease USP28 is required for MYC stability.* Nat Cell Biol, 2007. **9**(7): p. 765-74.
176. Wang, X., et al., *Phosphorylation regulates c-Myc's oncogenic activity in the mammary gland.* Cancer Res, 2011. **71**(3): p. 925-36.
177. Xie, X., et al., *Systematic discovery of regulatory motifs in human promoters and 3' UTRs by comparison of several mammals.* Nature, 2005. **434**(7031): p. 338-45.
178. Zeller, K.I., et al., *Global mapping of c-Myc binding sites and target gene networks in human B cells.* Proc Natl Acad Sci U S A, 2006. **103**(47): p. 17834-9.
179. Kohl, N.E., et al., *Human N-myc is closely related in organization and nucleotide sequence to c-myc.* Nature, 1986. **319**(6048): p. 73-7.
180. Stanton, L.W., M. Schwab, and J.M. Bishop, *Nucleotide sequence of the human N-myc gene.* Proc Natl Acad Sci U S A, 1986. **83**(6): p. 1772-6.
181. Meyer, N. and L.Z. Penn, *Reflecting on 25 years with MYC.* Nat Rev Cancer, 2008. **8**(12): p. 976-90.
182. Koppen, A., et al., *Dickkopf-1 is down-regulated by MYCN and inhibits neuroblastoma cell proliferation.* Cancer Lett, 2007. **256**(2): p. 218-28.
183. Valli, E., et al., *CDKL5, a novel MYCN-repressed gene, blocks cell cycle and promotes differentiation of neuronal cells.* Biochim Biophys Acta, 2012. **1819**(11-12): p. 1173-85.
184. Charron, J., et al., *Embryonic lethality in mice homozygous for a targeted disruption of the N-myc gene.* Genes Dev, 1992. **6**(12A): p. 2248-57.
185. Davis, A.C., et al., *A null c-myc mutation causes lethality before 10.5 days of gestation in homozygotes and reduced fertility in heterozygous female mice.* Genes Dev, 1993. **7**(4): p. 671-82.
186. Sawai, S., et al., *Defects of embryonic organogenesis resulting from targeted disruption of the N-myc gene in the mouse.* Development, 1993. **117**(4): p. 1445-55.
187. Stanton, B.R., et al., *Loss of N-myc function results in embryonic lethality and failure of the epithelial component of the embryo to develop.* Genes Dev, 1992. **6**(12A): p. 2235-47.
188. Zimmerman, K.A., et al., *Differential expression of myc family genes during murine development.* Nature, 1986. **319**(6056): p. 780-3.
189. Huang, M. and W.A. Weiss, *Neuroblastoma and MYCN.* Cold Spring Harb Perspect Med, 2013. **3**(10): p. a014415.
190. Matsumoto, M., et al., *Expression of proto-oncogene products during drug-induced differentiation of a neuroblastoma cell line SK-N-DZ.* Acta Neuropathol, 1989. **79**(2): p. 217-21.
191. Cinatl, J., et al., *In vitro differentiation of human neuroblastoma cells induced by sodium phenylacetate.* Cancer Lett, 1993. **70**(1-2): p. 15-24.
192. Han, S., R.K. Wada, and N. Sidell, *Differentiation of human neuroblastoma by phenylacetate is mediated by peroxisome proliferator-activated receptor gamma.* Cancer Res, 2001. **61**(10): p. 3998-4002.

193. Reddy, C.D., et al., *Anticancer effects of the novel 1alpha, 25-dihydroxyvitamin D3 hybrid analog QW1624F2-2 in human neuroblastoma.* J Cell Biochem, 2006. **97**(1): p. 198-206.
194. Wakamatsu, Y., et al., *Regulation of the neural crest cell fate by N-myc: promotion of ventral migration and neuronal differentiation.* Development, 1997. **124**(10): p. 1953-62.
195. Kang, J.H., et al., *MYCN silencing induces differentiation and apoptosis in human neuroblastoma cells.* Biochem Biophys Res Commun, 2006. **351**(1): p. 192-7.
196. Cotterman, R. and P.S. Knoepfler, *N-Myc regulates expression of pluripotency genes in neuroblastoma including lif, klf2, klf4, and lin28b.* PLoS One, 2009. **4**(6): p. e5799.
197. Loven, J., et al., *MYCN-regulated microRNAs repress estrogen receptor-alpha (ESR1) expression and neuronal differentiation in human neuroblastoma.* Proc Natl Acad Sci U S A, 2010. **107**(4): p. 1553-8.
198. Henriksen, J.R., et al., *Conditional expression of retrovirally delivered anti-MYCN shRNA as an in vitro model system to study neuronal differentiation in MYCN-amplified neuroblastoma.* BMC Dev Biol, 2011. **11**: p. 1.
199. Zaizen, Y., et al., *The effect of N-myc amplification and expression on invasiveness of neuroblastoma cells.* J Pediatr Surg, 1993. **28**(6): p. 766-9.
200. Benard, J., *Genetic alterations associated with metastatic dissemination and chemoresistance in neuroblastoma.* Eur J Cancer, 1995. **31A**(4): p. 560-4.
201. Goodman, L.A., et al., *Modulation of N-myc expression alters the invasiveness of neuroblastoma.* Clin Exp Metastasis, 1997. **15**(2): p. 130-9.
202. van Golen, C.M., et al., *N-Myc overexpression leads to decreased beta1 integrin expression and increased apoptosis in human neuroblastoma cells.* Oncogene, 2003. **22**(17): p. 2664-73.
203. Tanaka, N. and M. Fukuzawa, *MYCN downregulates integrin alpha1 to promote invasion of human neuroblastoma cells.* Int J Oncol, 2008. **33**(4): p. 815-21.
204. Beierle, E.A., et al., *N-MYC regulates focal adhesion kinase expression in human neuroblastoma.* J Biol Chem, 2007. **282**(17): p. 12503-16.
205. Song, L., et al., *Oncogene MYCN regulates localization of NKT cells to the site of disease in neuroblastoma.* J Clin Invest, 2007. **117**(9): p. 2702-12.
206. Hatzi, E., et al., *N-myc oncogene overexpression down-regulates IL-6; evidence that IL-6 inhibits angiogenesis and suppresses neuroblastoma tumor growth.* Oncogene, 2002. **21**(22): p. 3552-61.
207. Dungwa, J.V., et al., *Angiogenin up-regulation correlates with adverse clinicopathological and biological factors, increased microvascular density and poor patient outcome in neuroblastomas.* Histopathology, 2012. **60**(6): p. 911-23.
208. Chappell, J. and S. Dalton, *Roles for MYC in the establishment and maintenance of pluripotency.* Cold Spring Harb Perspect Med, 2013. **3**(12): p. a014381.
209. Slack, A., et al., *The p53 regulatory gene MDM2 is a direct transcriptional target of MYCN in neuroblastoma.* Proc Natl Acad Sci U S A, 2005. **102**(3): p. 731-6.
210. Chen, L., et al., *p53 is a direct transcriptional target of MYCN in neuroblastoma.* Cancer Res, 2010. **70**(4): p. 1377-88.
211. Dewitt, J., et al., *Constitutively active TrkB confers an aggressive transformed phenotype to a neural crest-derived cell line.* Oncogene, 2014. **33**(8): p. 977-85.
212. Iraci, N., et al., *A SP1/MIZ1/MYCN repression complex recruits HDAC1 at the TRKA and p75NTR promoters and affects neuroblastoma malignancy by inhibiting the cell response to NGF.* Cancer Res, 2011. **71**(2): p. 404-12.
213. Burkhart, C.A., et al., *Effects of MYCN antisense oligonucleotide administration on tumorigenesis in a murine model of neuroblastoma.* J Natl Cancer Inst, 2003. **95**(18): p. 1394-403.

214. Sidell, N., *Retinoic acid-induced growth inhibition and morphologic differentiation of human neuroblastoma cells in vitro.* J Natl Cancer Inst, 1982. **68**(4): p. 589-96.
215. Ciani, E., et al., *Nitric oxide negatively regulates proliferation and promotes neuronal differentiation through N-Myc downregulation.* J Cell Sci, 2004. **117**(Pt 20): p. 4727-37.
216. Sears, R., et al., *Multiple Ras-dependent phosphorylation pathways regulate Myc protein stability.* Genes Dev, 2000. **14**(19): p. 2501-14.
217. Welcker, M., et al., *The Fbw7 tumor suppressor regulates glycogen synthase kinase 3 phosphorylation-dependent c-Myc protein degradation.* Proc Natl Acad Sci U S A, 2004. **101**(24): p. 9085-90.
218. Yada, M., et al., *Phosphorylation-dependent degradation of c-Myc is mediated by the F-box protein Fbw7.* EMBO J, 2004. **23**(10): p. 2116-25.
219. Cage, T.A., et al., *Downregulation of MYCN through PI3K Inhibition in Mouse Models of Pediatric Neural Cancer.* Front Oncol, 2015. **5**: p. 111.
220. Liu, T., et al., *Activation of tissue transglutaminase transcription by histone deacetylase inhibition as a therapeutic approach for Myc oncogenesis.* Proc Natl Acad Sci U S A, 2007. **104**(47): p. 18682-7.
221. Gamble, L.D., et al., *MYCN sensitizes neuroblastoma to the MDM2-p53 antagonists Nutlin-3 and MI-63.* Oncogene, 2012. **31**(6): p. 752-63.
222. Delmore, J.E., et al., *BET bromodomain inhibition as a therapeutic strategy to target c-Myc.* Cell, 2011. **146**(6): p. 904-17.
223. Puissant, A., et al., *Targeting MYCN in neuroblastoma by BET bromodomain inhibition.* Cancer Discov, 2013. **3**(3): p. 308-23.
224. Yamashiro, D.J., et al., *Expression and function of Trk-C in favourable human neuroblastomas.* Eur J Cancer, 1997. **33**(12): p. 2054-7.
225. Zhu, S., et al., *Activated ALK collaborates with MYCN in neuroblastoma pathogenesis.* Cancer Cell, 2012. **21**(3): p. 362-73.
226. Weiss, W.A., et al., *Targeted expression of MYCN causes neuroblastoma in transgenic mice.* EMBO J, 1997. **16**(11): p. 2985-95.
227. Boon, K., et al., *N-myc enhances the expression of a large set of genes functioning in ribosome biogenesis and protein synthesis.* EMBO J, 2001. **20**(6): p. 1383-93.
228. Murphy, D.M., et al., *Dissection of the oncogenic MYCN transcriptional network reveals a large set of clinically relevant cell cycle genes as drivers of neuroblastoma tumorigenesis.* Mol Carcinog, 2011. **50**(6): p. 403-11.
229. Brockmann, M., et al., *Small molecule inhibitors of aurora-a induce proteasomal degradation of N-myc in childhood neuroblastoma.* Cancer Cell, 2013. **24**(1): p. 75-89.
230. Eggert, A., et al., *Expression of the neurotrophin receptor TrkA down-regulates expression and function of angiogenic stimulators in SH-SY5Y neuroblastoma cells.* Cancer Res, 2002. **62**(6): p. 1802-8.
231. Schramm, A., et al., *Prediction of clinical outcome and biological characterization of neuroblastoma by expression profiling.* Oncogene, 2005. **24**(53): p. 7902-12.
232. Pajtler, K.W., et al., *Expression of NTRK1/TrkA affects immunogenicity of neuroblastoma cells.* Int J Cancer, 2013. **133**(4): p. 908-19.
233. Sitek, B., et al., *Identification of dynamic proteome changes upon ligand activation of Trk-receptors using two-dimensional fluorescence difference gel electrophoresis and mass spectrometry.* Mol Cell Proteomics, 2005. **4**(3): p. 291-9.
234. Yao, R. and G.M. Cooper, *Requirement for phosphatidylinositol-3 kinase in the prevention of apoptosis by nerve growth factor.* Science, 1995. **267**(5206): p. 2003-6.
235. Gustafson, W.C. and W.A. Weiss, *Myc proteins as therapeutic targets.* Oncogene, 2010. **29**(9): p. 1249-59.

236. Barone, G., et al., *New strategies in neuroblastoma: Therapeutic targeting of MYCN and ALK.* Clin Cancer Res, 2013. **19**(21): p. 5814-21.
237. Sjostrom, S.K., et al., *The Cdk1 complex plays a prime role in regulating N-myc phosphorylation and turnover in neural precursors.* Dev Cell, 2005. **9**(3): p. 327-38.
238. Shigeishi, H., et al., *Maintenance of stem cell self-renewal in head and neck cancers requires actions of GSK3beta influenced by CD44 and RHAMM.* Stem Cells, 2013. **31**(10): p. 2073-83.
239. Duffy, D.J., et al., *GSK3 inhibitors regulate MYCN mRNA levels and reduce neuroblastoma cell viability through multiple mechanisms, including p53 and Wnt signaling.* Mol Cancer Ther, 2014. **13**(2): p. 454-67.
240. Mullis, K.B. and F.A. Faloona, *Specific synthesis of DNA in vitro via a polymerase-catalyzed chain reaction.* Methods Enzymol, 1987. **155**: p. 335-50.
241. Bradford, M.M., *A rapid and sensitive method for the quantitation of microgram quantities of protein utilizing the principle of protein-dye binding.* Anal Biochem, 1976. **72**: p. 248-54.
242. Shapiro, A.L., E. Vinuela, and J.V. Maizel, Jr., *Molecular weight estimation of polypeptide chains by electrophoresis in SDS-polyacrylamide gels.* Biochem Biophys Res Commun, 1967. **28**(5): p. 815-20.
243. Towbin, H., T. Staehelin, and J. Gordon, *Electrophoretic transfer of proteins from polyacrylamide gels to nitrocellulose sheets: procedure and some applications.* Proc Natl Acad Sci U S A, 1979. **76**(9): p. 4350-4.
244. Carney, D.N. and C.F. Winkler, *In vitro assays of chemotherapeutic sensitivity.* Important Adv Oncol, 1985: p. 78-103.
245. Fulwyler, M.J., *Electronic separation of biological cells by volume.* Science, 1965. **150**(3698): p. 910-1.
246. Schwartz, D.C. and C.R. Cantor, *Separation of yeast chromosome-sized DNAs by pulsed field gradient gel electrophoresis.* Cell, 1984. **37**(1): p. 67-75.
247. Krishan, A., *Rapid flow cytofluorometric analysis of mammalian cell cycle by propidium iodide staining.* J Cell Biol, 1975. **66**(1): p. 188-93.
248. Deitch, A.D., H. Law, and R. deVere White, *A stable propidium iodide staining procedure for flow cytometry.* J Histochem Cytochem, 1982. **30**(9): p. 967-72.
249. Taylor, W.R., *FACS-based detection of phosphorylated histone H3 for the quantitation of mitotic cells.* Methods Mol Biol, 2004. **281**: p. 293-9.
250. Vistica, D.T., et al., *Tetrazolium-based assays for cellular viability: a critical examination of selected parameters affecting formazan production.* Cancer Res, 1991. **51**(10): p. 2515-20.
251. Bryant, P.E., H. Mozdarani, and C. Marr, *G2-phase chromatid break kinetics in irradiated DNA repair mutant hamster cell lines using calyculin-induced PCC and colcemid-block.* Mutat Res, 2008. **657**(1): p. 8-12.
252. El-Khamisy, S.F., et al., *A requirement for PARP-1 for the assembly or stability of XRCC1 nuclear foci at sites of oxidative DNA damage.* Nucleic Acids Res, 2003. **31**(19): p. 5526-33.
253. Eschenburg, G., et al., *Smac mimetic LBW242 sensitizes XIAP-overexpressing neuroblastoma cells for TNF-alpha-independent apoptosis.* Cancer Res, 2012. **72**(10): p. 2645-56.
254. Lee, S., et al., *Robust selection of cancer survival signatures from high-throughput genomic data using two-fold subsampling.* PLoS One, 2014. **9**(10): p. e108818.
255. Barnard, S., S. Bouffler, and K. Rothkamm, *The shape of the radiation dose response for DNA double-strand break induction and repair.* Genome Integr, 2013. **4**(1): p. 1.

256. Gilabert, M., et al., *Poly(ADP-ribose) polymerase 1 (PARP1) overexpression in human breast cancer stem cells and resistance to olaparib.* PLoS One, 2014. **9**(8): p. e104302.
257. Barnes, D.J., et al., *Bcr-Abl expression levels determine the rate of development of resistance to imatinib mesylate in chronic myeloid leukemia.* Cancer Res, 2005. **65**(19): p. 8912-9.
258. Guo, W., et al., *Mechanisms of methotrexate resistance in osteosarcoma.* Clin Cancer Res, 1999. **5**(3): p. 621-7.
259. Cazzalini, O., et al., *p21CDKN1A participates in base excision repair by regulating the activity of poly(ADP-ribose) polymerase-1.* DNA Repair (Amst), 2010. **9**(6): p. 627-35.
260. Tentori, L., et al., *Pharmacological inhibition of poly(ADP-ribose) polymerase (PARP) activity in PARP-1 silenced tumour cells increases chemosensitivity to temozolomide and to a N3-adenine selective methylating agent.* Curr Cancer Drug Targets, 2010. **10**(4): p. 368-83.
261. Tanuma, S. and Y. Kanai, *Poly(ADP-ribosyl)ation of chromosomal proteins in the HeLa S3 cell cycle.* J Biol Chem, 1982. **257**(11): p. 6565-70.
262. Kashima, L., et al., *CHFR protein regulates mitotic checkpoint by targeting PARP-1 protein for ubiquitination and degradation.* J Biol Chem, 2012. **287**(16): p. 12975-84.
263. Moding, E.J., M.B. Kastan, and D.G. Kirsch, *Strategies for optimizing the response of cancer and normal tissues to radiation.* Nat Rev Drug Discov, 2013. **12**(7): p. 526-42.
264. Iliakis, G., et al., *DNA damage checkpoint control in cells exposed to ionizing radiation.* Oncogene, 2003. **22**(37): p. 5834-47.
265. Xu, B., et al., *Two molecularly distinct G(2)/M checkpoints are induced by ionizing irradiation.* Mol Cell Biol, 2002. **22**(4): p. 1049-59.
266. Zitouni, S., et al., *Polo-like kinases: structural variations lead to multiple functions.* Nat Rev Mol Cell Biol, 2014. **15**(7): p. 433-52.
267. Donzelli, M. and G.F. Draetta, *Regulating mammalian checkpoints through Cdc25 inactivation.* EMBO Rep, 2003. **4**(7): p. 671-7.
268. Kandel, E.S., et al., *Activation of Akt/protein kinase B overcomes a G(2)/m cell cycle checkpoint induced by DNA damage.* Mol Cell Biol, 2002. **22**(22): p. 7831-41.
269. Shtivelman, E., J. Sussman, and D. Stokoe, *A role for PI 3-kinase and PKB activity in the G2/M phase of the cell cycle.* Curr Biol, 2002. **12**(11): p. 919-24.
270. Combaret, V., et al., *Clinical relevance of CD44 cell-surface expression and N-myc gene amplification in a multicentric analysis of 121 pediatric neuroblastomas.* J Clin Oncol, 1996. **14**(1): p. 25-34.
271. Favrot, M.C., V. Combaret, and C. Lasset, *CD44--a new prognostic marker for neuroblastoma.* N Engl J Med, 1993. **329**(26): p. 1965.
272. Gross, N., et al., *CD44H expression by human neuroblastoma cells: relation to MYCN amplification and lineage differentiation.* Cancer Res, 1994. **54**(15): p. 4238-42.
273. Gross, N., K. Balmas Bourloud, and C.B. Brognara, *MYCN-related suppression of functional CD44 expression enhances tumorigenic properties of human neuroblastoma cells.* Exp Cell Res, 2000. **260**(2): p. 396-403.
274. Negroni, A., et al., *Decrease of proliferation rate and induction of differentiation by a MYCN antisense DNA oligomer in a human neuroblastoma cell line.* Cell Growth Differ, 1991. **2**(10): p. 511-8.

Supplement

List of Abbreviations

µg	Microgram
µl	Microliter
µm	Micrometer
°C	Degree Celsius
CB	Chromatid Breaks
cDNA	complementary DNA
A	Ampere
A-EJ	Alternative end joining
A.U.	arbitrary units
AF	AlexaFluor
ALK	Anaplastic Lymphoma Kinase
APC	Allophycocyanin
BDNF	Brain-Derived Neurotrophic Factor
bp	Basenpaare
BSA	Bovine Serum Albumin
Da	Dalton
DAPI	4,6-Diamidin-2-phenylindol
DMSO	Dimethylsulfoxid
DNA	Deoxyribonucleic Acid
DSB	Double-strand break
EDTA	Ethylendiamintetraacetat
ELISA	Enzyme Linked Immunosorbent Assay
FACS	Fluorescence-Activated Cell Sorting
FCS	Fetal Calf Serum
FITC	Fluoresceinisothiocyanat

Supplement

FSC	Forward Scatter
g	Gram
GFP	Green Fluorescent Protein
h	hour
HRP	Horseradish Peroxidase
HRR	Homologous Recombination Repair
IHC	Immunohistochemistry
INSS	International Neuroblastoma Staging System
Kbp	kilo base pairs
kDa	Kilo-Dalton
M	Molar
mA	Milliampere
MAX	MYC associated Factor X
mg	Milligram
MIBG	Methyliodbenzylguanin
min	Minute (s)
ml	Milliliter
mM	Millimolar
mRNA	messenger RNA
MTT	3-(4,5- dimethylthiazol-2-yl)-2,5-diphenyltetrazolium bromide
NB	Neuroblastoma
ng	Nanogram
NGF	Nerve Growth Factor
NHEJ	Non-homologous end joining
nm	Nanometer
PAGE	Polyacrylamid-Gelelektrophorese
PBS	Phosphate Buffered Saline
PCC	Premature Chromosome Condensation

PCR	Polymerase Chain Reaction
PE	Phycoerythrin
PFA	Paraformaldehyd
PFGE	Pulsed-field Gel Electrophoresis
pHH3	phosphorylated Histone H3
PI	Propidium Iodide
RIPA	Radioimmunoprecipitation Buffer
RNA	Ribonucleic Acid
rpm	rounds per minute
RPMI	Roswell Park Memorial Institute
RT	Room Temperature
SDS	Sodium Dodecyl Sulfate
SEM	Standard Error of the Mean
STDEV	Standard Deviation
s	second
SDS	Sodium Dodecylsulfate
SSC	Side Scatter
TBS	Tris-buffered Saline
TBST	Tris-buffered Saline + Tween20
TEMED	Tetramethylethylendiamine
Tet	Tetracycline
Trk	Tropomyosin receptor kinase
TRIS	Tris(hydroxymethyl)-aminomethane
UV	Ultra-violet light
V	Volt
WB	Western Blot
x g	fold earth acceleration

Supplement

List of Figures

List of Tables

Conference Contributions

Talk, 25th Annual Meeting of the Kind Philipp Foundation in Wilsede, June 2012

Poster, Research Day of the Medical Department of the University of Essen, November 2012

Poster, Research Day of the Medical Department of the University of Essen Poster, November 2013

Supplement

Poster, Advances in Neuroblastoma Research (ANR), May 2014

Poster, Radiation Biology and Cancer from Molecular Responses to the Clinic, February 2015

Supplement

Acknowledgements

I would like to thank my PhD advisor PD Dr. Alexander Schramm for giving me the opportunity to work in his research group, for guiding my research, and advising me throughout the entire time of my PhD research, while still always listening to my opinions and supporting my own theories regarding experiments.

I also want to thank everyone at the GRK1739, especially Prof. Dr. Verena Jendrossek, Dr. Gabriele Siedenburg and Ivonne Schulte, for providing me with a rich learning atmosphere and hundreds of memories of my time at the graduate school. Additionally, I would like to thank the DFG for the financial support for my project.

Prof. Dr. George Iliakis was very generous in allowing me to learn new methods and techniques in his lab under supervision of Dr. Aashish Soni and Dr. Fanghua Li. I would like to thank all of you for teaching me and supporting my research in such a valuable way.
Aashish, our collaboration and our scientific discussions were a lot of fun!

Furthermore, I want to thank Prof. Dr. Jens Fischer and Alexandra Schütze for taking part in another fruitful collaboration.

Most of all, I would like to thank my family, and especially my mother, for always supporting me in everything I do. I would not have been able to do any of this without you.

Supplement

Resume

Der Lebenslauf ist in der Online-Version aus Gründen des Datenschutzes nicht enthalten.

Supplement

Supplement

Statutory Declaration

Hiermit erkläre ich, gem. § 6 Abs. 2, f der Promotionsordnung der Math.-Nat. Fakultäten zur Erlangung des Dr. rer. nat., dass ich das Arbeitsgebiet, dem das Thema „The role of the receptor tyrosine kinase TrkA in checkpoint activation, DSB repair, and survival of neuroblastoma cell lines“ zuzuordnen ist, in Forschung und Lehre vertrete und den Antrag von Ines Rudolf befürworte.

Ort, Datum PD Dr. rer. nat. Alexander Schramm

Hiermit erkläre ich, gem. § 7 Abs. 2, c und e der Promotionsordnung der Math.-Nat. Fakultäten zur Erlangung des Dr. rer. nat., dass ich die vorliegende Dissertation selbständig verfasst und mich keiner anderen als der angegebenen Hilfsmittel bedient habe und alle wörtlich oder inhaltlich übernommenen Stellen als solche gekennzeichnet habe.

Ort, Datum Ines Rudolf

Hiermit erkläre ich, gem. § 7 Abs. 2, d und f der Promotionsordnung der Math.-Nat. Fakultäten zur Erlangung des Dr. rer. nat., dass ich keine anderen Promotionen bzw. Promotionsversuche in der Vergangenheit durchgeführt habe, dass diese Arbeit von keiner anderen Fakultät abgelehnt worden ist, und dass ich die Dissertation nur in diesem Verfahren einreiche.

Ort, Datum Ines Rudolf